University of Helsinki
Dissertationes Universitatis Helsingiensis
71/2025

Doctoral Programme in Clinical Research, Faculty of Medicine
HUS Diagnostic Center, Radiology
University of Helsinki and Helsinki University Hospital
Finland

# IMAGING OF COMPLICATING INJURIES IN THE ANKYLOSED SPINE

**Riku Vierunen**

DOCTORAL DISSERTATION

To be presented for public discussion with the permission of
the Faculty of Medicine of the University of Helsinki,
in lecture hall 3, Biomedicum 1, Meilahti
on 14th March 2025, at noon.

Helsinki 2025

**Supervised by**
Frank V. Bensch MD, PhD
Radiology
HUS Diagnostic Center
Helsinki University Hospital, Helsinki, Finland

Docent Mika P. Koivikko MD, PhD
Radiology
HUS Diagnostic Center
Helsinki University Hospital, Helsinki, Finland

**Reviewed by**
Docent Jaakko Niinimäki MD, PhD
Diagnostic radiology
University of Oulu and Oulu University Hospital, Oulu, Finland

Docent Jukka Huttunen MD, PhD
Department of Neurosurgery
Neurocenter
Kuopio University Hospital, Kuopio, Finland

**To be discussed with**
Professor Roberto Blanco Sequeiros MD, PhD
Department of Diagnostic Radiology
Faculty of Medicine, University of Turku
Turku University Hospital, Turku, Finland

The Faculty of Medicine uses the Urkund system (plagiarism recognition) to examine all doctoral dissertations.

Publisher: Helsingin yliopisto
Series: Dissertationes Universitatis Helsingiensis 71/25

ISBN 978-952-84-0231-2 (print)
ISBN 978-952-84-0230-5 (online)
ISSN 2954-2898 (print)
ISSN 2954-2952 (online)

PunaMusta, Joensuu 2025

# TABLE OF CONTENTS

# ABSTRACT

Ankylosis of the spine is caused by excess bone growth along the vertebrae resulting in mechanical fusion of the vertebral column. Known causes are inflammation from ankylosing spondylitis (AS), or idiopathic from diffuse idiopathic skeletal hyperostosis (DISH), or degenerative from degenerative spondylosis (DS), as well as iatrogenic from surgical fusion. Differentiating AS, DISH, and DS by radiologic imaging alone may prove impossible, and often the latter two are not even documented in the electronical medical records with the corresponding International Classification of Diseases, Tenth Revision (ICD-10) codes.

Ankylosis predisposes the spine to unstable fractures and spinal hematoma as well as to blunt cerebrovascular injury (BCVI), which are the main focus of this thesis. The studies took place in Töölö Hospital, the only level-1 trauma center in Finland at the time, where severe orthopedic and neurosurgical traumas were managed until February 2023. Spinal hematoma and BCVI are serious injuries which may cause permanent neurological impairment if not diagnosed and treated promptly.

A manual review of 2256 urgent or emergency referrals in the first study (I) revealed 28 AS patients had fully ankylosed spines. Of these 28, 19 (68%) had spinal epidural hematomas (SEH) and 5 (18%) had spinal subdural hematomas (SSH). The most common trauma mechanism was a fall from standing height in 20 patients (71%). Surgery improved patients' neurological status ($p = 0.008$). Impingement found in MRI resulted in more severe neurological status ($p = 0.012$). Hematomas' T1 heterogeneity occurred in MRIs after a median delay of four days ($p = 0.047$).

The second study (II) focused on patients with ankylosed cervical spine and on the incidence of concomitant BCVI. A manual review of 5867 computed tomographic angiographies (CTA) revealed 153 patients with blunt trauma and ankylosis of at least three consecutive cervical vertebrae. Of these 153, 29 (19%) had a total of 36 BCVIs which caused two anterior and four posterior circulation strokes. Of the BCVIs, 32 (89%) were in the vertebral arteries. The classification of BCVIs according to Biffl et al. were as follows: 17 grade II, 4 grade III, 14 grade IV, and one grade V. The most common trauma mechanism was a fall from standing height in 125 patients (82%). A fracture in the cervical spine proved to be the only

significant predictor for BCVI (OR 7.44). DS was the most common cause for ankylosis of the cervical spine.

The third study (III) focused on spinal hematomas and their relation to neurological status in DISH patients with blunt trauma. In the same cohort of 2256 referrals studied in Study I, 70 had ankylosis from DISH and blunt trauma. Of these 70, 37 (53%) had spinal hematoma, 47 (67%) had spinal cord impingement, and 43 (61%) had spinal cord injury (SCI); 34 (49%) hematomas were epidural and 3(4%) subdural.

# LYHENNELMÄ

Poikkeavaa luun kasvua selkärangan ympärillä, mikä johtaa nikamien yhteen luutumiseen, kutsutaan selkärangan ankyloosiksi. Selkärankareuma (SR), diffuusi idiopaattinen skeletaalinen hyperostoosi (DISH) ja degeneratiivinen spondyloosi (DS) ovat tunnettuja syitä ankyloosille, jotka kehittyvät tulehduksellisten (SR) ja tuntemattomien (DISH) tekijöiden sekä selkärangan rappeuman (DS) myötä. Selkärangan jäykistys- eli luudutusleikkauksen jälkeen nikamat menettävät myös mahdollisuutensa luonnolliselle liikkeelle. Ankyloosi altistaa selkärangan epästabiileille murtumille, selkäydinkanavan verenpurkaumille eli spinaalisille hematoomille ja tylpille kaulasuonivammoille (TKS), jotka ovat vakavia vammoja sekä tämän väitöskirjan aiheita.

Tässä väitöskirjatutkimuksessa tutkittiin retrospektiivisesti 2011 tammikuun ja 2020 maaliskuun välisenä aikana kuvattuja 2256 potilaan selkärangan magneettikuvauksia ja 5867 potilaan kaularangan ja kaulasuonten tietokonetomografisia angiografia-tutkimuksia.

Ensimmäisessä osatyössä (I) tutkittiin spinaalisia hematoomia 28:lla SR -potilaalla, joilla oli täysin ankyloituneessa selkärangassa murtuma. 19:llä (68 %) oli spinaalinen epiduraalinen hematooma (SEH) ja 5 (18 %) spinaalinen subduraalinen hematooma (SSH).

Toisessa osatyössä (II) 153:lla potilaalla löytyi vähintään 3 perättäisen nikaman osalta ankyloitunut kaularanka ja tylppä vamma. 36 TKS:ää löytyi 29:ltä (19 %) potilaalta, joista suurin osa (32, 89%) oli nikamavaltimoissa ja jotka aiheuttivat 2 etu- ja 4 takakierron aivoinfarktia.

Kolmannessa osatyössä (III) tutkittiin spinaalisia hematoomia tylpän vamman saaneilla DISH -potilailla. DISH:n aiheuttama ankyloosi löytyi 70:ltä tylpän vamman saaneelta potilaalta, joista 37:llä (53 %) oli spinaalinen hematooma, 47:llä (67 %) selkäytimen pinne ja 43:llä (61 %) oli selkäydinvaurio. 34 potilaalta löytyi 49% ilmaantuvuudella SEH ja 3 potilaalla 4% ilmaantuvuudella SSH.

Kaikissa osatöissä kaatuminen seisaaltaan oli yleisin vammamekanismi. Selkärangan ankyloosi altistaa potilaan vakaville vammoille, jotka ovat tässä potilasryhmässä kohtalaisen yleisiä.

# LIST OF ORIGINAL PUBLICATIONS

This thesis is based on the following publications, which are referred to in the text by their Roman numerals I-III:

I **Vierunen RM**, Koivikko MP, Siironen JO, Kerttula LI, Bensch FV. Post-traumatic spinal hematoma in ankylosing spondylitis. Emerg Radiol. 2021 Jun;28(3):601-611. doi: 10.1007/s10140-020-01881-3. Epub 2021 Jan 16. PMID: 33452963.

II **Vierunen RM**, Haapamäki VV, Koivikko MP, Bensch FV. Ankylosis of the cervical spine increases the incidence of blunt cerebrovascular injury (BCVI) in CTA screening after blunt trauma. Emerg Radiol. 2022 Jun;29(3):507-517. doi: 10.1007/s10140-022-02022-8. Epub 2022 Mar 16. PMID: 35296926; PMCID: PMC9123032.

III **Vierunen RM**, Haapamäki VV, Koivikko MP, Bensch FV. Post-traumatic spinal hematoma in diffuse idiopathic skeletal hyperostosis (DISH). Eur Radiol. 2023 Dec;33(12):9425-9433. doi: 10.1007/s00330-023-09866-9. Epub 2023 Jun 29. PMID: 37382616; PMCID: PMC10667401.

# ABBREVIATIONS

| | |
|---|---|
| ALARA | as low as reasonably achievable |
| ACDF | anterior cervical discectomy and fusion |
| ALL | anterior longitudinal ligament |
| AS | ankylosing spondylitis |
| BCVI | blunt cerebrovascular injury |
| CCA | common carotid artery |
| CCJ | craniocervical junction |
| CR | computed radiography |
| CSF | cerebrospinal fluid |
| CT | computed tomography |
| CTA | computed tomographic angiography |
| CTJ | cervicothoracic junction |
| DEXA | dual-energy x-ray absorptiometry |
| DISH | diffuse idiopathic skeletal hyperostosis |
| DR | direct radiography |
| DSA | digital subtraction angiography |
| DS | degenerative spondylosis |
| HU | Hounsfield unit |
| ICA | internal carotid artery |
| ICD-10 | International Classification of Diseases, Tenth Revision |
| IVD | intervertebral disc |
| IQR | interquartile range |
| MRA | magnetic resonance angiography |
| MRI | magnetic resonance imaging |
| MVA | motor vehicle accident |
| NEXUS | National Emergency X-Radiography Utilization Study |
| OPLL | ossification of the posterior longitudinal ligament |
| PLL | posterior longitudinal ligament |

| | |
|---|---|
| SCI | spinal cord injury |
| SEH | spinal epidural hematoma |
| SI | sacroiliac |
| SpA | seronegative spondylarthropathy |
| SSH | spinal subdural hematoma |
| TBI | traumatic brain injury |
| TLJ | thoracolumbar junction |
| VA | vertebral artery |
| WBCT | whole-body CT |

# 1 INTRODUCTION

Additional bone growth along the vertebral column forming bony bridges between two vertebrae is called ankylosis, which in its advanced stage leads to rigid spine, preventing normal movement between the affected vertebrae. Due to rigidity of ankylotic spine, patients are vulnerable to severe trauma with far less trauma energy in comparison to the situation in patients with a normally mobile spine. Even low-energy trauma such as a fall from standing height may cause an unstable spinal fracture, which is a severe injury capable of causing permanent neurological impairment (Shah et al. 2019).

Chronic back pain is a common complication in patients with ankylosing diseases and disorders. Therefore, when a harmless-seeming stumble on ground level causes a well-positioned but unstable fracture running transversely through the vertebral column, it may go unnoticed by both patient and attending physician (Einsiedel et al. 2006, Teunissen et al. 2017). Advanced spinal ankylosis results in altered biomechanics, as the formerly mobile vertebrae are fused and act like a single long bone. The normal slightly forward-curving kyphosis in the thoracic spine is accentuated, and the weight of the head acts as a lever force for the upper spine when falling backwards. Falling forward, the face hits the ground as the mass of the body around the rigid spine follows. Both of the previous mechanisms cause hyperextension to the spine which is broken in two. Sharp fracture edges abrade the neurovascular structures, causing neurological deficits and hemorrhage next to the fracture. A spinal hematoma itself can cause spinal cord impingement and, without treatment, can cause permanent neurological deficits (Lawton et al. 1995).

Spinal ankylosis is caused by seronegative spondyloarthropathies (SpA), diffuse idiopathic skeletal hyperostosis (DISH), degenerative spondylosis (DS), or by spinal fusion.

Ankylosing spondylitis (AS) is the most common SpA, of which the others are psoriatic arthritis, arthritis associated with inflammatory bowel disease, and reactive arthritis. Axial SpA causes inflammation of the spine in the apophyseal joints and spinal ligaments adjacent to the intervertebral discs (IVD), which in its advanced form results in a fully ankylosed spine (Sieper & Poddubnyy 2017). The radiological appearance of AS is not always distinguishable from DISH and DS; all of these (three) entities may occur even in the same patient (Teunissen et al. 2017, Kuperus et al. 2018, Slonimsky et al. 2018).

DISH is a bone-generating disease of unknown mechanism but is related to overweight, type 2 diabetes, old age, and male sex (Weinfeld et al. 1997, Westerveld et al. 2008, Kuperus et al. 2020). The original criterion by Resnick & Niwayama defines it as anterior flowing or wavy bone protrusions at the level of at least three consecutive IVDs without signs of SpA or DS (Resnick & Niwayama 1976). These protrusions, called syndesmophytes, may fuse and usually occur in the cervical and upper thoracic spine, causing ankylosis in the anterior aspect of the spine.

DS or osteoarthritis of the spine is related to old age. Before the spine is ankylosed, the hallmark features of degenerative spinal disease are visible in radiological imaging. The IVDs and facet joint spaces are narrowed, sclerosis and osteophytes grow next to the endplates and joint surfaces, and eventually the affected vertebrae are fused (Sarzi-Puttini et al. 2005, Gellhorn et al. 2013).

Degeneration and trauma causing pathological vertebral displacement may result in neurological deficits and chronic pain, which is managed surgically by spinal fusion. Treatment aiming at pain relief and return to daily life causes ankylosis of the affected vertebrae as well as acceleration of the degeneration of the adjacent IVD (Matsunaga et al 1999, Shah et al. 2019).

Ankylosis and the trauma of patients with ankylosed spine are imaged by radiography, computed tomography (CT), and magnetic resonance imaging (MRI). Ankylosis, depending on the etiology, is often visible on radiographs, but a well-positioned fracture may be occult. CT and MRI are superior to radiographs in detecting fractures of an ankylosed spine. Osteoporosis and the sharp edges of fractures along the thin cortices of vertebrae, as seen in AS patients, as well as the differing ankylosis types are visibleon CT. The soft tissue contrast of MRI is superior to CT, enabling the detection of soft-tissue injuries as well as spinal hematomas. (Shah et al. 2019)

Blunt cerebrovascular injury (BCVI) results mainly from high-energy trauma seen in motor vehicle accidents (MVA), falling, and bicycle accidents, causing abrupt stretching of the cervical arteries when the head follows immediately the body after the collision (Rutman et al. 2018, Bensch et al.2019). BCVI is a serious injury which may cause acute ischemic stroke (Biffl et al. 1999). For imaging of BCVI, computed tomographic angiography (CTA) has become the most common imaging method, whereas digital subtraction angiography (DSA) remains the gold standard (Berne et al. 2006, Eastman et al. 2006, Stein et al. 2009, Bromberg et al. 2010, Wang et al. 2012).

AS patients have more spinal hematomas than the general trauma population, the incidence of which has been based on findings in surgery and imaging studies (Foo & Rossier 1982, Jacobs & Fehlings 2008, Westerveld et al. 2009b, Al-Mutair & Bednar 2010, Vazan et al. 2019, Shah et al. 2021). AS patients are mostly already known in healthcare and often specific ICD-10 codes. The literature on AS and DISH patients with injured ankylosed spine tends to focus

primarily on management, trauma mechanisms, and other injuries than spinal hematoma. Only a few case reports concern those with a BCVI.

Study I focuses on the incidence and MRI features of spinal hematoma in AS patients after blunt trauma. The aims of Study II are to discover the incidence and grade of BCVI, as well as the related strokes in patients with ankylosed cervical spine. Study III focuses on spinal hematoma and its relation to neurological status in patients with DISH after blunt trauma.

# 2 REVIEW OF THE LITERATURE

## 2.1 Anatomy of the spine

The bony spinal column consists of 7 cervical, 12 thoracic, 5 lumbar, 5 sacral, and 4 coccygeal vertebrae with their own anatomical properties. The sacral and coccygeal vertebrae are most often fused as single bones called the sacrum and coccyx, which in turn may, by a bony union or fibrocartilaginous joint, fuse to one another. Joined as one upon the other by the separating IVDs, they form the vertebral column. Supporting the cranium and providing axial support for the rest of the body in an upright posture is the primary function for the spine. The sacrum has bilateral fibrocartilaginous joints that transfer the weight of the torso and upper body to the iliac bones and the lower extremities. (Bogduk 2016, Dalley & Agur 2023)

The bony vertebrae attached to each other protect the spinal cord and allow passage for the nerve roots via the neural foramina below the pedicles. The need for mobility without predisposing the spinal cord and nerve roots to impingements between the mobile and surrounding bony and fibrocartilaginous structures affects the shape and anatomy of vertebrae, which differ across the vertebral column. (Bogduk 2016, Dalley & Agur 2023)

Vertebrae in the regions described differ from each other by their structural properties for mobility and by their orientation. The cervical spine is the most mobile portion and carries less axial load than the lower vertebrae. The thoracic spine is the most rigid part of the spine where mobility is mostly reduced by ribs that join with two articulations bilaterally and are supported by their associated ligaments. The adult vertebral column has four physiological curvatures in the cervical, thoracic, and lumbar spine, as well as in the sacrum. The posteriorly convex and concave parts of the spine are respectively known as kyphosis and lordosis. The thoracic vertebrae are in kyphosis, bowing slightly backwards. The cervical and lumbar spine have a slight forward bowing lordosis. The cervical spine adjoining the thoracic spine forms the cervicothoracic junction (CTJ) and the thoracic spine adjoining the lumbar spine forms the thoracolumbar junction (TLJ). Forward bowing lumbar lordosis is more convex than the cervical lordosis and accentuated by the sacrum that is tilted forward and connected to the fifth lumbar vertebra, thus forming the lumbosacral angle. The IVDs together with these several

curvatures provide, for the vertebral column, both shock absorption and flexibility. (Bogduk 2016, Dalley & Agur 2023)

The cranium, working as a center of mass and a significant vector in deceleration forces such as MVA, affects the upper parts of the spine. Two adjoining columns of vertebrae with different properties in mobility cause additional structural stress in the intersection. These tendencies and restrictions by anatomical composition affect each other, which becomes apparent in a general trauma population and causes peaking of spinal fractures in CTJ and TLJ (Fig. 1, Niemi-Nikkola et. al 2018).

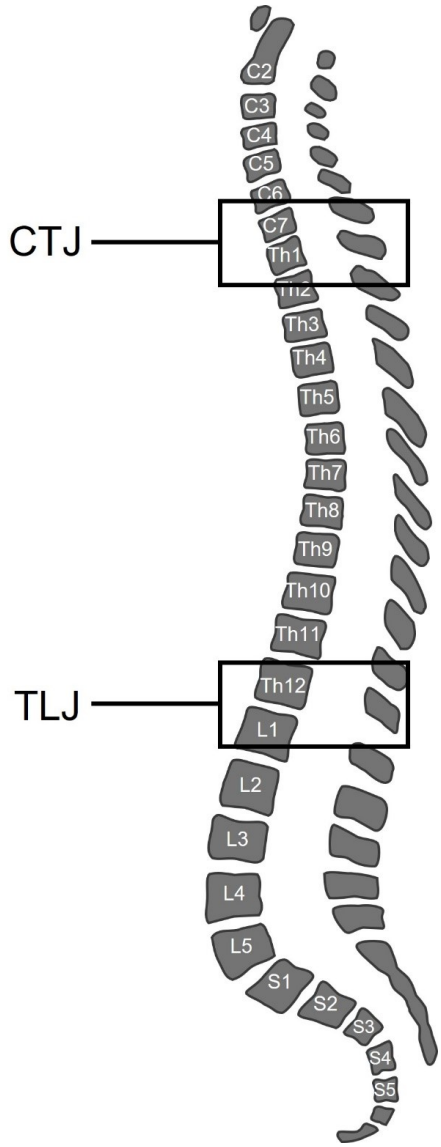


**Figure 1** Anatomy of the vertebral column. Cervicothoracic junction (CTJ) and thoracolumbar junction (TLJ) in boxes.

### 2.1.1 Vertebrae

A typical vertebra consists of a body, vertebral arch, two transverse processes, one spinous process, and two articular processes at each posterolateral aspect of the arch (Fig. 2). Vertebrae are nominated alphanumerically, meaning that the letter indicates region, and the number indicates level. For instance, C1 refers to the first cervical vertebra (C=cervical vertebrae, Th=thoracic vertebrae, L=lumbar vertebrae, S=sacral vertebrae) (Fig. 1).

The vertebral body, being the largest part of the vertebra, is the cylindrical anterior part carrying most of the axial load. Vertebrae as well as IVDs are generally larger the lower they are located in the spine. The vertebrae develop from annular epiphyses that later fuse to the body and form slightly thicker endplates at the outer margins of each upper and lower end. The epiphyseal remnants of permeable hyaline cartilage supply the vertebral body with fluid and nutrients, providing protection from impacts together with the IVDs. Most of the body consists of cancellous bone and hematopoietically active red (in children) or fatty yellow bone marrow (in adults). Posterior intercostal arteries in the thoracic spine and lumbar arteries in the lumbar spine originate directly from the aorta and run along the anterior and lateral surface of the respective vertebral body. These arteries have smaller periosteal, equatorial, and posterior branches supplying the vertebral body and posterior arch. Smaller branches supplying the cervical vertebrae originate from vertebral and ascending cervical arteries, and those supplying the sacrum from lateral sacral arteries in the pelvis. The basivertebral vein supplies drainage of the bodies via the sinus situated in the posterior cortex of each vertebral body. (Dalley & Agur 2023)

The vertebral bodies have differing and specific features across the spine for each functional segment. The upper endplate of a typical cervical vertebra slants downward anteriorly, which allows for a higher range of motion for flexion and extension (Bodguk 2016). Cranially pointing edges known as the uncinate processes arise from both lateral margins of the upper endplates of a typical cervical vertebra, forming a downward concave impression visible in the coronal plane for accommodating the intervertebral disc and lower endplate of the next higher vertebra. The combination of anterior downward slant and the upwards facing uncinate processes of the upper endplate of a typical cervical vertebral body forms a saddle joint that enables easy extension, flexion, and lateral flexion movements (Bogduk 2016).

The body of a typical thoracic vertebra has a combination of four cartilaginous facets at the posterior and lateral aspect, two at the level of the upper endplate, and two at the level of the lower endplate, all for costovertebral articulations (Dalley & Agur 2023). The costovertebral articulations along with their ligamentous and muscular structures limit the movement and axial rotation

of the thoracic spine, which is markedly more rigid than the cervical and lumbar spine (Fujimori et al. 2012, Shin et al. 2013, Dalley & Agur 2023).

The body of each lumbar vertebra is larger than the ones above it, reflecting the increased axial load (Dalley & Agur 2023). Even though they bear more axial load than the ones located more cranially, lumbar vertebrae still have a moderate ability to rotate, which is well illustrated by anatomical 3D models (Shin et al. 2013). Axial rotation was thought to be limited to approximately 2° per vertebra in the lumbar spine (Pearcy & Tibrewal 1984). The more recent study by Shin et al. convincingly showed that lumbar spine axial rotation below the L2 ranges from 4.4° to 6.7° (Shin et al. 2013). That study also revealed that during axial rotation, the two upper vertebrae showed coupled bending opposite to the axial rotation, and that the two lower vertebrae had coupled bending in the same direction as the axial rotation.

Bilateral pedicles connect the vertebral body to the posterior vertebral elements while transmitting forces between each other (Bogduk 2016, Dalley & Agur 2023). In the upper parts of the thoracic spine, where the pedicles are the narrowest, the pedicles, on cross-sectional images have a tear-drop and outwardly convex shape (Panjabi et al. 1997). Th4 has the narrowest pedicles, from which point their width gradually reaches its peak width at L5 (Morita et al. 2021). Th1 has the shortest pedicles, from which pedicle length gradually reaches its peak at Th3 (Morita et al. 2021). The superior and inferior surface of each pedicle forms the inferior and superior borders of the respective adjacent neural foramina (Dalley & Agur 2023). The anterior margin of the neural foramina is formed by the posterior wall of the body and the IVD, whereas the posterior margin is formed by the facet joints (Dalley & Agur 2023).

From the posterior and medial margin of the pedicles, bilateral vertically oriented thin layers called laminae form the bony posterior margin of the spinal canal and unite at the posterior midline, forming the vertebral arch (Dalley & Agur 2023). The laminae are widest in the cervical spine, with the greatest being 15.6 mm in mean width at C2, which is halved in the thoracic spine and gradually increases again, reaching its peak of 15.7 mm at L5. The height and thickness of the laminae is least in the upper parts of the cervical spine excluding C2, which corresponds to its measurement(s) at the lower thoracic and lumbar spine of approximately 5 mm. (Xu et al. 1999)

Bilateral transverse processes at the posterior and lateral margin of the pedicles and the long, posteriorly protruding spinous process at the posterior midline of the vertebral arch serve as attachment for the surrounding muscles controlling spinal movement (Bogduk 2016, Dalley & Agur 2023). Transverse processes differ between cervical, thoracic, and lumbar vertebrae. In the cervical spine, the transverse processes from C1 to C6 are perforated craniocaudally by the transverse foramina which protect the vertebral arteries (Fig. 3) (Travan et al. 2015,

Dalley & Agur 2023). The diameters decrease gradually from C6 to C2 (Travan et al. 2015). Normal variants are frequent findings in transverse processes of the cervical spine. Transverse foramina have smaller remnants or are usually absent in C7 (Dalley & Agur 2023). Accessory or double transverse foramina are smaller foramina next to the actual ones (Travan et al. 2015). C1 is the widest vertebra, and known as atlas based on ancient Greek mythology of a giant carrying the (actual) world on his shoulders. It has most normal variations such as retrotransverse canals, arcuate foramina, and supratransverse foramina (Travan et al. 2015, Dalley & Agur 2023). An incomplete form of a foramen known as retrotransverse groove is more frequently seen than the complete form, with the latter being observable in 17.8% (Travan et. al 2015). The transverse processes in the thoracic vertebrae have anterolaterally facing cartilaginous facets for costotransversal articulations. The lumbar transverse processes lack foramina and cartilaginous facets, being larger than those previously described. Spinous processes are smallest in the cervical spine excluding C1 and C2, which lack spinous processes, and C7 which actually has the longest process of all the mobile vertebrae (Dalley & Agur 2023). Spinous processes in the thoracic spine are longer, with each overlapping the one below, whereas the ones in the lumbar spine are shorter and more horizontally oriented (Dalley & Agur 2023).

The zygapophyseal joints, also known as facet joints, are diarthrodial synovial joints with articular cartilages at the posterolateral aspects of the posterior arch (Fig. 3) (Jaumard et al. 2011, Bogduk 2016, Dalley & Agur 2023). The sum of the subsequent facet joints forms bilateral posterior columns that carry part of the axial load, in addition to (the aid of) vertebral bodies (Dalley & Agur 2023). The orientation of facet joint surfaces differs among the three regions with mobile vertebrae. In the cervical spine, the median inclination of the superior articular joint surface in the sagittal plane is a 40° angle compared to the vertical axis drawn along the posterior cortex of the respective vertebral body (Nowitzke et al. 1994). The inclination in the sagittal plane varies across the spine and gradually becomes more vertically oriented towards the lumbar spine (Jaumard et al. 2011, Dalley & Agur 2023). Articular surfaces in the thoracic spine are nearly vertical and further restrict rotation (Fujimori et al. 2012, Dalley & Agur 2023). Towards the lower parts of the cervical spine, flexion and extension decrease, while the height of the superior articular processes in facet joints increases (Nowitzke et al. 1994).

The high mobility of the cervical spine, which provides support for the cranium, requires a specific functional anatomy. C1 has two lateral masses which are connected by the anterior and posterior arches. The superior articular processes of the lateral masses are semi-lunate-shaped, slanted medially, and concave, forming the synovial atlanto-occipital joints together with the convex occipital condyles (Fig. 4). The atlanto-occipital joints also prevent any rotational movement

between the cranium and C1 but allow some degree of extension and flexion. (Bogduk 2016, Dalley & Agur 2023)

The vertically oriented median atlantoaxial joint at the midline between the anterior arch of the C1 and C2's odontoid process's anterior surface as well as two bilateral horizontally oriented joints between the lateral masses of C1 and laterally sloped superior articular processes of C2 forms the synovial atlantoaxial joint (Fig.4 and Fig.5). Movement between C1 and C2 in the bilateral atlantoaxial joints generates approximately 50% of the axial rotational movement for the cranium, while the remaining rotation is cumulatively generated by facet joints and vertebral bodies with the IVDs of the lower cervical spine (Bogduk & Mercer 2000). While C1 is moving against bilateral and primally horizontally oriented joint surfaces of C2 in rotation, it also serves as a rack for the cranium, through which rotational movement is transmitted (Bogduk 2016). The transverse ligament is a part of the cruciate ligament, runs posteriorly to the odontoid process, attaches to the medial surfaces of both C1 lateral masses, and holds the median atlantoaxial joint in place (Dalley & Agur 2023). The normal interval at the median atlantoaxial joint ranges from 3 mm in adults to 5 mm in children (Bogduk 2016). As the weight of the cranium is transmitted by two axial force vectors from both atlanto-occipital joints to the rest of the spine, the weight distributes itself into three vectors beginning from C3 (Fig. 5) (Bogduk 2016, Dalley & Agur 2023).

Atlanto-occipital, atlantoaxial, and facet joints of the cervical spine have synovial capsules including anterior and posterior folds next to the joint surfaces at the anterior and posterior margins; these folds are known as meniscoids (Friedrich et al. 2008). The joint capsules of facet joints limit the range of motion while the crescent-shaped meniscoids provide support for the articular surfaces (Friedrich et al. 2008, Bogduk 2016). Meniscoids consist of adipose and fibrous tissue, or a mix of both (Farrell et al. 2016). The median meniscoid diameter measured antero-posteriorly ranges from 2 to 4 mm in cadaveric dissections, whereas the greatest diameter on 3T MRI in vivo was 5 mm in the lateral atlantoaxial joints (Farrell et al. 2016, Friedrich et al. 2008).

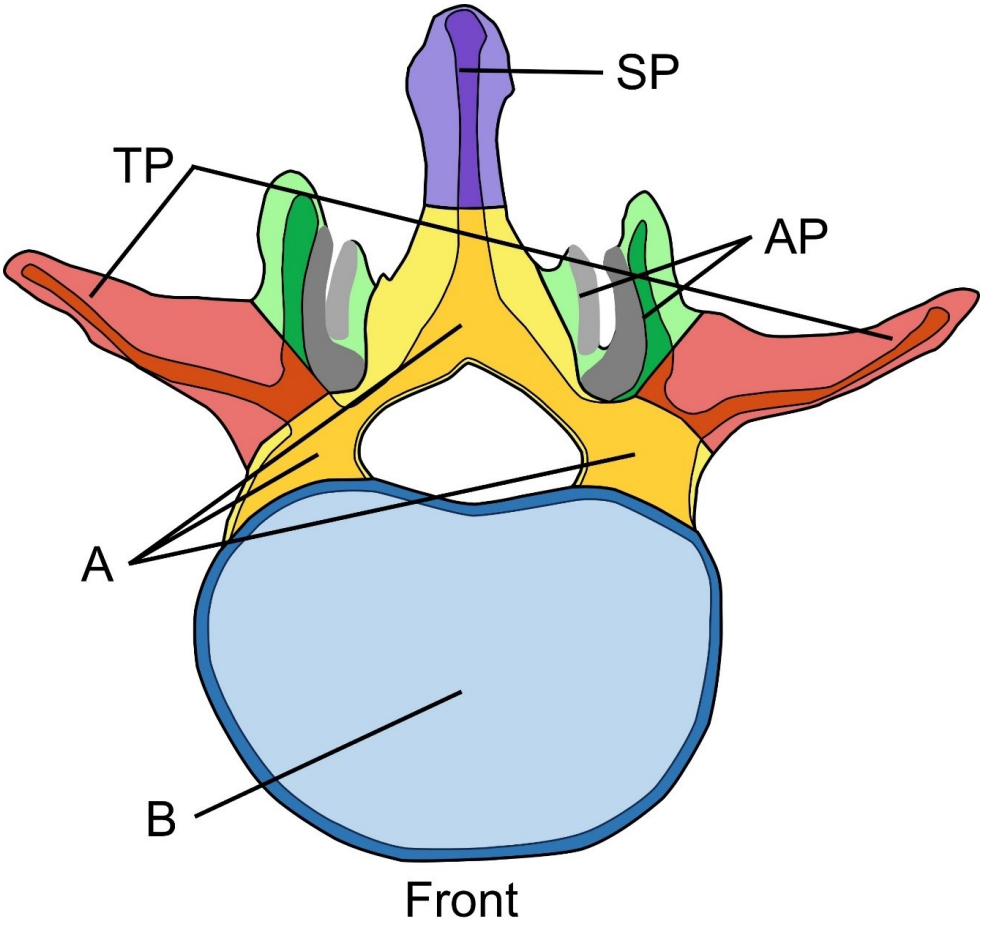


**Figure 2** Basic anatomy of a lumbar vertebra from a superior view. The anteriorly located vertebral body (B, blue) bears most of the axial load. Pedicles and the laminas form the vertebral arch (A, yellow), and protect the spinal canal and its contents. Muscles moving the spine attach to the transverse processes (TP, red) and to the spinous process (SP, purple). Bilateral superior and inferior articular processes (AP, green) have superior (dark grey) and inferior joint surfaces (light grey) that form facet joints above and below.

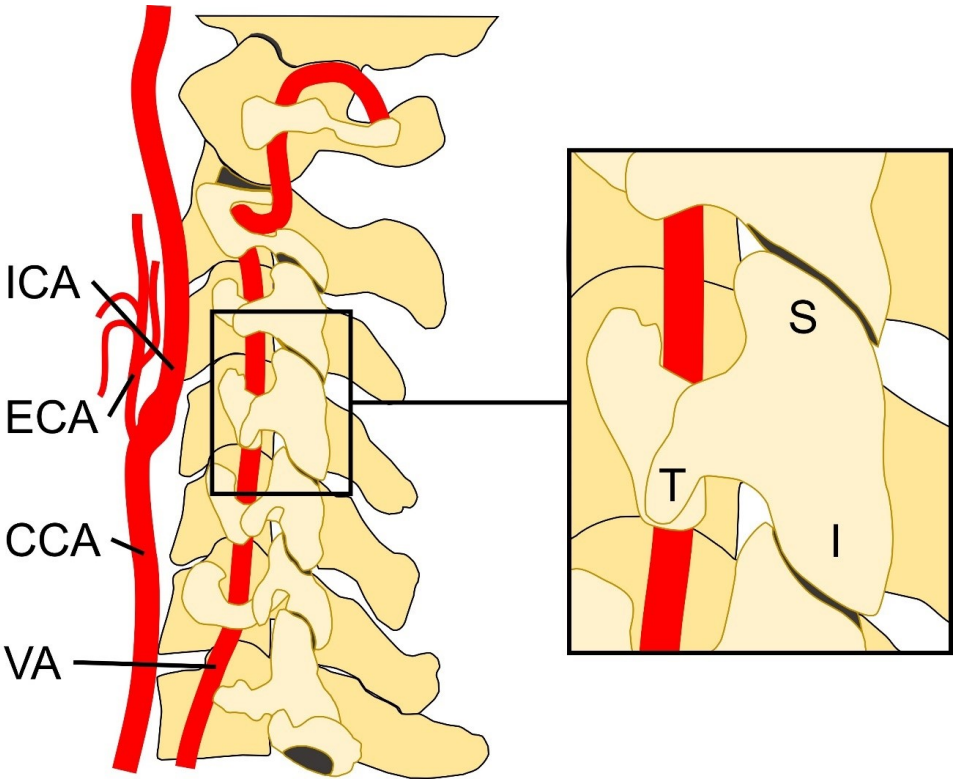


**Figure 3** Cervical spine viewed from the left showing the facet joints and cervical arteries. Superior articular process (S) and inferior articular process (I) as well as transverse process (T) of the C4 are shown in the enlarged area on the right. The vertebral artery (VA) penetrates through the transverse processes from C6 to C1. The common carotid artery (CCA), internal carotid artery (ICA), and the external carotid artery (ECA) are located anteriorly to the cervical spine.

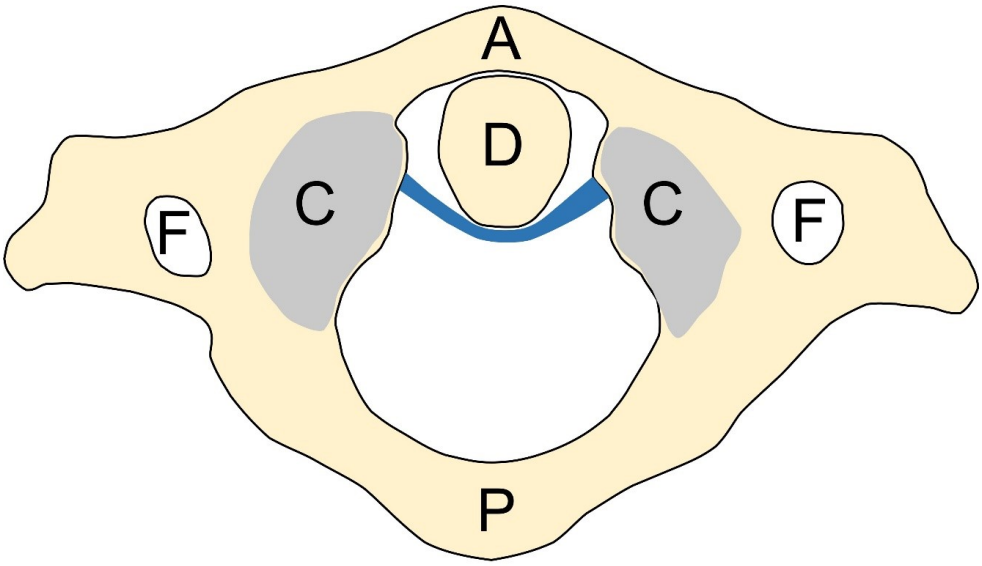


**Figure 4** Superior view of C1 known as the atlas. Anterior (A) and posterior arches (P) hold together lateral masses which have depressions in their superior articular processes for occipital condyles. Transverse processes extending bilaterally from the lateral masses have vertebral foramens (F) forming passages for vertebral arteries. Transverse ligament (blue) of the cruciate ligament blocks the posterior movement of the odontoid process (D) of the second cervical vertebra from moving posteriorly into the spinal canal. The median atlantoaxial joint is formed of the posterior surface of the anterior arch and the anterior surface of the odontoid process.

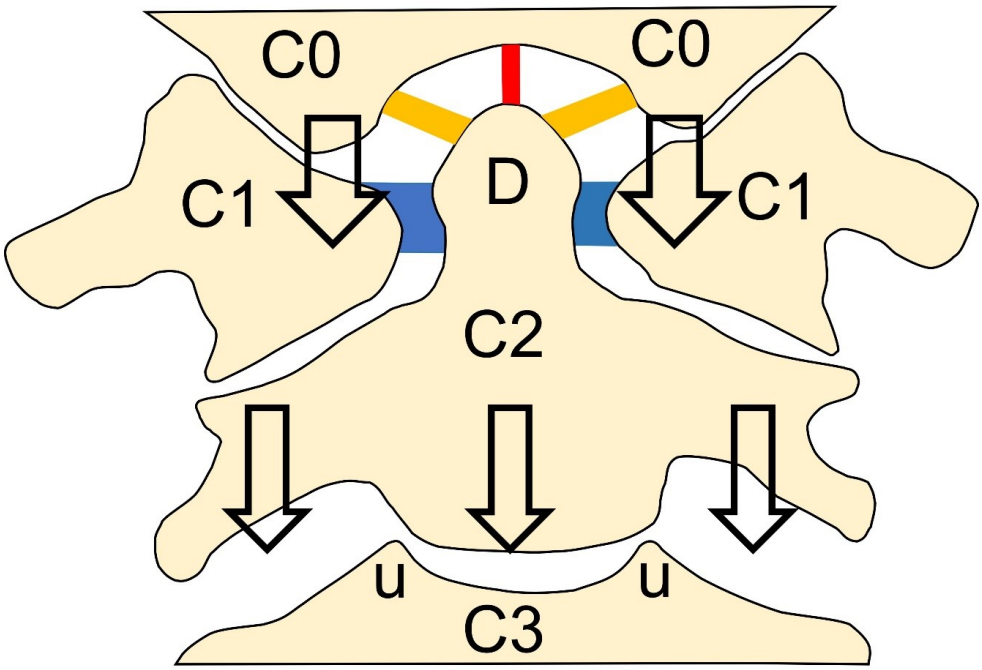


**Figure 5** Anterior view of the craniocervical junction with the anterior arch of C1 removed. Occipital condyles (C0) lie on the superior articular processes of C1, forming the atlanto-occipital joints from which the weight of the cranium (arrows) is transmitted to the rest of the cervical spine. The transverse ligament (blue) is connected between medial aspects of lateral masses of C1 from behind the odontoid process (D) of C2. Bilateral alar ligaments (orange) connect from the tip of the odontoid process to medial surfaces of occipital condyles. The apical ligament (red) connects between the tip of the odontoid process to the anterior aspect of the foramen magnum known as the clivus. C3 is the first typical cervical vertebrae of which uncinate processes (u) appear at the lateral margins of its upper endplate.

### 2.1.2 Intervertebral discs

IVDs, along with the spinal ligaments, connect the vertebral bodies into a flexible column, which, together with the aforementioned curvatures, creates flexibility suited for absorbing forces within physiological limits (including walking, running, and jumping), which even extends to minor trauma (Dalley & Agur 2023). IVDs connect all vertebrae between C2 and S1. At birth, half of the intervertebral space is filled with cartilaginous endplates, which is at that particular stage of development supplied by abundant vasculature. Within the first decade of life, the vasculature diminishes, and the intervertebral space is replaced by extracellular matrix, especially in the middle of the IVD, which contains mainly two cell types producing type-I and type-II collagen (Roberts et al. 2006). Roundish nucleus pulposus cells, resembling chondrocytes usually produce type-II collagen in the gelatinous parts of the IVD (Chelberg et al. 1995, Roberts et al. 2006, Dalley & Agur 2023).

The mature disk consists of a collagen-rich peripheral ring called the annulus fibrosus (Fig. 6) (Dalley & Agur 2023). The annulus fibrosus consists of approximately 15 to 25 layers of parallel oriented thin and fibrotic lamellae (Marchand & Ahmed 1990). Cells within these lamellae are akin to elongated fibroblasts and produce type-I and type-II collagen (Roberts et al. 2006). Each lamella has fibrotic strands running at an approximately 30° angle to the horizontal and an adjacent layer having strands running in the opposite direction of an at least 60° angle, providing resistance to torque between the vertebrae (Dalley & Agur 2023). Annulus fibrosus cells produce mainly type-I and type-II collagens, and a small amount of elastin, only 2% the dry weight of the annulus, is evident between the lamellae (Chelberg et al. 1995, Yu et al. 2005). With aging, the structure of the lamellae becomes more complex, as interdigitations and thickness increase (Marchand & Ahmed 1990).

Around the age of 2.5 years, the vascularity of the endplates is significantly reduced, and in adults only a few blood vessels remain at the periphery of the annulus, making the IVD the body's largest avascular tissue (Edelson & Nathan 1988, Roberts et al. 2006). Cervical IVDs deviate slightly from this pattern by changing from a gelatinous nucleus pulposus in children and young adults to a uniformly fibrocartilaginous disc in adults (Oda et al. 1988, Mercer & Bogduk 1999). This change takes place around the age of 30 (Oda et al. 1988). The annulus fibrosus of a cervical IVD is thinner at the posterior margin and extends bilaterally into the posterior edges of the uncinate processes (Bogduk 2016). At the posterior margin of the uncinate processes (Fig. 5) from C3 to C6 or C7, a small area of disc cartilage is covered by a connective tissue capsule connected to the posterolateral margin of the IVD. The resulting space is filled with extracellular fluid. The whole structure is

considered to be a synovial joint or be degenerative spaces associated with normal aging, also known as uncovertebral joints (Dalley & Agur 2023).

IVDs, due to their particular structure, adapt to changes in axial load and in vertebral alignment. An increase in axial load flattens the IVD by placing pressure on the nucleus pulposus, which, due to the incompressibility of fluids, causes outward bulging of the annulus fibrosus. Extension extends the distance between the endplates anteriorly and stretches the annulus fibrosus, and simultaneously the distance between the endplates posteriorly decreases, bulging the IVD outward (Dalley & Agur 2023). Unphysiological bulging or extrusion of the nucleus pulposus, especially into the spinal canal or neural foramina, can cause pain, nerve dysfunction, or even nerve palsy through nerve impingement. In a protrusion, the annulus fibrosus remains intact or thinned; in extrusions, the lamellae of the annulus fibrosus become torn, with parts of the nucleus pulposus (being) pushed through the resulting defect; in sequestrations, the herniated nucleus becomes separated from its IVD or origin (Roberts et al. 2006).

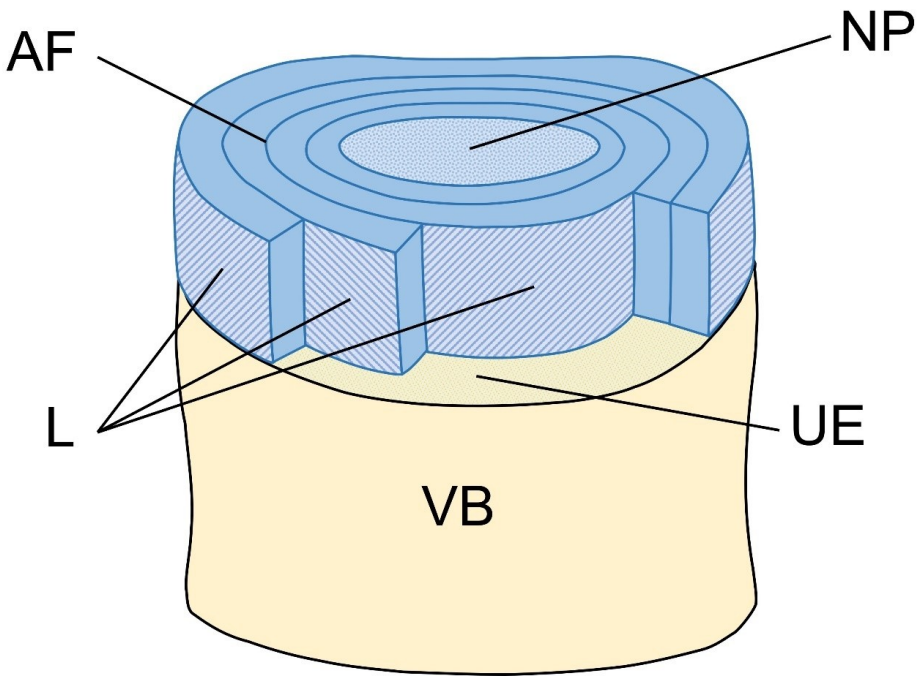


**Figure 6** Anterior view of an intervertebral disc on top of a lumbar vertebral body (VB). The anterior part of the annulus fibrosus (AF) is partly removed. The annulus fibrosus consists of multiple concentric circular lamellae (L) containing the central nucleus pulposus (NP). The upper endplate (UE) is partly exposed.

### 2.1.3 Spinal ligaments

The anterior longitudinal ligament (ALL) is broad and strong, extending superiorly from the skull base and the anterior atlanto-occipital membrane to the anterior arch of C1, continuing over the whole length of the spine to the anterior sacrococcygeal ligament. It connects to both the anterior periosteum of the vertebral bodies and to the IVDs. ALL is the only spinal ligament preventing hyperextension of the spine (Fig. 7) (Dalley & Agur 2023). In the cervical spine, it keeps the vertebrae firmly in the midline during axial rotation, whereas the superior and inferior articular processes of facet joints can slide transversely against each other (Bogduk 2016).

The posterior longitudinal ligament (PLL) is markedly narrower than the ALL and runs along the posterior aspect of the spinal canal's vertebral bodies from C2 to the S1 (Fig. 7). The PLL fuses at the level of C2 with the tectorial membrane and extends over the odontoid process and transverse ligament attaching to the posterior surface of the clivus, a portion of the occipital bone forming the anterior edge of the foramen magnum (Dalley & Agur 2023).

The PLL attaches both to the IVDs and to the vertebral bodies and provides some resistance to hyperflexion as well as to bulging or herniation of the IVDs, which therefore tends to occur posterolaterally. The PLL's loose contact with the posterior wall of the vertebrae allows for venous plexuses and a small amount of fat between the ligament and the bone (Dalley & Agur 2023)

The highly flexible ligamenta flava connect the anterior surface of the laminae of the vertebral arches, limit the amount of movement between the posterior arches of adjacent vertebrae, and facilitate return to a neutral position (Fig. 7). The ligaments appear macroscopically as paired structures connecting adjacent laminae, yet they are connected by a thin fibrous structure in the posterior midline. Ligamenta flava form the posterior wall of the spinal canal between the posterior arches and tend to increase in thickness the lower they are situated in the spine. (Dalley & Agur 2023)

Thin interspinous ligaments, oriented in the sagittal plane, attach to the inferior and superior surface of spinous processes at the midline (Fig. 7). The supraspinous ligament attaches to the tips of the spinous processes from C7 continuing to S1 (Fig. 7). (Dalley & Agur 2023)

Ligamenta flava, interspinous, and supraspinous ligaments resist hyperflexion of the spine. The interspinous and supraspinous ligaments continue cranially from C7 as the nuchal ligament, which attaches to the external occipital protuberance and posterior margin of the foramen magnum (Dalley & Agur 2023). The nuchal ligament is composed of a main ligamentous structure running in the posterior midline and an unusual component of thin strains of muscle fibers originating from the posterior processes of the cervical spine (Bogduk 2016).

The broad transverse ligament running posterior to the odontoid process of C2 is part of the cruciate ligament. The superior longitudinal and inferior

longitudinal band are thinner and together form the cruciate ligament, reflecting its cross-like appearance. The vertically oriented superior longitudinal band attaches to the inferior edge of the clivus. The apical ligament is a thin vertically oriented band in the midline, in front of the superior longitudinal band, and attaches to the tip of the odontoid process and to the inferior border of the clivus (Fig. 5). The inferior longitudinal band is also vertically oriented and continues beneath the transverse ligament, attaching to the posterior aspect of C2. (Dalley & Agur 2023)

The alar ligaments bilaterally connect the occipital condyles to the apicolateral parts of the odontoid process and function as a primary support structure of the atlanto-occipital joints by limiting rotation (Fig. 5) (Bogduk 2016). A tear in one or both alar ligaments therefore lead to atlanto-occipital rotatory instability (Dvorak et al. 1987).

The anterior atlanto-occipital membrane running from the anterior arch of C1 to the anterior border of the clivus, and the posterior atlanto-occipital membrane running from the posterior arch of C1 to the posterior margin of the foramen magnum (both) support the atlanto-occipital joints. The anterior atlanto-axial membrane running from the anterior arch of C1 to the anterior body of C2, and the corresponding posterior membrane running from the posterior arch of C1 to the posterior arch of C2 (both) offer some additional support. (Dalley & Agur 2023)

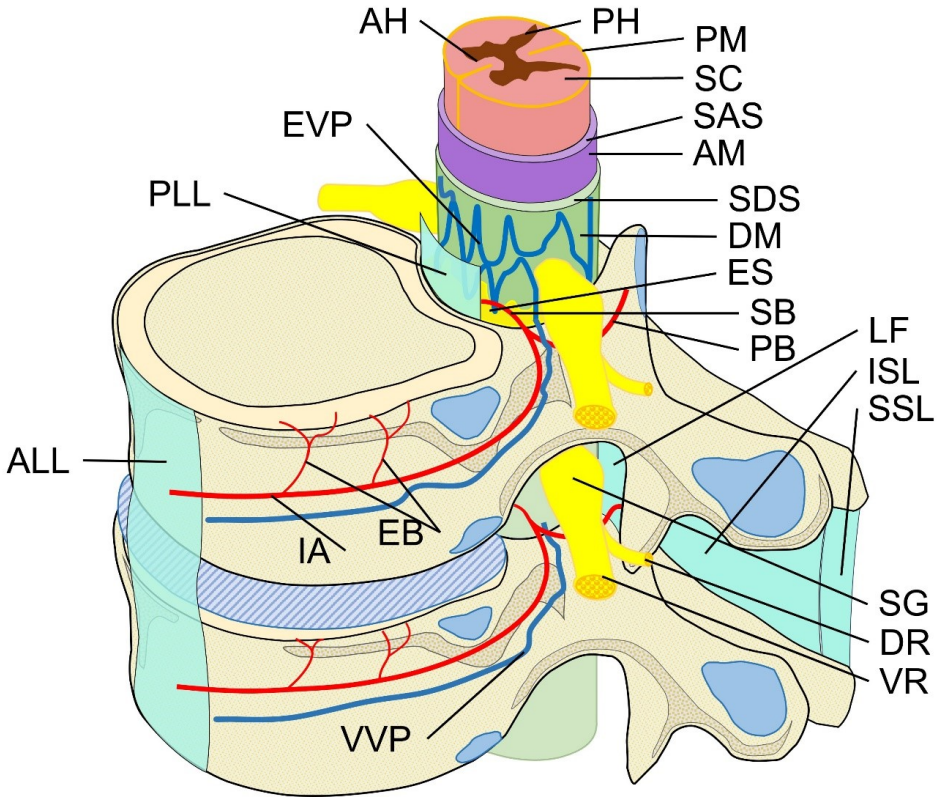


**Figure 7** Anterolateral view of two thoracic vertebrae with ribs removed. Anterior longitudinal (ALL), posterior longitudinal (PLL), interspinous (ISL), supraspinous ligament (SSL), and ligamentum flavum (LF) are in light turquoise. Equatorial branches (EB), spinal branch (SB), and posterior branch (PB) of the posterior intercostal artery (IA) are in red. The epidural venous plexus (EVP) exiting the neural foramina and forming the larger vertebral venous plexuses (VVP) are in blue. Anterior (AH) and posterior gray horns (PH) are shown in brown within the dark-red white matter of the spinal cord (SC). The orange pia mater (PM) covers the SC. The subarachnoid space (SAS) is located beneath the (purple) arachnoid mater (AM). The subdural space is a potential space between the dura mater (DM) and AM, and is enlarged in the image. The spinal nerves form the spinal ganglia (SG) in the neural foramina and separate again into a ventral (VR) and dorsal ramus (DR).

### 2.1.4 Contents of the spinal canal

The spinal canal is bounded anteriorly by the posterior walls of the vertebrae and IVDs, posteriorly by the posterior arches and the ligamenta flava, and bilaterally by the pedicles and neural foramina. (Dalley & Agur 2023)

In the cervical spine, branches of the vertebral arteries and posteroinferior cerebellar artery form three longitudinal arteries running along the spinal cord, the anterior spinal artery, and two posterior spinal arteries. In the thoracic and lumbar spine, spinal branches (Fig. 7) entering the spinal canal via the neural foramina provide the circulation for the spinal cord. The anterior and posterior segmental medullary arteries derived from spinal branches form the three longitudinal arteries in the thoracic and lumbar spine. Segmental medullary arteries also have medullary branches that supply the spinal cord, with the radial arteries deriving also from spinal branches. (Dalley & Agur 2023)

The artery of Adamkiewicz, (also known as the great radicular artery of Adamkiewicz or the great anterior segmental medullary artery) supplies two-thirds of the spinal cord from the level of Th8 to the conus medullaris (Taterra et al. 2019, Dalley & Agur 2023). It is present in 84.6% of the general population, and its origin varies greatly, from the intercostal arteries at the level of Th3 to the lumbar arteries at the level of L4, with the majority having a lumbar origin (Taterra et al. 2019). Just under 77% originate from the left side, 89% between the Th8 and L1, and for those with an artery of Adamkiewicz present, 11.3% had two arteries, of which 26.7% were bilateral (Taterra et al. 2019). A major proportion of spinal ischemias are related to an injury or other impairment of this singular artery responsible for supplying circulation for a large area of the spinal cord (Dalley & Agur 2023).

Promoting understanding of the anatomy of the artery of Adamkiewicz by MRI, CTA, or DSA (DSA being the gold standard) may help to prevent postoperative ischemic injuries to the spinal cord in patients having surgery or radiological procedures affecting the thoracoabdominal aorta, and may help to prevent postoperative ischemic injuries to the spinal cord (Taterra et al. 2019, Takagi et al. 2015).

The veins of the spinal cord accompany the spinal arteries, forming epidural venous plexuses in the epidural space and draining to the vertebral venous plexuses exiting the spinal cord via the neural foramina (Fig. 7) (Dalley & Agur 2023).

The epidural space contains fat and these same venous plexuses between the periosteum of the surrounding bones and the outermost spinal membrane called the dura mater or spinal dura (Fig. 7). The epidural space occupies the spinal canal from the foramen magnum to the sacral hiatus at the lower end of the sacrum (Bagheri & Govsa 2017, Dalley & Agur 2023).

#### 2.1.4.1 Spinal meninges

The spinal meninges encase the spinal cord and spinal nerve roots and contain the cerebrospinal fluid (CSF) while providing protection and structural support (Fig. 7). Surrounded by the epidural space, the spinal dura mater is the outermost spinal meninx, consisting mainly of fibrous tissue with some elastic fibers forming the dural sac. The dura mater ends cranially at the foramen magnum and caudally merges with the filum terminale, which is anchored to the coccyx by the coccygeal ligament (Vandenabeele et al. 1996, Dalley & Agur 2023). Unlike the intracranial portion, the spinal dura mater is not made up of nerve structures, and acts primarily as a protective barrier (Vandenabeele et al. 1996), but small recurrent meningeal nerves originating distal to the ganglia end on the meningeal surface (Dalley & Agur 2023). In the neural foramina, the dura mater ends as tapering sleeve-like elongations blending with the epineurium distally to the spinal ganglia (Dalley & Agur 2023).

The spinal arachnoid mater is an avascular membrane containing the CSF, the spinal cord, spinal nerve roots, and spinal ganglia in the neural foramina. The arachnoid mater consists of fibrous and elastic tissue and is in contact with the innermost layer of the dura mater. It has thin elongations called the arachnoid trabeculae on its inner surface which resemble the strands of a spider web and are in contact with the pia mater (Dalley & Agur 2023). The spinal subdural space does not exist as a natural cavity between the dura and arachnoid mater. Thin and elongated neurothelial cells with numerous interconnecting digitations form 4 to 8 parallel layers between the meninges (Reina et al. 2002). Bleeding or movement of other fluids caused by trauma or needle puncture can damage the neurothelial cells and separate the adjacent meninges, thereby creating a potential spinal subdural space (Smith et al. 1984, Reina et al. 2002).

The soft, fibrous, thin, and transparent pia mater covers the whole of the spinal cord, the spinal nerve roots, and the spinal blood vessels as the deepest of the spinal meninges (Fig. 7). Fibrous denticulate ligaments numbering 20 to 22 extend from the surface of the pia mater and attach to the inner surface of the dura mater. Each denticulate ligament originates from the lateral surfaces of the spinal cord between the posterior and anterior nerve roots. CSF flows in the subarachnoid space between the arachnoid and pia mater. (Dalley & Agur 2023)

#### 2.1.4.2 Spinal cord and the nerve roots

The cylindrical spinal cord serves as the neural pathway between the brain and the body, starting as a continuation from the brain stem, and ending as conus medullaris between Th12 and L3. On each spinal level, two anterior and two posterior nerve roots exit on each side of the spinal cord. The level and the portion of the spinal cord from which bilateral rootlets form the nerve roots is defined as a

spinal cord segment. The spinal cord has 31 segments with their spinal nerves. (Dalley & Agur 2023)

The cross-section of the spinal cord shows its gray matter in a letter H configuration with two prominent anterior and two smaller posterior gray horns (Fig. 7). In the middle and lateral aspects, there exist prominences on each side called lateral horns. Efferent motor-neuron fibers originating from the anterior and lateral horns form the anterior root, while afferent sensory fibers form the posterior root. Anterior and posterior roots join together into a spinal nerve ganglion consisting of mixed afferent and efferent nerves inside the neural foramen, in which the anterior and posterior branches of the spinal nerves originate. The thicker anterior branch supplies the anterior and lateral parts of the trunk as well as the upper and lower extremities. The posterior branch supplies the vertebral column in addition to the muscles and skin of the back. (Dalley & Agur 2023)

Spinal nerves are named according to the vertebra of the same segment: such as L3 for the nerves of the third lumbar segment (Dalley & Agur 2023). In clinical practice, the distinction between nerves and vertebrae is made by referring to the nerve with Roman numerals. In the cervical spine are eight spinal nerves, but only seven vertebrae. The first spinal nerves exit above the lateral masses of C1, and the eighth spinal nerves exit the neural foramina between C7 and Th1 (i.e. below the pedicles of C7). Starting from Th1, all spinal nerves exit the spinal canal through the neural foramens below the pedicles of their same segment (Dalley & Agur 2023)

## 2.2 Cerebrovascular anatomy

The internal carotid arteries (ICA) and the vertebral arteries (VA) supply the entire brain circulation (Fig. 3). The right common carotid (CCA) artery originates from the bifurcation of the brachiocephalic trunk, and the left from the arch of the aorta. Both arteries travel cranially to the upper margin of the thyroid cartilage where they divide into the ICA and external carotid artery. Anterior to the longus capitis muscles, the cervical portions of the ICAs ascend to the base of the skull, where they enter the carotid canal within the petrous part of the temporal bone, followed by the cavernous and the cerebral part, the latter of which is the origin of the ophthalmic artery. The widened part of the ICA immediately distal to the bifurcation is called the carotid bulb. (Dalley & Agur 2023)

VAs originate from the subclavian arteries and travel vertically through the transverse foramina of C6 to C1 (Fig. 3). In a study of 200 patients, an anatomical variant in which the left vertebral artery ascends directly from the aortic arch showed a prevalence of 6% (Yaprak et al. 2021). After exiting the C1 transverse foramina cranially, VAs turn laterally and posteriorly while circling around the lateral masses of C1, after which they penetrate the atlanto-occipital membrane, the

dura mater, and the arachnoid mater, entering the subarachnoid space at the level of the foramen magnum (Dalley & Agur 2023). The VAs have four segments: The V1 segment ranges from the origin to the cervical vertebra where VAs enter the most inferior transverse foramen, the V2 segment runs through the transverse foramina, the V3 segment ranges from the exit of the C1 transverse foramina to the penetration of the subarachnoid mater, and the V4 segment from the dura mater to the confluence and formation of the basilar artery at the anterior aspect of the pons (Yaprak et al.)

### 2.2.1 Radiological differential diagnostics of the carotid arteries

An increase in vascular imaging of the cervical arteries has revealed a large spectrum of variations as well as secondary findings related to diseases and individual anatomy which may complicate the treatment of patients in need of endovascular thrombectomy, which is currently a major accepted treatment for acute ischemic stroke. (Benson et al. 2020, Culleton et al. 2021, Nageler et al. 2023).

Atherosclerosis is a common disease, causing thickening of the arterial walls and luminal narrowing and may cause stenosis of the ICA predominantly at the bulb level. Atherosclerotic stenosis in the carotid bulb develops turbulent flow acting as a source of thromboembolisms and a major cause of strokes. CTA is a common method in the investigations of cerebral ischemia (Culleton et al. 2021). The accepted level for measuring degree of stenosis, according to North American Symptomatic Carotid Endarterectomy Trial criteria, is at the bulb of the ICA (Barnett et al. 1991).

Arterial wall plaque ulceration following a plaque rupture offers an increased risk for stroke. An intraluminally developing thrombus, which is associated with ipsilateral acute stroke, appears as an intraluminal filling defect on angiographic images. An intraplaque hemorrhage is a sign of a vulnerable plaque, which is usually not visible on basic angiographic images, but does appear on MRI with T1-weighted images (Culleton et al. 2021).

The tortuosity of the ICA had first been documented in the early 20$^{th}$ century, presenting as loops, kinks, or coils, which are considered developmental variations and increase with age (Cairney 1924, Benson et al. 2020, Mokin et al. 2021).

A carotid web appears as a sharply demarcated shelf-like intraluminal thickening at the posterior or lateral wall of the ICA bulb (Culleton et al. 2021). This anatomical variant is also seen in younger patients without atherosclerosis, where the posterior or lateral wall of the ICA is narrowed slightly on angiographic images. Reconstructed images in the sagittal plane usually show the structure of a carotid web more sharply and verify the diagnosis. A carotid web predisposes patients to risk for stroke and for recurrent strokes (Guglielmi et al. 2021).

Vasculitides such as giant cell arteritis or Takayasu's arteritis can affect the cervical arteries. Inflammation causes thickening and contrast enhancement of the arterial wall on both CTA and MRI. Intraluminal changes up to stenosis and occlusion may occur in advanced disease (Culleton et al. 2021).

Fibromuscular dysplasia causes abnormal cellular proliferation in the musculature of arterial walls, causing a tortuous and beaded, string-like appearance of these arteries on CTA, MRI, or DSA. Fibromuscular dysplasia is a non-inflammatory, non-atherosclerotic, and idiopathic disease which can be either focal or multifocal. It can occur in any artery, but especially its multifocal type occurs predominantly in the renal and carotid arteries. (Gornik et al. 2019)

### 2.2.2 Radiological differential diagnostics of the vertebral arteries

The VAs differ from the ICAs by being tightly enclosed by the transverse foramina of the transverse processes of the cervical vertebrae C1-C6, but also by having collateral arteries. In a study demonstrating collateral arteries in patients with blunt cerebrovascular artery injuries, of 46 (patients) with vertebral artery injuries 19 had collateral arteries from the ascending muscular or thyrocervical trunk arteries (Fink et al. 2011).

A vertebral fenestration is an uncommon anatomical variant in which a short segment of the VA appears with a split lumen, which, according to modern understanding, represents a congenital disorder with a prevalence of 0.1% to 0.2 % and occurs most commonly in the V4 segment (Kim 2016, D'Sa et al. 2020). Accurate differentiation of fenestration from injury is paramount, since the latter may cause strokes and permanent neurological impairment, whereas the former is considered harmless (D'Sa et al. 2020).

## 2.3 Spinal ankylosis

Spinal ankylosis is defined as the mechanical fusion of the vertebral column that limits movement of the affected vertebrae. Ankylosis can develop from inflammatory diseases such as AS in mostly younger patients as well as from other SpAs, from DISH or DS found predominantly in older patients, or even from the surgical fusion to treat acquired instability (Figs. 8–11). Spinal ankylosis fundamentally changes the mechanical properties of the affected segment and predisposes patients to unstable spinal fractures with a high degree of complications; this can result even from minimal trauma such as a fall from standing height. Therefore, in the presence of suspected spinal ankylosis, patients even with low-energy trauma should undergo a thorough clinical examination

based on awareness of the risks related to spinal ankylosis and also have careful scrutiny of (their) imaged examinations. (Shah et al. 2019)

### 2.3.1 Ankylosing spondylitis and other seronegative spondyloarthropathies

Chronic inflammation in the axial skeleton affects mainly the entheses and is mainly caused by AS, psoriatic arthritis, arthritis associated with inflammatory bowel disease, or reactive arthritis, and is commonly referred to as axial spondyloarthritis or SpA (Sieper et al. 2017, Shah et al. 2019). AS is the most common type of SpA, occurring usually in men under the age of 30 with a male-to-female ratio of 2-3:1, and a prevalence of 0.5% in European populations. Genetic association with HLA-B27 tissue antigen, and pathogenesis related to inflammation-mediated pathways with the tumor necrosis factor α, (and with) interleukins 17 and 23, are well established, though the exact mechanisms remain largely unclear. Early clinical symptoms of axial SpA include ache and morning stiffness in the lumbar region. Inflammation in axial SpA in the cartilaginous part of the sacroiliac (SI) joints at the interface of cartilage and bone visible on MRI usually starts as developing bone marrow edema, which in later stages progresses to structural changes such as proliferative bone growth and damaged cartilage. Without medical treatment, these changes usually progress until the SI joints are completely fused i.e. ankylosis. (Sieper et al. 2017)

The term “non-radiographic SpA” relates to the modified New York classification criteria, which historically did not recognize SpA patients without radiographic signs of sacroiliitis (van der Linden et al. 1984, Sieper et al. 2017). This set of criteria is outdated, because radiographical images were then able only to show late-stage changes related to chronic disease, whereas MRI is capable of demonstrating the inflammatory changes even at a very early stage. This situation led to an updated classification of axial SpA (Rudwaleit et al. 2009).

Diagnosis of axial SpA is a clinical diagnosis. Although the radiological diagnosis is based on active inflammation found in the SI joints, the disease causes chronic inflammation in the rest of the spine as well (Sieper et al. 2017). Active inflammation can occur from the craniocervical junction (CCJ) to all vertebral endplates, as well as to facet, costotransversal, and costovertebral joints and spinal ligaments, and such inflammation leads to ankylosis of the spine through usually narrow syndesmophytes. This further leads to a rigid spine incapable of dispersing the energy from even minor trauma (Fig. 8) (Leone at al. 2016). The thoracic spine usually develops a pronounced kyphosis, and the overall bone structure becomes osteoporotic due to chronic inflammation and reduced mobility, which further promotes the risk for fractures in low-energy trauma (Bessant et al. 2002, Shah et al. 2019).

### 2.3.2 Diffuse idiopathic skeletal hyperostosis (DISH)

DISH is a systemic disorder causing excess bone growth mainly in the thoracic and cervical spine (Resnick et al. 1976, F at al. 2009a). Its etiology and pathological mechanisms remain unclear, but it shows a well-established association with aging, overweight, type 2 diabetes, atherosclerosis, and male sex (Weinfeld et al. 1997, Westerveld et al. 2008, Kuperus et al. 2020).

Radiographic criteria for spinal DISH were introduced as wavy osteophytes from the anterolateral margin of endplates in a consecutive column of at least four adjacent vertebrae without radiographic findings from degenerative changes or SpA (Resnick et al. 1976). In the thoracic spine, the anterolateral aspect of DISH osteophytes is contralateral to the aorta (Sebro 2018). Although the IVD should maintain its height, the original criteria were noticed to overlap with changes from degeneration and even from SpA, during the era when imaging resolution was improving, with CT scans becoming more readily available (Kuperus et al. 2018, Slonimsky et al. 2018).

In a study of 172 patients with either AS or DISH, differentiation between those two entities was unavailing in 12 (Teunissen et al. 2017). The original criteria were also challenged by a recent study which shows that the anatomical distribution of DISH osteophytes extends also to the lumbar spine (Misaki et al. 2022). The DISH osteophytes are most prevalent from Th4 to Th11 and have a higher density than the rest of the vertebral bone, which, invalidates the previous presumptions regarding DISH patients, such as their having a higher overall bone density (Westerveld et al. 2009a) or as having osteoporotic bone analogous to that of AS patients (Caron et al. 2010).

Bridging osteophytes along the anterolateral aspect of the vertebrae and along the ALL can cause ankylosis, which interferes with the normal biomechanical properties of the IVDs (Fig. 9). The rigid segment including the junctional areas are predisposed to injury from low-energy trauma (Shah et al. 2019). The posterior parts of the vertebrae and the IVDs usually remain unaffected, allowing for some residual flexibility and durability, thus aiding in absorption of physiological and even non-physiological impacts. Features of DISH often overlap with those of AS and of degenerative spondylosis (DS), making any radiological diagnosis challenging (Okada et al. 2017, Teunissen et al. 2017).

### 2.3.3 Degenerative spondylosis

DS is defined as osteoarthritis of the spine (Shah et al. 2019). Related to aging, DS affects the IVDs and the facet joints, causing narrowing of the intervertebral space and hypertrophic osteophyte formation (Sarzi-Puttini et al. 2005, Gellhorn et al. 2013). The literature on spinal ankylosis caused by DS is scarce. The mid and lower region of the cervical spine and the lower parts of the lumbar spine are generally

most affected (Shah et al. 2019). As the intervertebral space disappears, the edges of endplates fuse with prominent osteophyte formation (Shah et al. 2019). Facet joint degeneration and hypertrophy eventually causes ankylosis and also causes narrowing of the spinal canal, which predisposes patients to spinal stenosis and spinal cord or cauda equina impingement (Rustagi et al. 2017). The etiologies of spinal DS vary and are related to inflammation, metabolic conditions, and postural errors which are all related to aging (Rustagi et al. 2017).

### 2.3.4 Spinal fusion

The vertebral column may become mechanically unstable because of vertebral fractures from acute trauma, a fracture of the pars interarticularis due to constant strain (spondylolysis), or degeneration of the facet joints. Such structural changes may allow the vertebral body to move forward over the one above which is called spondylolisthesis when occurring with a spondylolysis. (Dalley et al. 2023)

Pathological instability and malalignment of the vertebral column narrows the spinal canal and the neural foramina, eventually causing compression of neural structures, chronic and radiating pain, paresthesia, or even paralysis. Symptomatic and pathological instability is an indication for surgical fusion of the affected vertebrae. Fusion surgery involves typically metal hardware for posterior, or for anterior fixation, involves interbody devices, and bone grafts (Shah et al. 2019).

Degenerative spondylosis and uncovertebral joint arthrosis in the cervical spine causing radiating pain and paresthesia is treated by anterior cervical decompression and fusion (ACDF). ACDF relieves radiating symptoms and fuses the treated intervertebral space which becomes filled with bone growth within 6 months for 75% and within 12 months for 90 % of patients (Noordhoek et al. 2019, Shah et al. 2019). Change in the biomechanics of the treated segment results in an increase in degenerative changes emerging at the adjacent IVD space of the superior or inferior end (Matsunaga et al. 1999).

Due to surgical fusion, whether ACDF or posterior fixation, the affected vertebrae lose their normal ability to absorb shock and move naturally. The surgically fused spine should be considered vulnerable to unstable injury from low-energy trauma as is an ankylosed spine with others of these etiologies (Fig. 11) (Shah et al. 2019).

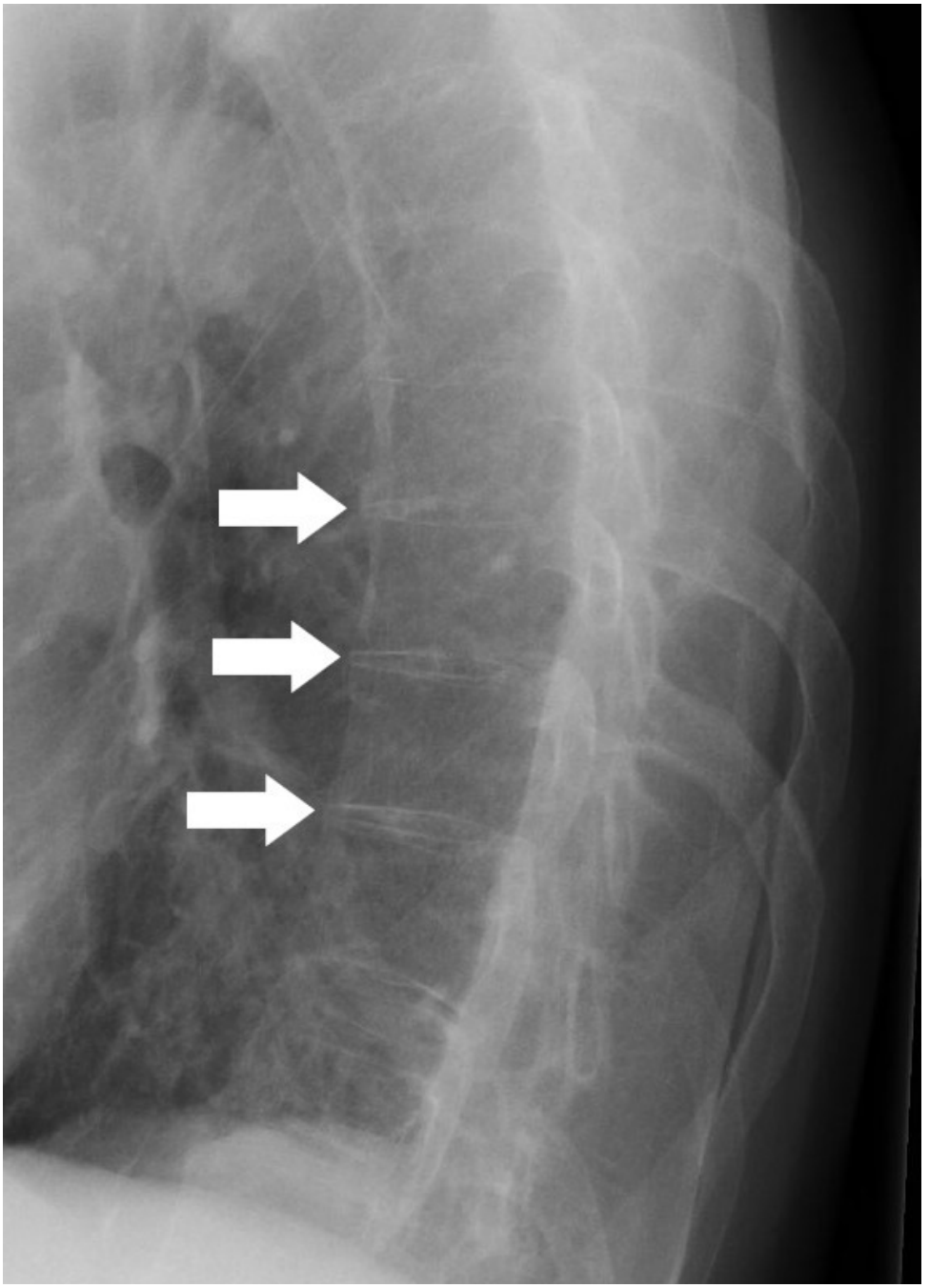

**Figure 8** Chest radiograph of a 68-year-old man with ankylosing spondylitis. Arrows indicate the narrow syndesmophytes caused by chronic inflammation.

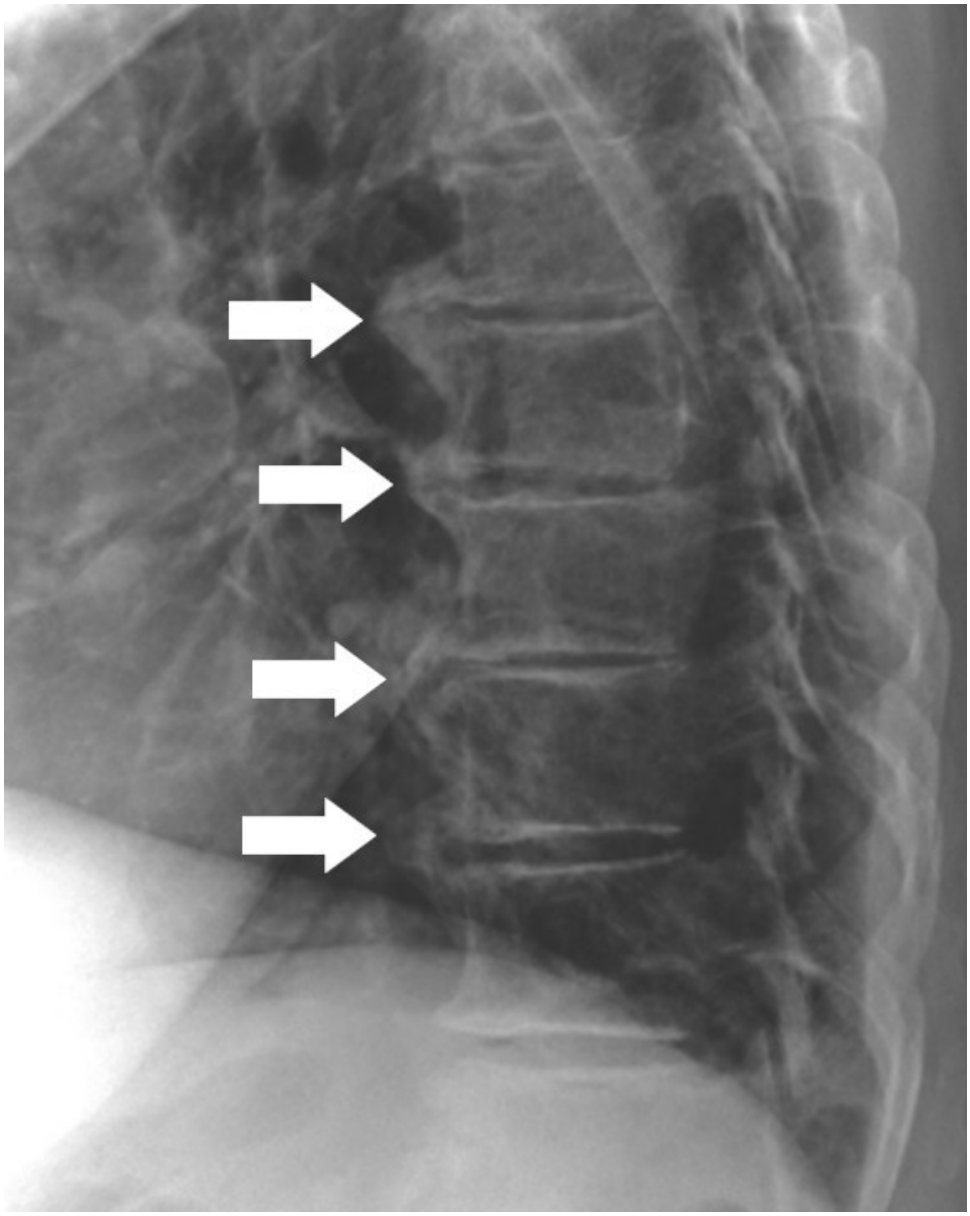

**Figure 9** Radiograph of an 80-year-old woman. Arrows indicate prominent bridging osteophytes from DISH at the mid-region of the thoracic spine.

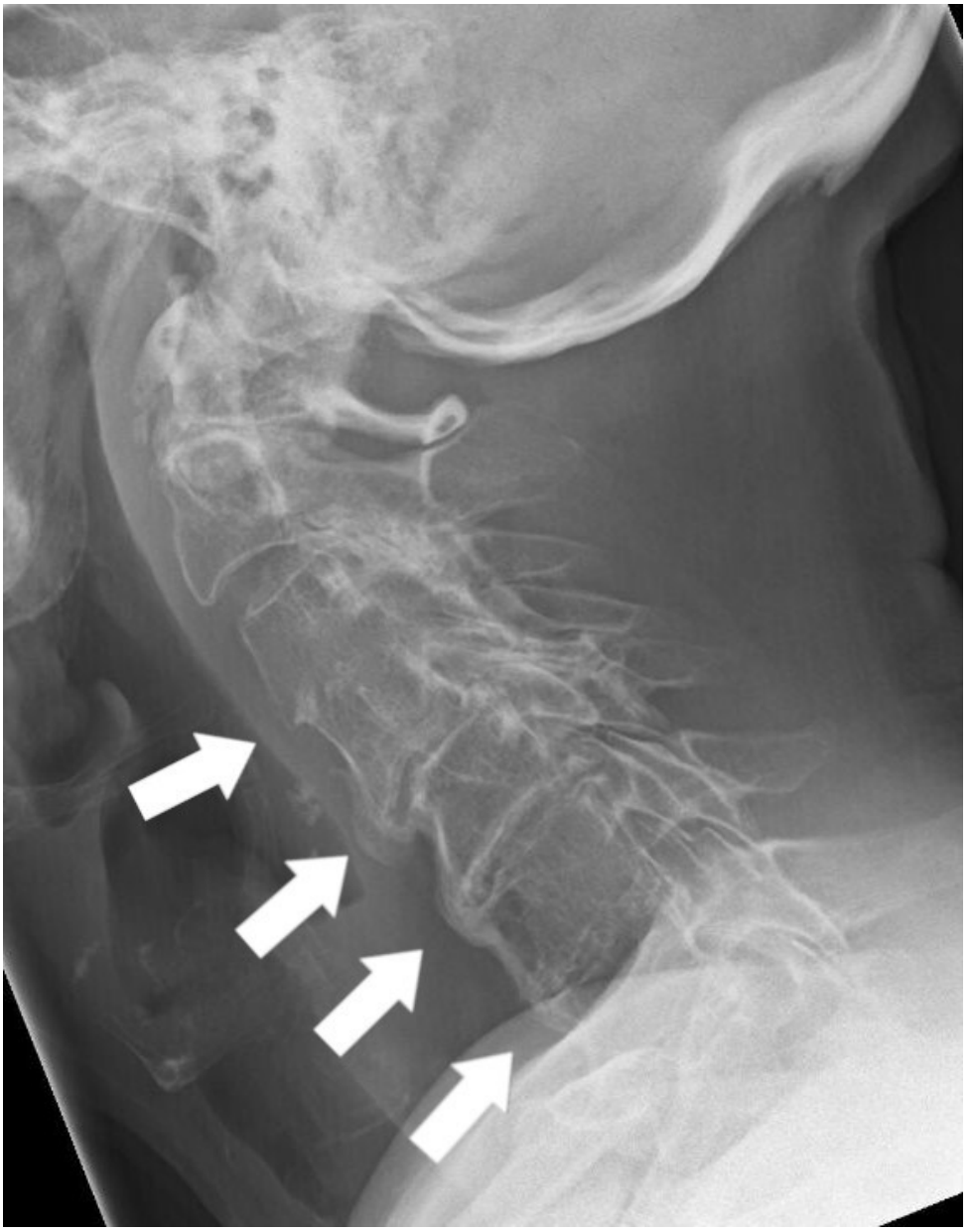

**Figure 10** Radiograph of an 86-year-old woman with degenerative changes in the intervertebral discs causing fusion of C3 through C7. Arrows indicate collapse of the intervertebral spaces and anteriorly protruding and bridging osteophytes.

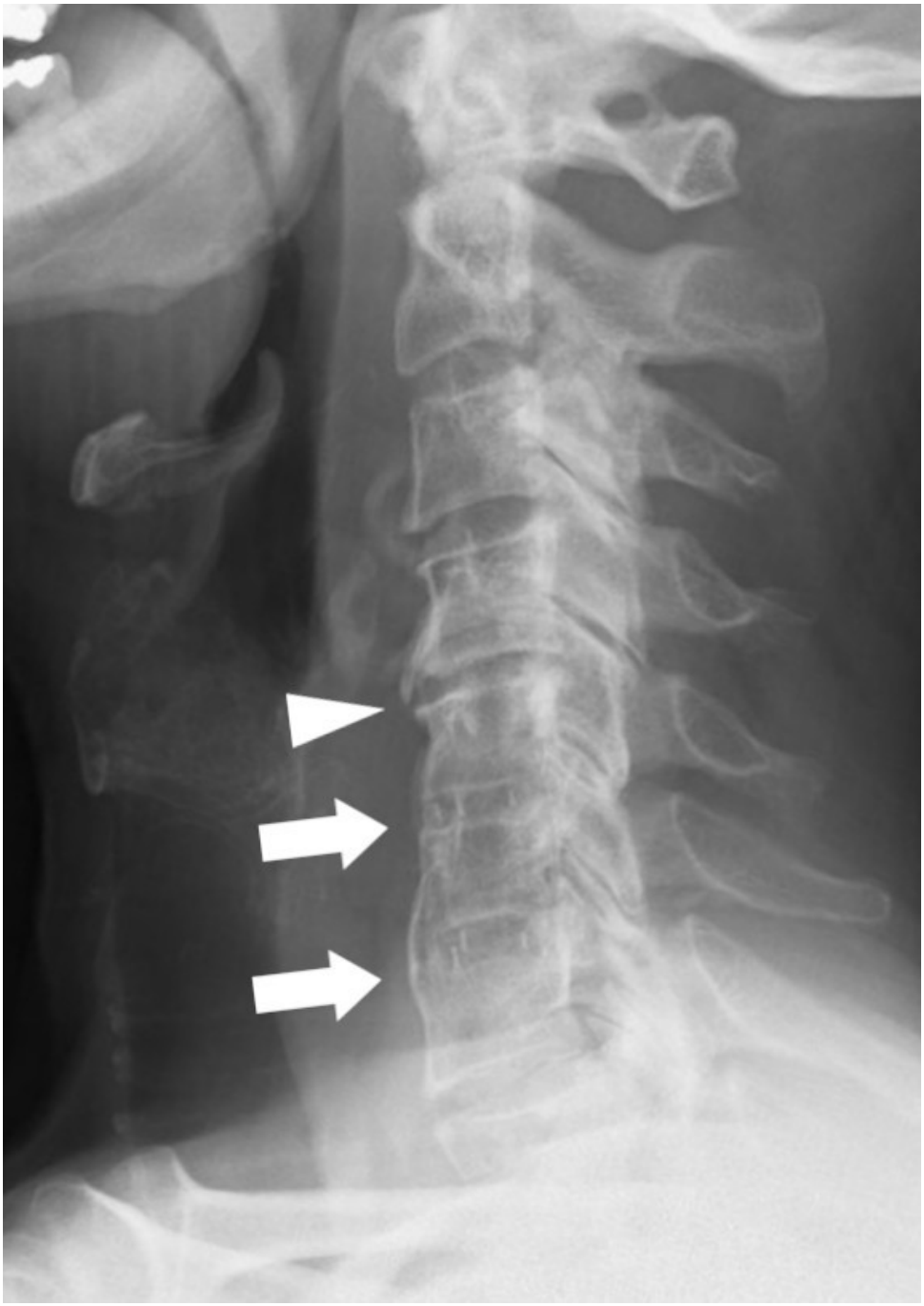

**Figure 11** Radiograph of a 67-year-old man with history of anterior cervical decompression and fusion (ACDF) indicated by arrows. This led to fusion from C5 through C7. The arrowhead indicates the adjacent disc space superiorly being reduced with increased sclerosis at the endplates, and formation of anteriorly protruding but not yet contiguous osteophytes.

## 2.4 Spinal trauma

Spinal trauma has the potential to cause severe impairment of quality of life through a restricted range of motion and especially injury to neurological structures. This may manifest as inability to accomplish everyday tasks or as deficits ranging from chronic pain to permanent lack of motor function. The burden of SCI on the public healthcare system in Ontario, Canada, was estimated at $336,000 per person net lifetime cost (Chan et al. 2019).

Mechanisms causing spinal trauma are associated with high-energy trauma, with the most common being MVA followed by bicycle accidents, falls from heights, and motor-vehicle collisions involving pedestrians (Oliver et al. 2012, Niemi-Nikkola et al. 2018, Smits et al. 2020). Younger patients are overrepresented in MVAs, while the elderly are more commonly affected by ground-level falls (Oliver et al. 2012, Niemi-Nikkola et al. 2018, Smits et al. 2020). In the cervical spine trauma of older patients, SCI results from ground-level falls more commonly than from other trauma mechanisms (Niemi-Nikkola et al. 2018). A study in the United States found that although the severity of injuries remained the same from the mid-90's to the late 2000's, the management and outcome of patients was improving, as the mortality of MVA- and non-MVA-injured patient groups was decreasing (Oliver et al. 2012). That study found that the incidence of SCI related to MVAs also decreased, which may possibly be explained by improved road-traffic safety, public health campaigns, automobile-safety legislation, and technology. A common finding in epidemiological studies is that in western countries, the average age of SCI patients increases as the population grows older (Oliver et al. 2012, Niemi-Nikkola et al. 2018, Smits et al. 2020). Other factors suspected of causing SCI in the elderly include osteoporosis, osteopenia, and degenerative changes.

### 2.4.1 Vertebral fracture classification

Classification of vertebral fractures facilitates treatment decisions between conservative and surgical alternatives, the latter of which are necessary if a fracture is prone to further malposition to and endangerment of neural structures.

A description of risk of further instability and progression of neurological deficits in thoracolumbar fractures and dislocations was suggested based on the appearance on imaging in a report by Nicoll (Nicoll 1949). Holdsworth described the posterior ligamentous complex and classified fractures into five main categories based on radiographic and clinical findings: wedge fractures caused by flexion, unstable fracture-dislocations caused by flexion-rotation, osseo-ligamentous injuries involving the IVD caused by extension, burst fractures caused by

compression, and forward displacement of the vertebral body by shearing forces (Holdsworth 1963).

In 1983, Denis suggested a three-column concept consisting of an anterior, middle, and posterior column (Fig. 12). The anterior column consists of the ALL and anterior two-thirds of the vertebral body. The middle column consists of the posterior third of the vertebral body, the annulus fibrosus of the IVD, and the PLL. The posterior column was described by Holdsworth as the posterior ligamentous complex and consists of all posterior osseous and ligamentous structures including the posterior arch and the spinous and transverse processes, as well as the facet joints. Denis' classification is applicable to the vertebral column from the cervical to the lumbar spine and remains a popular way to acquire a rough estimate of fracture stability (Denis 1983).

In 1994, Magerl et al. proposed a more detailed and systematic classification of thoracolumbar fractures including 64 fracture subtypes, which was of course more arduous to apply in clinical practice (Magerl et al. 1994, Blauth et al. 1999). Acknowledgement of these disadvantages led to the development of a more pragmatic system including morphology, the posterior ligamentous complex and neurological status in 2005 and 2007, which consists of the TLICS (Thoracolumbar Injury Classification and Severity System), and SLICS (Subaxial Cervical Spine Injury Classification and Severity System) classification systems, respectively (Vaccaro et al. 2005, Vaccaro et al. 2007). The most comprehensive spinal fracture classification to date is the Arbeitsgemeinschaft für Osteosynthesefragen (AO; Davos, Switzerland) Spine Trauma Classification system, which supplements the aforementioned principles with the additional criteria of morphological appearance on radiologic examinations, division of the vertebral column into four regions (upper cervical, subaxial cervical, thoracolumbar, and sacral spine), prioritization of the most severe injury, neurological status, and clinical modifiers such as poor quality of bone as well as vascular injury or abnormality (Vaccaro et al. 2013).

#### 2.4.1.1 Compression fracture

Compression injuries are classified as type A in the AOSpine Trauma Classification System. A common fracture seen in trauma related to falls from heights and at ground level is a type A1 or wedge-compression fracture, where the upper endplate is compressed in a wedge-like morphology with some possible comminution (Fig. 13). A compression fracture is a stable injury with little risk of progression which can safely be treated conservatively. (Divi et al. 2019)

#### 2.4.1.2 Burst fracture

Burst fracture is caused by axial compression similar to wedge compression fracture and is classified as a type A injury, where the trauma energy is higher than in the latter (Divi et al. 2019). Holdsworth described an injury mechanism for burst fracture in which the nucleus pulposus of the IVD, due to the incompressibility of fluids, penetrates through the vertebral endplate, causing a sudden increase in pressure, that the vertebral body is unable to withstand, causing explosive radial displacement of fracture fragments (Fig. 13) (Holdsworth 1963). The trauma mechanism causing this distinct morphology requires sudden deceleration forces in the craniocaudal direction such as in a fall from a height (Rosenthal et al. 2018). These fractures are classified by the AOSpine as A3 and A4 injuries that may involve, respectively, either comminution of the upper endplate or of the whole body up to the posterior wall (Divi et al. 2019). In the Denis classification, a burst fracture includes at least the anterior and middle columns, making it an unstable injury (Denis 1983). The fragments from the posterior wall often protrude into the spinal canal centrally (Rosenthal et al. 2018, Divi et al. 2019). In addition to neurological status, which may improve also with conservative management, and the involvement of the posterior column or posterior ligamentous complex, the alignment of the spine at the level of injury also affects the decision between conservative and surgical managements (Rosenthal et al. 2018, Divi et al. 2019).

#### 2.4.1.3 Transverse fractures

Transverse spinal fractures may involve any or all osseous or ligamentous structures and are mainly to be regarded as unstable. This includes trauma mechanisms causing extension and flexion associated with rotational forces (Fig. 13). The AOSpine classification of transverse thoracolumbar fractures includes type B and C injuries, in which the latter is associated with rotational forces and is prone to dislocations. Transosseous disruption caused by flexion-distraction forces such as in a two-point seat belt injury causes a fracture through the spinous process and the facet joints, as well as either or both articular process all the way through to the anterior border of the vertebral body, which is described as a classic Chance fracture (Chance 1948, Divi et al. 2019). A flexion-distraction injury may also consist of a combination of a torn posterior ligamentous complex. Transverse disco-ligamentous injury disrupts the posterior ligaments that are resisting hyperflexion as well as disrupting the IVD from either endplate and possibly also affects the ALL (Divi et al. 2019).

#### 2.4.1.4 Fractures of the ankylosed spine

The AOSpine classification takes into account a weakened bone structure secondary to osteoporosis by adding the clinical modifier M3 in AS patients (Divi et al. 2019, Shah et al. 2019). The loss of elasticity due to ankylosis in AS patients alters the biomechanics from a flexible spine consisting of multiple articulations to that of a singular bone resembling a tubular long bone also referred to as "bamboo spine." Any fracture occurring in SpA patients with ankylosis of the spine should therefore be considered a pathological fracture. The combination of rigidity, osteoporosis, and pronounced kyphosis of the thoracic spine exposes AS patients to a markedly elevated risk of unstable spine injuries even from low-energy trauma (Shah et al. 2019). When an AS patient with a fully ankylosed spine falls forward at ground level, which is probable because of the kyphosis-caused forward shift of the center of gravity, the head or face is likely to hit the ground, while the downward momentum persists in the torso, which causes hyperextension to the lower parts of the cervical spine or the upper or mid-parts of the thoracic spine. Conversely, when falling backwards, the apex of the thoracic kyphosis hits the ground, while the inertia of the upper parts of the upper body and especially the mass of the cranium, as well as the lower parts of the body continue their downward momentum, causing hyperextension exacerbated by the long fulcrum of the ankylosed spine. As the bone has lost all elasticity and is weakened further by osteoporosis, the most likely result of hyperextension is a highly unstable three-column fracture (Shah et al. 2019).

Spinal fractures in AS present most frequently as extension-type injuries, followed by the rotational type. Due to osteoporosis, purely compression-type fractures may also occur (Westerveld et al. 2009b, Shah et al. 2019). Since all normally flexible structures become ossified, the course of the fracture line does not usually respect anatomical structures as would be expected in a healthy spine (Fig. 14) (Lukasiewicz et al. 2016, Rustagi et al 2017).

In DISH, the anterolaterally ossified syndesmophytes cause only anterior fusion of spinal segments, which correlates with a local increase in bone density (Westerveld et al. 2009a). Some residual flexibility is maintained posteriorly in the IVDs, facet joints, and between the posterior arches. Fractures are therefore mainly caused by extension forces, with fracture lines running either through the disc space or through the vertebral body, often compromising the anterior and middle columns (Brandsford et al. 2012, Balling et al. 2015, Okada et al. 2017, Okada et al. 2019). This finding was further confirmed in a study of 160 DISH and 85 AS patients where isolated vertebral body fractures were found in a respective 58% and 17% (Shah et al. 2021). Although wedge and burst fractures do occur in DISH, the extension type running through multiple levels occurred in 9 patients from a cohort of 147 with low-energy trauma, most likely related to the strongly ankylosing nature of the syndesmophytes (Lantsman 2020).

In a study of 112 patients with ankylosis caused by AS and DISH from Caron et al., spinal fractures in 72 DISH patients corresponded with the distribution and morphology of advanced AS, occurring most commonly in the lower parts of the cervical spine, followed by the thoracic and lumbar spine (Caron et al. 2010, Lukasiewicz et al. 2016, Teunissen et al. 2017). This distribution was supported by a recent study of 160 DISH and 85 AS patients (Shah et al. 2021). In studies of DISH patients by Okada et al. in 2017 and 2019, fractures had a tendency to occur in the thoracic spine followed by the lumbar and cervical spine (Okada et al. 2017, Okada et al. 2019). In another study of 147 DISH patients, fractures occurred in the lumbar spine, followed by the thoracic and cervical spine (Lantsman et al. 2020).

When a fracture occurs in a substantially ankylosed spine of either etiology, the patient might paradoxically feel a subjective sense of relief and increased mobility, due to the spine's gaining some increased range of motion, albeit completely non-physiological. This newly acquired mobility, combined with strong local forces attributable to the long levers of the ankylosed segments, leads to a marked increase in risk for complications such as hemorrhage and impingement on neural structures. Sharp fracture edges in close proximity to adjacent neurovascular structures further increase complication risks. This type of fracture is likely to appear very well-positioned on images to the point where the fracture line is barely visible on CT, and secondary neurovascular injuries might occur only after a delay when the patient feels comfortable enough to start moving. This leads to underappreciation of both fracture instability and of complications. Pain caused by the fracture may be masked by chronic pain related to the disease, which may lead to delay in treatment (Teunissen et al. 2017). When such a patient becomes mobilized, the fractured bone ends start to pivot and shear due to the strong leverage, putting neurovascular structures at great risk. This mechanism is also known as secondary neurological deterioration related to SCI (Leone et al. 2016).

The reported incidence of SCI revealed by clinical examination ranges widely, has been between 21% and 97% in AS patients with a spinal fracture (Einsiedel et al. 2006, Westerweld et al. 2009a, Lukasiewicz et al. 2016, Teunissen et al. 2017). Compared to the general population, patients with AS have an 11.4 times increased relative risk for traumatic SCI (Alaranta et al. 2002). Especially a fracture at the level of the cervical spine of an AS patient may have catastrophic outcomes, including death, and was found to be a leading cause of in-hospital mortality independent of other diagnoses such as cardiovascular disease, pneumonia, or respiratory failure (Wysham et al. 2017).

An ossified PLL (OPLL) had occurred in 15% of DISH patients with neurological deficit, which might indicate its being an independent causal factor for SCI in DISH patients (Okada et al. 2019). The OPLL is associated with DISH at a prevalence ranging from 1.9% in Japan to 3.7% in the United States (Sasaki et al. 2014, Yoshimura et al. 2014, Okada et al 2019).

Secondary neurological deterioration leads to a delay in diagnosis and treatment in 35% to 44% of traumatic AS patients (Einsiedel et al. 2006, Teunissen et al. 2017), while 9.5% had delayed diagnosis of DISH with spinal fractures (Caron et al. 2010). This share increased in a study of 285 DISH patients to 40%, of which 59% comprised physicians' failure to diagnose the fracture, the rest being patients' delay in seeking medical care within 24 hours from the onset of a fracture (Okada et al. 2019).

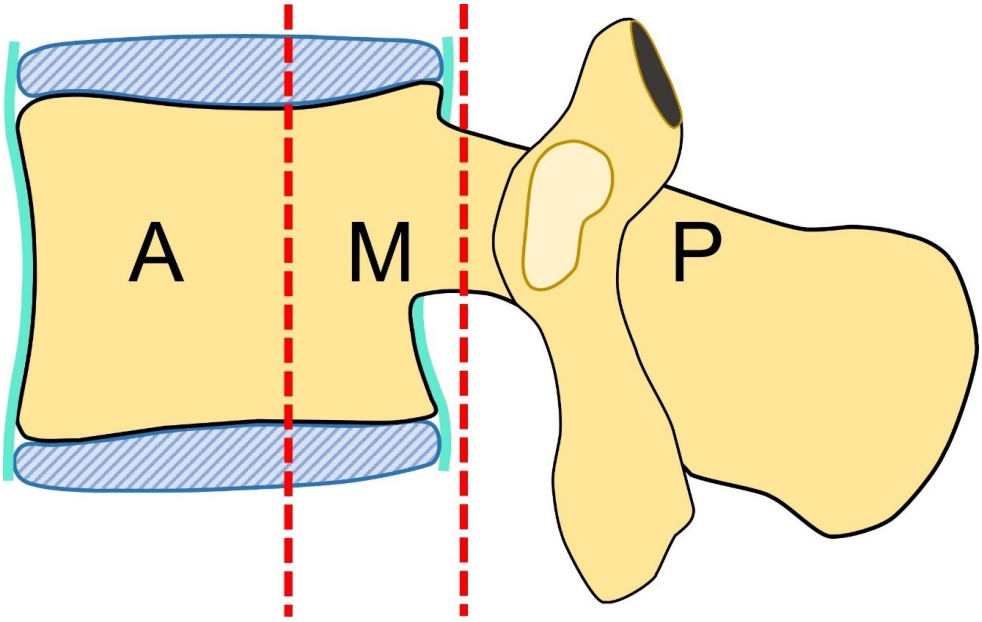


**Figure 12** The three columns of Denis are separated by the dotted lines. The anterior column (A) consists of the anterior two-thirds of the vertebral body, the annulus fibrosus, and the anterior longitudinal ligament. The middle column (M) consists of the posterior third of the vertebral body, the annulus fibrosus, and the posterior longitudinal ligament. The posterior column (P) consists of the posterior osseous and ligamentous structures behind the posterior longitudinal ligament.

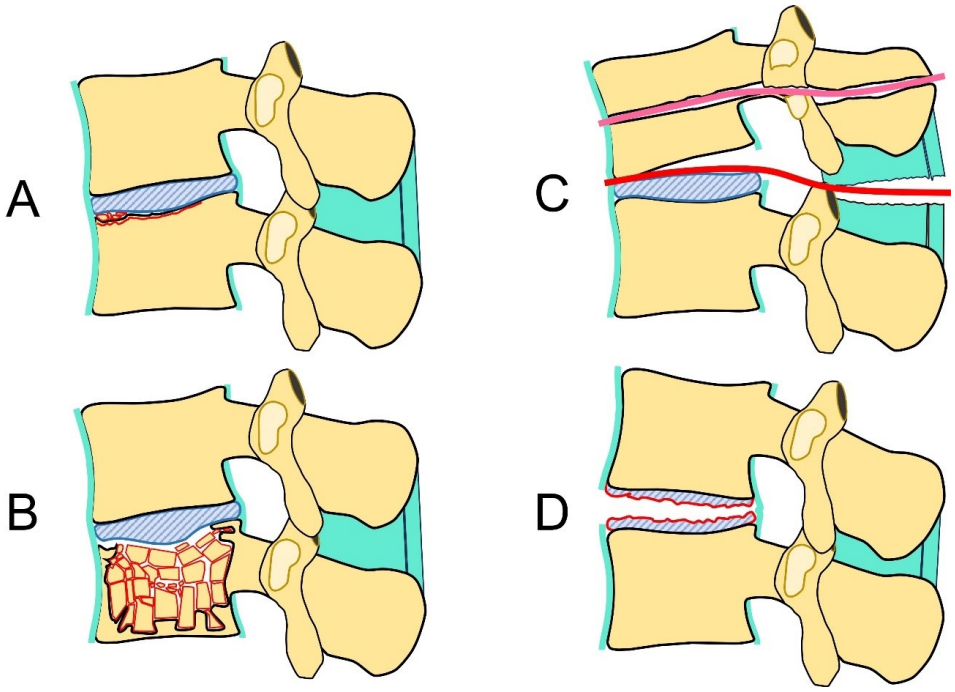


**Figure 13** (A) A compression fracture usually occurs in the anterior upper endplate, causing a wedge-shaped appearance. (B) For a burst fracture, at least two columns are affected and usually severely comminuted. The fracture may, also be limited to either but always involves the posterior column. (C) A combination of flexion and distraction forces typically causes a transverse fracture affecting all columns also known as a Chance fracture (pink line), or alternatively a disco-ligamentous injury (red line) affecting the IVD and ligamentous structures. (D) Extension forces causing a tear of the anterior longitudinal ligament and the IVD may also involve the posterior longitudinal ligament.

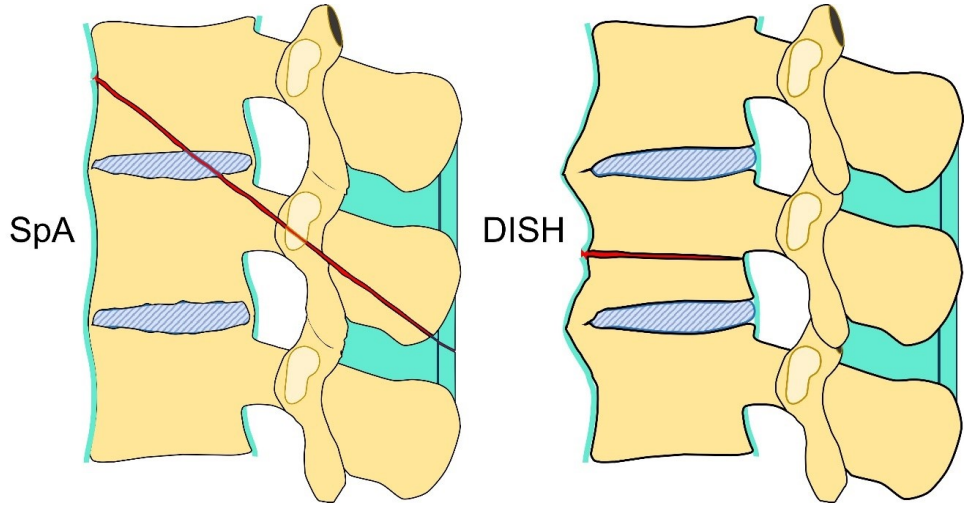


**Figure 14** Due to the ossification of soft tissue structures in the ankylosed spine in SpA combined with osteoporosis, extension forces cause unstable fractures crossing anatomical structures and affecting all three columns. In DISH patients, the anterolateral syndesmophytes support the IVD, which makes a fracture more likely to run through the vertebral body.

### 2.4.2 Spinal hematoma

Spinal hematoma after trauma occurs from injured venous plexuses or small arterioles in the epidural space and in between the spinal meninges and from the fractured bone itself (Foo et al. 1982, Jacobs et al. 2008, Al-Mutair et al. 2010, Anipindi et al. 2017). The anatomical location varies: it may be within the epidural space, the potential subdural space, the subarachnoid space, or within the spinal cord. Venous plexuses are most abundant in the epidural space, where 75% of spinal hematomas originate at an incidence of 1 per million. Of spinal hematomas, 40% are idiopathic. Other causes are anticoagulation therapy, malignancies, arteriovenous malformations, or are iatrogenic (Han et al. 1999, Pierce et al. 2018)

The primary symptom of spinal hemorrhage is pain, followed by neurological deficit, the latter of which may, without timely diagnosis and decompression, progress to permanent impairment. An epidural hematoma will appear uneven and poorly delineated on imaging studies due to its usual position within the adipose tissue of the epidural space. A spinal subdural hematoma (SSH), by contrast, is situated in the potential space between the dura and arachnoid mater, presenting as a collection of blood smoothly delineated from both sides, where the denticulate ligaments are occasionally identifiable. The spinal subarachnoid space, containing cerebrospinal fluid, is a continuation of the intracranial subarachnoid space and may therefore be affected by an intracranial subarachnoid hemorrhage. A hematoma within the spinal cord usually presents as a diffuse hemorrhage rather than as a delineated collection. (Pierce et al. 2018)

## 2.5 Blunt cerebrovascular injury (BCVI)

Blunt cerebrovascular injuries (BCVI) are defined as damage to the intima layer of the cervical arteries caused by a sudden stretching or rotation of the neck, by direct impact from a blunt force, or by shearing from adjacent rigid structures, mostly related to dislocations or fractures (Rutman et al. 2018). The estimated incidence of BCVI in blunt trauma ranges from 1% to 2.7%, and affects up to 9.2% of hospitalized patients (Fleck et al. 2011, Weber et al. 2018, Leichtle et al. 2020). Without appropriate treatment, the condition may cause severe complications such as brain ischemic stroke via thromboembolism or occluded artery (Cothren et al. 2004, Stein et al. 2009, Esnault et al. 2017).

The morphology and grading according to Biffl et al. for blunt cerebrovascular injury, as used in this study, is in Figure 15 (Biffl et al. 1999).

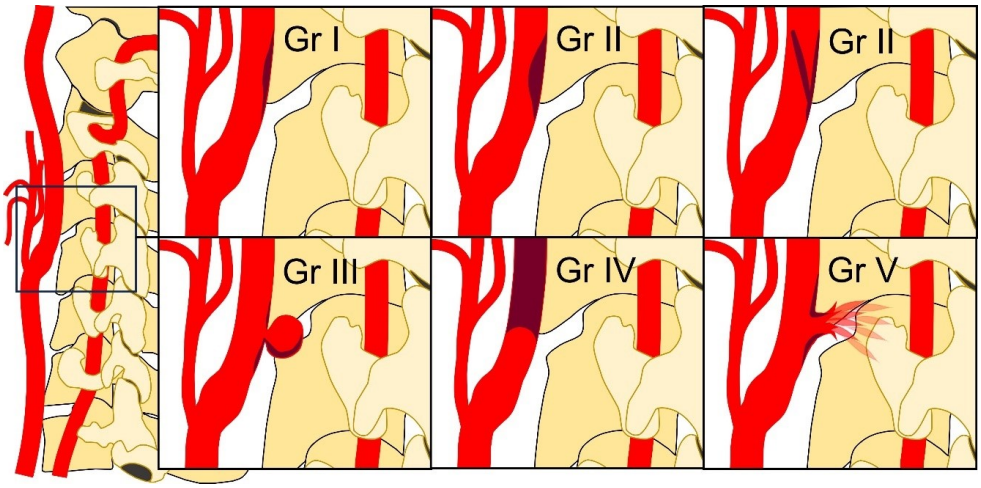


**Figure 15** Grading of BCVI according to Biffl et al. of an injured internal carotid artery (Biffl et al. 1999). Injury grades as follows: Gr I = luminal irregularity or dissection with < 25% luminal narrowing; Gr II = dissection or intramural hematoma with ≥ 25% luminal narrowing, intraluminal thrombus, or raised intimal flap; Gr III = pseudoaneurysm; Gr IV = occlusion; Gr V = transection with free extravasation.

## 2.6 Imaging of the ankylosed spine

ALARA (as low as reasonably achievable) is the basic principle behind the choice of imaging modality, in order to balance the benefit from diagnostic information to guide treatment versus radiation dose. Choosing the appropriate imaging method is critical and may be lifesaving in trauma patients. Medical imaging results in an average effective dose per patient ranging from 0.01 mSv to 10 mSv in computed radiography (CR) to 2 mSv to 20 mSv in CT (Mettler et al. 2008). Trauma, the leading cause of death in the United States in those below middle age, often necessitates in non-symptomatic patients a CT examination for exclusion of occult trauma (Roberts et al. 2020). At the same time, concern is growing regarding excessive imaging. Although effective doses below 100 mSv will cause only stochastic ionizing damage, a linear correlation exists between damage and doses in excess of 100 mSv; this is especially relevant in cases of consecutive CT imaging (Martin et al. 2022). The ionizing long-term effects are of larger concern for pediatric than for elderly patients, but apply to both. The “low” in ALARA is also applicable to cost, since imaging does contribute to overall public healthcare expense (Hendee et al. 2010, Skjødt et al. 2023).

Efforts to support decision-making for imaging based on clinical examination have led to clinical guidelines such as the National Emergency X-

Radiography Utilization Study (NEXUS) criteria or the Canadian cervical spine (CCS) rule, each of which strives to reduce unnecessary imaging (Hoffman et al. 2000, Stiell et al. 2001). Compared to general trauma patients, the NEXUS criteria have appeared to be insufficient for the exclusion of cervical spine fractures in the elderly (Paykin et al. 2017). Refinement of imaging criteria enables increasingly precise decision rules and criteria, which also takes into account the limited share of general trauma patients who require imaging with MRI in addition to CT to exclude ligamentous injury (Duane et al. 2013, Duane et al. 2016).

Patients with ankylosing spinal disorders often suffer from chronic pain, which may be a cause for unnecessary imaging. Patients with an ankylosed spine do, however, need multimodality imaging for appropriate treatment to avoid permanent neurological deficit (Shah et al. 2019). Understanding the biomechanical properties of the ankylosed spine, along with the limitations of imaging modalities, can provide guidance for decisions concerning both imaging and optimal treatment.

### 2.6.1 Radiography

The discovery of x-rays and their reliable creation via cathode tube by Wilhelm Conrad Rœntgen in 1895 provided the basis for medical imaging. The main difference between historical radiography and current digital radiography is detector technology. The former uses photographic screen films which directly visualize opacification via a chemical reaction proportional to the amount of absorbed radiation. Modern technology, digital radiography, is based on reusable detector plates which are either scanned by a laser beam in computed radiography (CR), or which immediately convert the absorbed radiation into a digital format in direct radiography (DR). Radiography provides an image with all anatomical structures inside the imaged volume projected on top of each other. The amount of opacification visible on images is directly proportional to the density and therefore to the radiation absorption of a structure. (Bansal 2006, Schaefer-Prokop et al. 2009)

Detection on radiographs of narrow spinal syndesmophytes is challenging in hospitalized patients, due to the overlay of body parts comprised of tissues with varying densities and of possible tubes and wires (Fig. 8). Radiologic diagnosis must therefore take into account the overall morphology of the spine and bone structure, including signs of osteoporosis (Fauny et al. 2020). Although the symptoms and course of AS are generally well-known, some patients do not receive a definitive diagnosis based on imaging findings (Koivikko et al. 2004).

The narrow syndesmophytes bridge the intervertebral space on the surface of the annulus fibrosus, and the intervertebral spaces are spared from the lowering changes of degeneration, which altogether cause the spine to resemble a bamboo

stick, hence the moniker “bamboo spine” (Takahashi et al. 2023). In advanced disease, even the facet joints and costovertebral joints also tend to fuse.

The anterolateral wavy or flowing syndesmophytes in DISH can usually be readily identified on a sagittal radiograph (Misaki et al. 2022), whereas overall bone density, excluding the syndesmophytes, appears normal (Westerweld et al. 2009b).

DS is a frequent finding which often coincides with AS and DISH, but findings identifying it as a primary cause for ankylosis are scarce (Okada et al. 2017, Slonimsky et al. 2018). DS affects both the endplates and facet joints (Gellhorn et al. 2013).

A fracture in AS patients with a fully ankylosed spine may be hidden if the affected vertebrae are in an almost normal position, which along with thinned cortices and low contrast due to osteoporosis makes fracture detection from a radiograph a challenge (Fauny et al. 2020). The only hint for the presence of a fracture may in fact be some signs of advanced AS themselves. The definitive diagnosis of such a fracture usually requires CT (Koivikko et al. 2004, Werner et al. 2016).

### 2.6.2 Computed tomography (CT)

The basis for reconstruction of CT images from a data set is a mathematical algorithm called a Radon transform, which was developed by Johann Radon in 1917. In 1972, Cormack and Hounsfield assembled the first CT scanner able to produce images in the axial plane by positioning patients inside a gantry with a rotating xray tube and opposing detectors. Modern scanners move the patient along the longitudinal axis while the rotating gantry produces a three-dimensional volumetric dataset, from which images in any plane can be reconstructed. The development of multi-slice CT scanners began in 1998, making possible the parallel acquisition of multiple slices, thereby markedly reducing scan time and imaging artefacts, while increasing resolution. (Rogalla et al. 2009)

Iterative reconstructions with artificial intelligence algorithms, back projection, tube filters controlling the photon current, layered detectors for photons with different energies, energy-resolving detectors, dual-energy CT with two separate tubes or a single tube with different voltages are common approaches. They function during data acquisition and post-processing of the volumetric dataset to enhance image quality and to make possible further reductions in scan time and effective dose. Using water and air as references, Hounsfield units (HU) provide a measure of object density which remains constant even across different scanners. Iodine contrast media widens the contrast of soft tissues and of the circulatory system, which helps highlight pathological processes. Image quality, scan time, and radiation safety are constantly being improved, with state-of-the-art current CT scanners being fitted with up-to-128-slice detectors, gantries with friction-free air bearings, and dual-energy X-ray sources allowing for spectral absorption analysis

such as for microscopic amounts of gout crystals. (Rogalla et al. 2009, Agostini et al. 2022)

CT is widely available and represents the primary tool in modern medical imaging for trauma, which outperformed radiography in detecting spinal fracture already two decades ago (Brown et al. 2005, Roberts et al. 2020). For the detection of well-positioned (occult) spinal fractures in AS patients, careful scrutiny of the usually osteoporotic bone often reveals the unstable and severe fracture crossing atypically across the ankylosed anatomical structures (Fig. 14).

In a study of 20 AS patients imaged with both modalities, CT detected 6 fractures and MRI detected 2, none of which were seen by the other modality (Koivikko & Koskinen 2008). These results may be explained by the proportion of well-positioned fractures in the pathologic bone of AS patients. As the authors discussed, increased intraosseous fat content and reduced cancellous bone may associate with less bone edema with less obvious appearance of the fracture on MRI, especially when located in the IVD. Due to unusual posture combined with a painful and unstable spine fracture, AS patients may not fit into the tube or be able to maintain the correct position for the duration of an MRI scan ranging from 20 to 30 minutes. Withstanding the pain and the forced imaging position may cause unintended movement leading to suboptimal image quality consequently explaining the altered visualization of fractures in MRI. As the recommended modality, CT detects the bone structure precisely, and the imaging time is only a fraction of that of MRI, although MRI does provide detection for ligamentous injuries, spinal hematomas, or SCI.

In a study of 42 DISH patients with spinal fractures, 35% had a delayed diagnosis due to initially incorrect assessment (Okada et al. 2017). Any delay caused by patients is related mostly to their reluctance to seek treatment; this is, however, less than the delay related to initial misdiagnosis (Okada et al. 2019). Iatrogenic delay was estimated to be avoidable by more aggressive CT imaging of asymptomatic DISH patients who experienced low-energy trauma (Okada et al. 2019).

In a study of 129 DISH patients imaged with radiographs and CT, 18 fractures were missed and 6 were diagnosed as false positives on radiographs (Lantsman et al. 2020). In DISH patients with neurological deficit, suspicion of posterior ligamentous complex injury, or SCI, a further MRI examination is advisable (Okada et. al 2017, Shah et al. 2021).

### 2.6.3 Magnetic resonance imaging (MRI)

MRI is an imaging modality based on interactions between tissue hydrogen, an external magnetic field, and radiofrequency excitation pulses which therefore does not expose patients to harmful ionizing radiation. Its inherent high soft-tissue contrast even without contrast enhancement offers superior diagnostic information on soft tissue conditions. Its high sensitivity for edema in any tissue is helpful in occult fracture detection as well as in fracture age classification or in identification of a pathologic component. Drawbacks include low availability, high cost, long imaging times, contraindications such as metallic foreign material as well as limited space inside the scanner for larger patients, and the demand for highly trained staff. (Azhar et al. 2023)

Time for recovery and reaction to excitation from radiofrequency pulse in T1-weighted imaging (T1WI) and T2-weighted imaging (T2WI) are applicable in the description of tissue properties. Bright signal is referred to as hyperintensity, while dark signal is referred to as hypointensity, in a grayscale image. In T1WI fat, white matter and methemoglobin appear hyperintense; muscle, grey matter, spinal cord, cartilage and most intra-abdominal parenchymal organs appear intermediate; air, cortical bone, ligaments, tendons, and fluids such as cerebrospinal fluid appear hypointense. In T2WI fat, fluids or tissues containing diffusely spread fluid appear hyperintense; muscle, most parenchymal intra-abdominal organs, white matter, and brown fat tissue appear intermediate; air, cortical bone, ligaments, and tendons appear hypointense. In short-tau inversion recovery (STIR) images, the fat is being suppressed and fat therefore appears reliably dark, while fluid signal in tissues such as edema is bright. Fat saturation in STIR is unaffected by metal artefacts due to the initial inversion pulse, but lacks image resolution compared to that of other imaging sequences. (Azhar et al. 2023)

AS patients require especially careful transfer and positioning due to both the inherent instability of their fractures and the usually pronounced kyphosis. Staff needs to be alert that even small movements can generate considerable forces at the fracture site, because the cranium and the cervical and upper thoracic spine form a lever in the supine position, pivoting at the level of CTJ, which is also the most common level for a fracture (Caron et al. 2010, Lukasiewicz et al. 2016, Teunissen et al. 2017). This brings another new meaning to the ALARA principle, because an incorrectly performed MRI scan might put patients at risk, while the “L” might indicate low imaging time which benefits the patient.

Only MRI offers sufficient soft tissue contrast for the detection of ligamentous injuries or occult fractures, which was essential for the evaluation and management of our patients in this study (Fig. 18). Presymptomatic spinal

hematoma generally remains undetectable without MRI (Pierce et al. 2018). In patients with CT-verified spinal fracture without neurological deficit, MRI scans detected additional findings in 71% with AS and 18% with DISH (Shah et al. 2021). The signal behavior of blood breakdown products within the blood-brain barrier as a function of time follows a predictable sequence for the appearance of spinal hematomas (Bradley 1993).

Heterogeneity of an epidural hematoma may be explained by the venous plexuses and epidural fat (Fig. 19). An SSH occurs within the potential space between the dura and arachnoid mater and may also seem heterogeneous on MRI due to the mixing of cerebrospinal fluid and blood (Fig.20). An SCI is usually apparent on clinical examination and is an important imaging finding visible only on MRI. Another differential diagnostic criterion reliably visible only on MRI is bulging of the IVD into the spinal canal, especially in DISH and DS patients, since their IVD and posterior disk space is usually preserved (Fig.21) (Pierce et al. 2018).

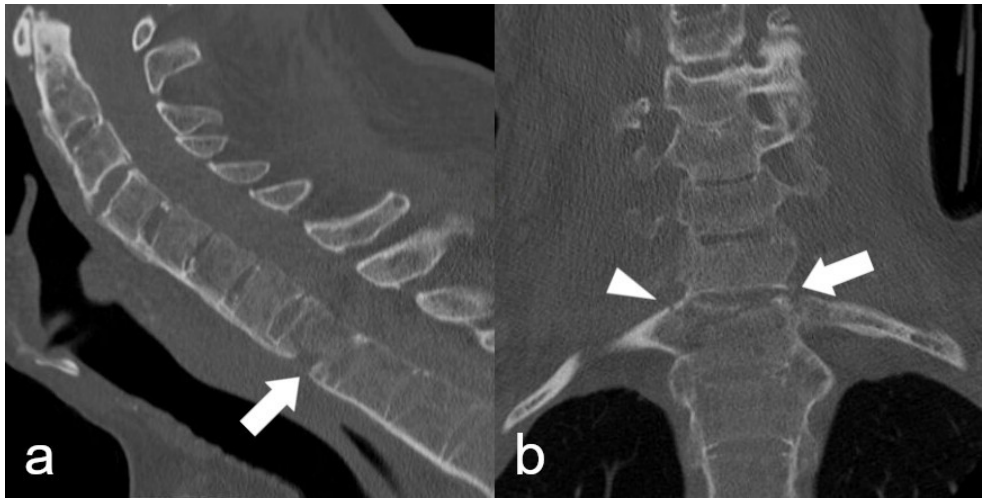


**Figure 16** A 61-year-old man had a CT scan three days after loss of strength in the right upper extremity and tenderness in his neck. The arrows indicate an unstable fracture passing through the ALL, the anterior and middle columns on a sagittal and coronal CT image. (a,b). The fracture line runs through the first right rib (arrowhead) and ankylosed right costovertebral joint (b).

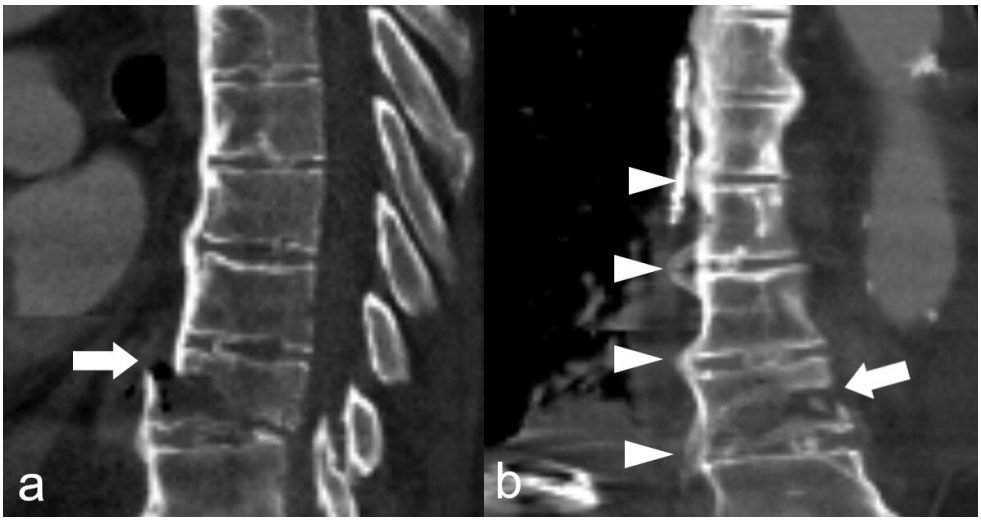


**Figure 17** An AOSpine classification Type B fracture in a 92-year-old man who fell at ground level and was unable to move his lower limbs. Arrows indicate the fracture running through the anterior and middle columns of the Th10 vertebral body on sagittal CT (a). Arrowheads on the left indicate the DISH osteophytes protruding anterolaterally at the level of intervertebral discs from Th7 to Th11 and avoiding the aorta to the contralateral side. The arrow on the right indicates the fracture running through the body of Th10 (b).

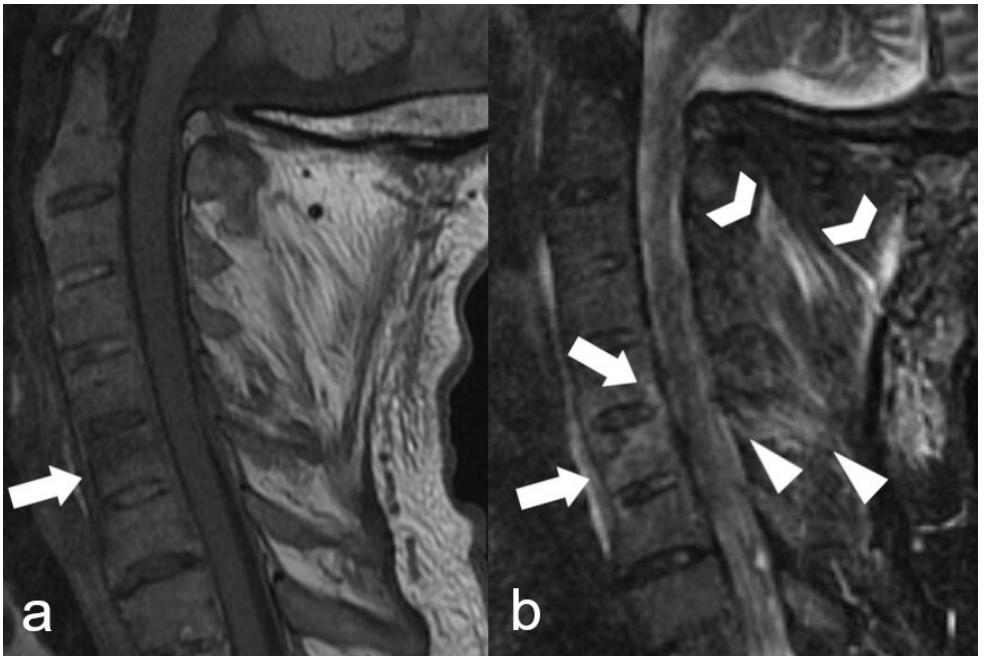


**Figure 18** A 73-year-old man fell asleep while driving and drove off the road. Sagittal T1WI MRI on the left (a) and sagittal STIR MRI on the right (b) show a flexion injury and a fracture (arrow) of the C6 vertebral body. On sagittal STIR, the fracture continues to the lower endplate of C5 (arrows). Posteriorly in the area of the ligamentum flavum and interspinous ligaments (arrowheads), as well as the nuchal ligament (chevrons), note tears in the posterior ligaments (b).

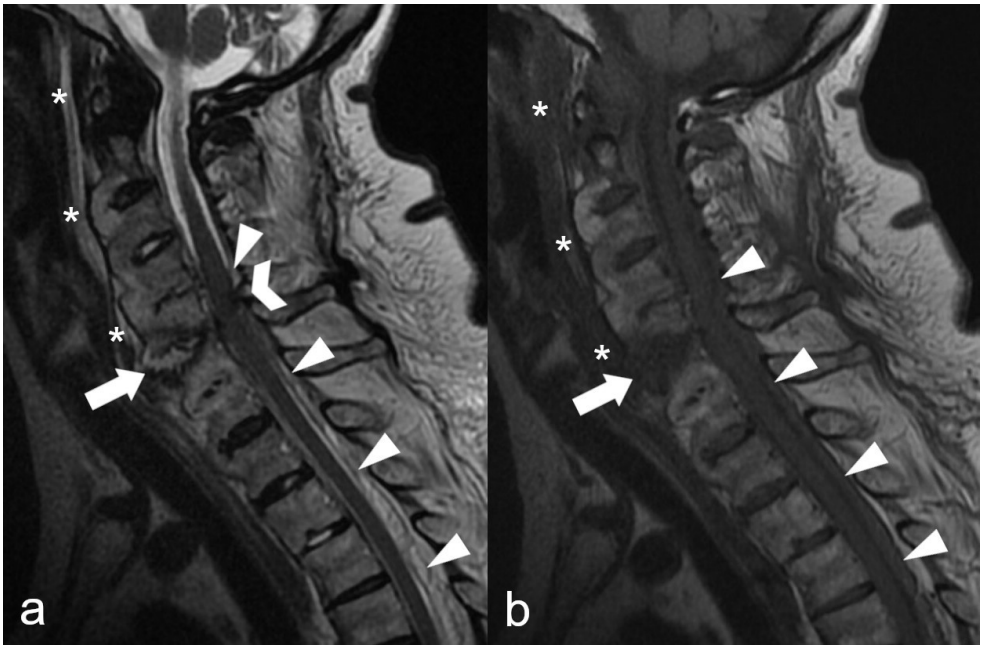


**Figure 19** A 77-year-old woman with ankylosing DISH after a fall from standing height. Sagittal T2WI (a) and sagittal T1WI (b) show the fracture line through the intervertebral disc between C5 and C6 indicated by arrows. The fracture continues as a tear in the ligamenta flava indicated by a chevron (a). A posterior epidural hematoma indicated by arrowheads shows heterogenous high signal intensity on T2WI (a) and homogeneously intermediate signal intensity on T1WI (b). Asterisks indicate a prevertebral hematoma extending from fracture level to the level of C1.

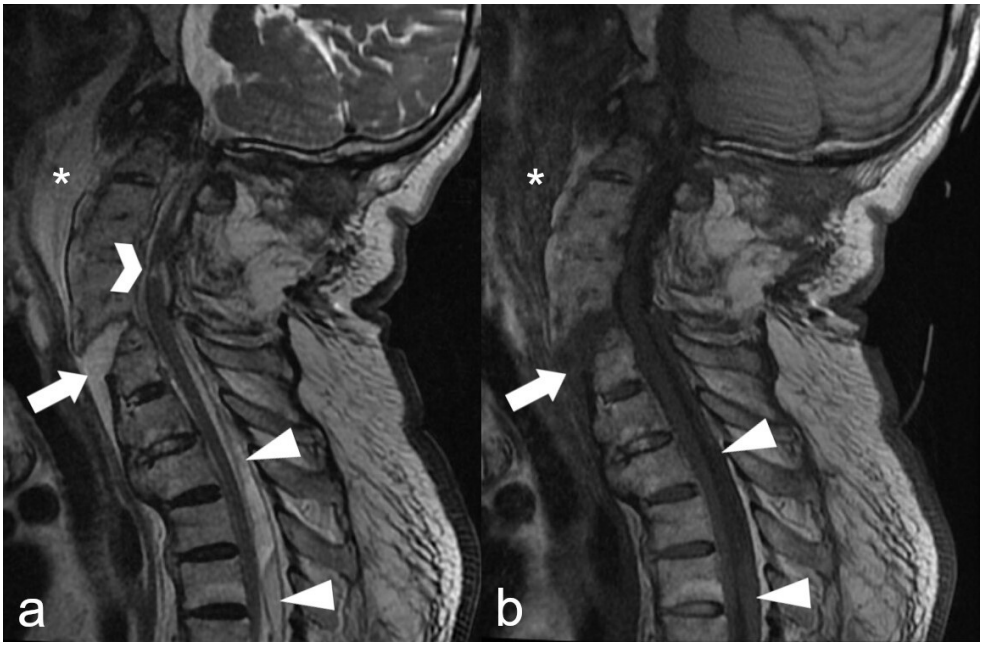


**Figure 20** An 87-year-old man with AS fell on his back and within hours developed a tingling sensation in his hands. Sagittal T2WI (a) and T1WI (b) show a hyperextension injury with an unstable fracture running through the anterior column of C7, the IVD above, and through the posterior parts of the C6 lower endplate (arrows). A SCI is shown as high signal intensity on T2WI at the level of the IVD space between C4 and C5 (chevron). A spinal subdural hematoma is visible on both images as a heterogeneous fluid collection delineated posteriorly by the smooth interface between dura and epidural fat (arrowheads). Asterisks indicate a prevertebral hematoma extending from fracture level to the base of the skull.

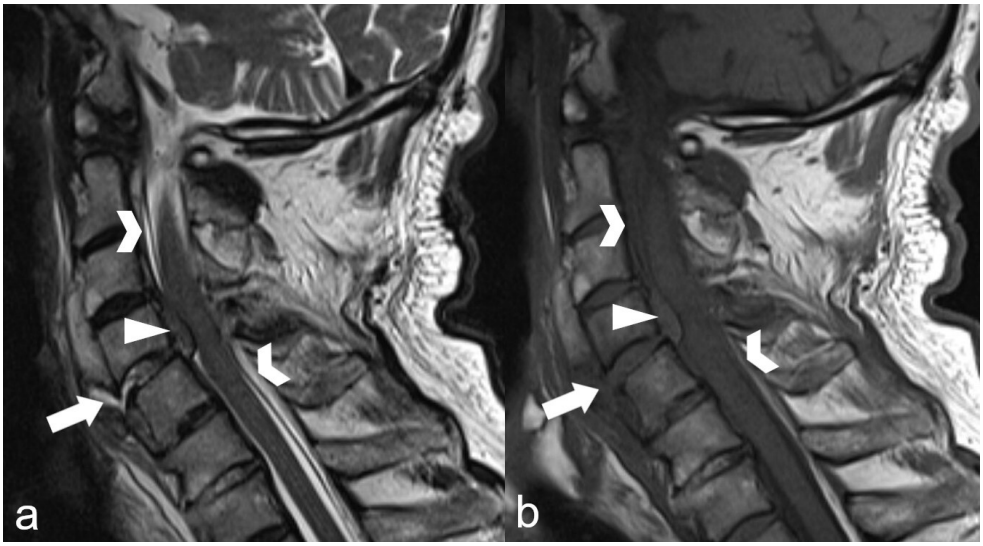


**Figure 21** A 69-year-old man with ankylosing DISH who had fallen forward on his forehead, after which he complained of progressive tenderness in the neck. Sagittal T2WI (a) and T1WI (b) show an injury through the ALL and the intervertebral disc space between $C_4$ and $C_5$ (arrows). Part of the IVD has herniated into the epidural space posterior to $C_4$ (arrowheads). An epidural hematoma (chevrons) is visible anteriorly above and posteriorly below the injury level.

## 2.7 Treatment of fractures of the ankylosed spine

Management is based on clinical examination with the focus on neurological status, because unstable spinal fractures carry a high risk for both primary and secondary injury to neurovascular structures. Among AS patients, 54% to 57% and 52 to 55% of DISH patients will be managed surgically (Westerveld et al. 2009b, Westerveld et al. 2014). Although unstable injury and neurological deficit are absolute indications for surgery, 46% of patients of both etiologies have been treated without surgery due to risks of treatment related to comorbidities or refusal (Westerveld et al. 2009b).

Posterior long-segment fixation is the most common method for patients with AS and DISH (Westerveld et al. 2014). Patients requiring surgery are recommended for fixation of at least 3 to 4 segments above and below the injury level (Rustagi et al. 2017). After posterior fixation, a combination of anterior and posterior fixation is the next most common surgical option (Westerveld et al. 2009b, Westerveld et al. 2014, Vazan et al. 2019).

The anterior approach is recommended for a minority of patients, allowing removal of bony fragments, epidural hematoma, or bulging IVDs from the anterior epidural space (Vazan et al. 2019). Westerveld et al. reported 15 % of patients treated with anterior fixation alone (Westerveld et al. 2009b). After anterior fixation for their cervical spine, patients usually wear a collar for support until the additional posterior fixation takes place. For fractures of the thoracolumbar spine, a mini-thoracotomy or lateral retroperitoneal approach is required for anterior surgery. (Vazan et al. 2019)

Posterior fixation is performed either with a midline approach or a minimally invasive percutaneous technique with or without fluoroscopy support. Screws to fix the vertebrae in place are drilled through the pedicles and fixed to long rods. The posterior approach provides access to the posterior epidural space for the removal of bony fragments or of (any) spinal hematoma. (Vazan et al. 2019)

Conservative treatment is a viable option for patients of advanced age or with contraindications for surgery such as cardiorespiratory diseases or other comorbidities. Options for conservative treatment include halo traction, halo immobilization, a collar, brace, plaster jacket, bed rest, treatment in an intensive care unit, or in a regular ward where immobilization is less restricted. (Westerveld et al. 2014)

The aim of both surgical and conservative management is to stabilize the fracture, allowing for fracture healing while preventing secondary injury to the spinal cord and further complications. An injured spinal cord is predisposed to further damage from decreased perfusion, which is additionally dependent on blood pressure and pulmonary function. Patients with an unstable fracture of the ankylosed spine and SCI therefore tend to benefit from treatment in an intensive care unit with adjusted blood-pressure levels and with prophylaxis against venous

thrombosis, while also benefiting from decubitus-ulcer prevention, aggressive treatment of genitourinary and pulmonary infections, and early and adequate nutrition (Bradley et al. 2008).

## 2.8 Imaging of BCVI

Since its introduction in the early 1980s, digital subtraction angiography (DSA) had been, in addition to physical examination, the only viable imaging method for injuries of the intimal lining of blood vessels (Fabian et al. 1990, Davis et al. 1990). BCVI was historically recognized as a pathology of mainly the common and internal carotid arteries. In 1996, with an increase in MVAs and better understanding of the effects of sudden deceleration forces with differing trauma mechanisms causing BCVI, more aggressive imaging developed, with a screening protocol using DSA (Biffl et al. 1998). Shortly thereafter, Biffl et al. established the current grading system for BCVI (Biffl et al. 1999). The cumulative data of the screening protocol that began in 1996, which also included vertebral-artery injuries, called into question the concept of the harmlessness of vertebral artery injury and further confirmed the need for vertebral artery imaging (Biffl et al. 2000).

DSA, while still being the gold standard for BCVI imaging, is aninvasive imaging modality with the additional disadvantage of inflicting high radiation exposure. Moreover, it needs significantly longer to perform and is more resource intensive and expensive than any of the other imaging modalities. Ultrasound, which is widely available, quick to perform, and free of any radiation exposure, is limited to vascular segments situated outside of any bony structures. It furthermore depends highly on patient cooperation and operator experience, while being easily limited by factors such as patient habitus. The development of CTA led to a far less invasive and more tolerable imaging option, more readily available without the need for a local angiography suite, with the possibility of vascular imaging being integrated into regular CT for trauma, (along) with an option for multiplanar reconstruction (Figs. 22–24). Data from first- generation CTA compared to DSA revealed that the former was unreliable to detect BCVIs of grades I, II, and III (Biffl et al. 2002). Furthermore, improper timing could lead to nondiagnostic CTA images, but CTA was nevertheless recommended for patients without access to DSA. Rapid developments in CT technology especially after the introduction of multidetector CT improved image quality and scanning time significantly while reducing artifacts to the point of becoming negligible. This has led to CTA being established as the primary imaging method for BCVI screening because of its speed, reliability, availability, and cost-effectiveness, as well as its ability to image all four relevant arteries simultaneously, while claiming sensitivity of 97.7% and specificity of 100% (Berne et al. 2006, Eastman et al. 2006, Stein et al. 2009, Bromberg et al. 2010, Wang et al. 2012).

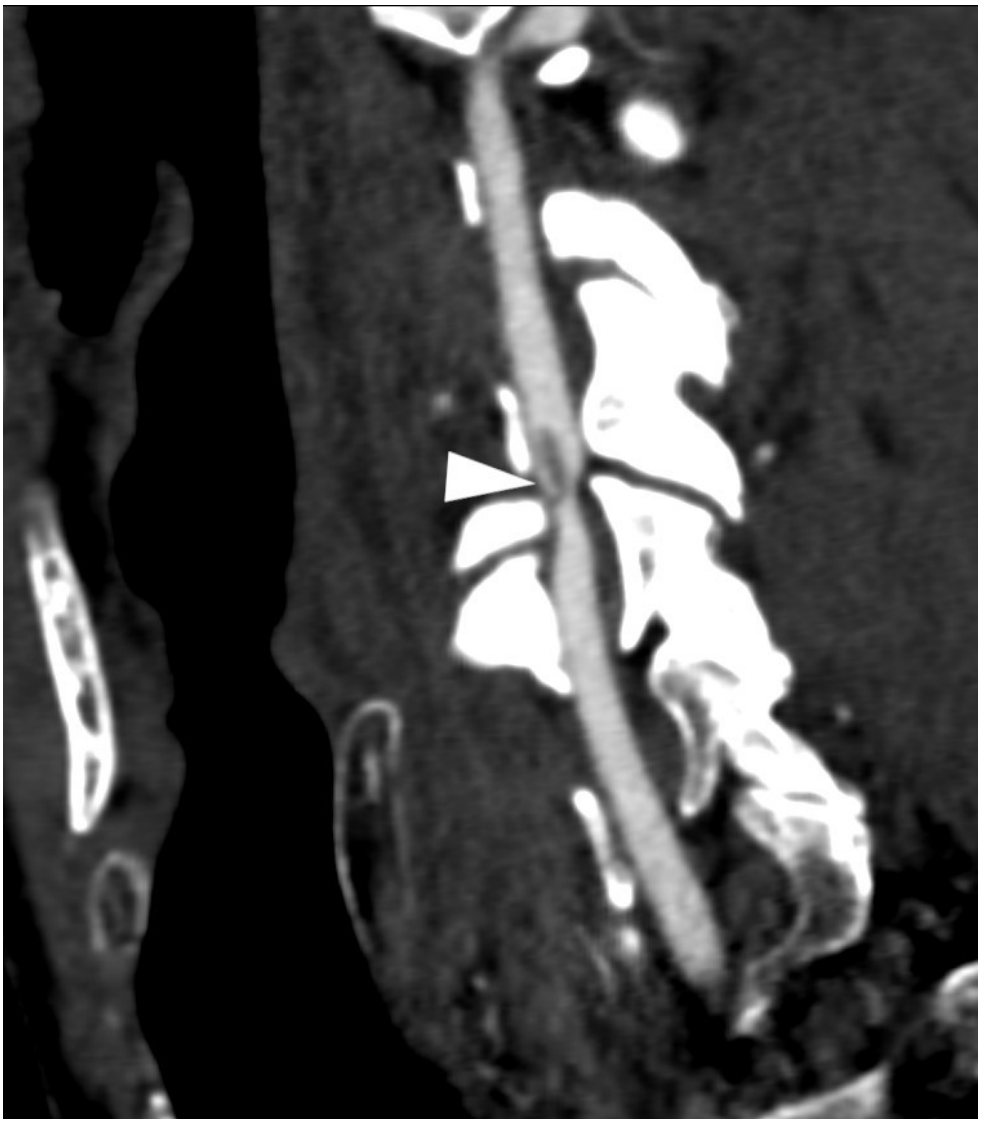

**Figure 22** Collapsing scaffolding hit a 66-year-old man in the head, causing an unstable injury through the intervertebral space between C4 and C5 and a bilateral vertebral artery injury. Arrowhead indicates a grade II BCVI in the left vertebral artery with an intraluminal thrombus. The cervical spine was ankylosed by DS from C5 to C7.

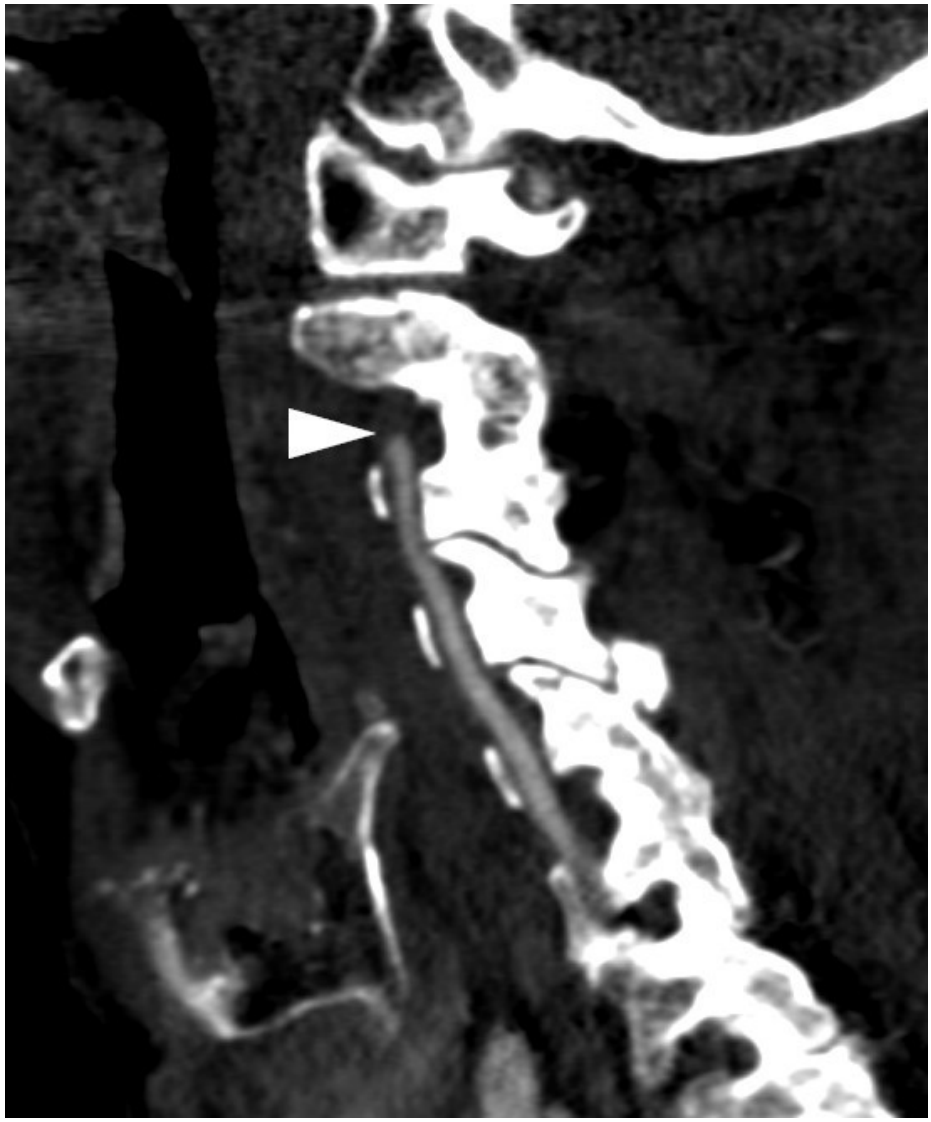

**Figure 23** A 79-year-old woman after falling on a bus and hitting her head on a pole, causing a C2 fracture and a gr IV BCVI on the same level in the right vertebral artery. The cervical spine was ankylosed by DISH from C5 to C7.

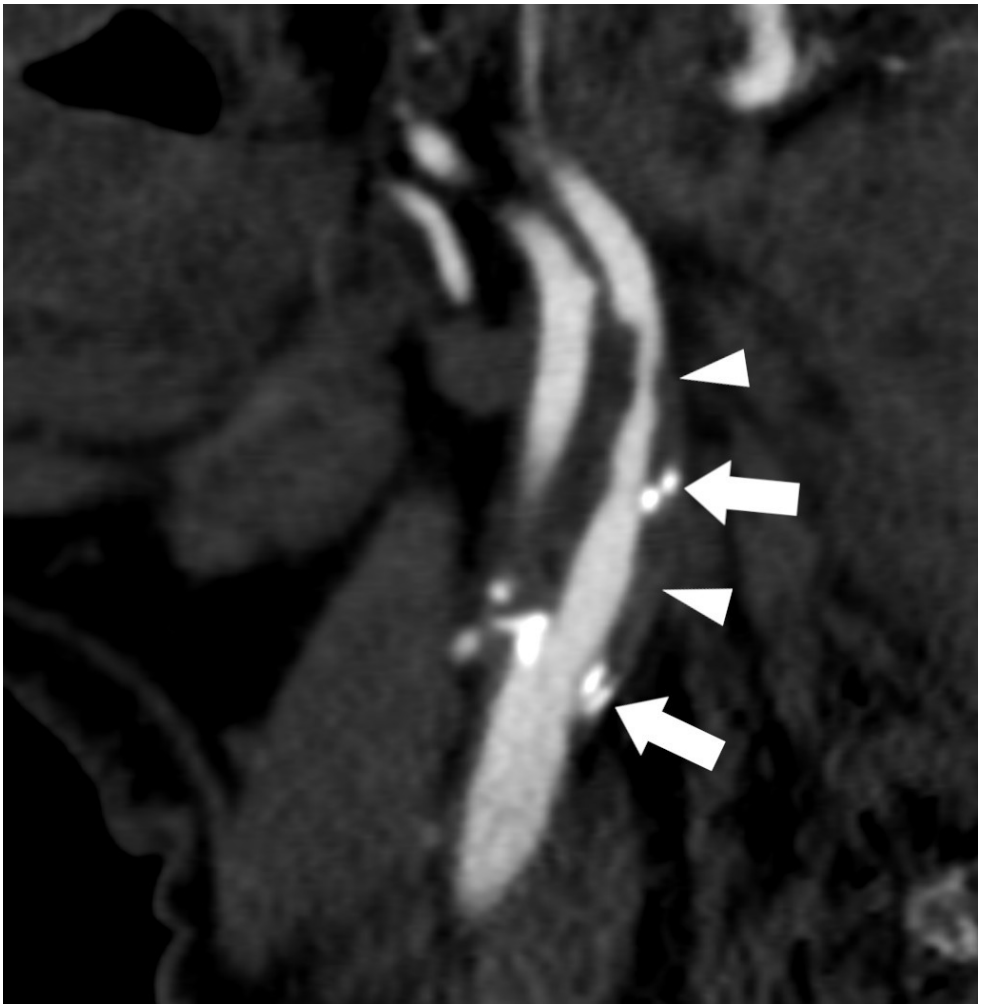

**Figure 24** Atherosclerosis causing luminal narrowing without signs of acute injury in the left internal carotid artery of a 74-year-old man who fell on his back. Arrowheads indicate the soft atherosclerotic plaque, and arrows indicate solid intramural calcifications.

## 2.9 Treatment of BCVI

If the injured artery is occluded or transected, symptoms usually occur immediately. In less severe injuries, the uneven and injured intimal surface reveals the thrombogenic collagen-gathering platelets which further promote a turbulent blood flow, leading eventually to a local or distant thrombosis and stroke (Biffl et al. 2001). The time between onset of trauma and stroke, the latent period, ranges from 18 hours to 7 days (Biffl et al. 2001, Cothren et al. 2004).

Antiplatelet or anticoagulation therapy is recommended for preventing stroke (Fabian et al. 1996, Cothren et al. 2004, Stein et al. 2009). Not all patients can be treated with anticoagulation, because of a number of contraindications including concomitant brain or vascular trauma, or hemodynamically unstable injuries with active extravasation requiring endovascular treatment (Stein et al. 2009).

However, antiplatelet or anticoagulation therapy should commence after the detection of BCVI, as the treatment will not further aggravate concomitant traumatic brain injury or solid organ injury (Shahan et al. 2016).

# 3 AIMS OF THE STUDY

The purpose of this study is to

*(I)* *establish the incidence, location, and MRI features of spinal hematoma in AS patients after blunt trauma,*

*(II)* *establish the incidence, location, and grade of BCVI, as well as the incidence of associated strokes in patients with ankylosed cervical spine after blunt trauma,*

*(III)* *establish the incidence and location of spinal hematoma, and their relation to neurological deficit in DISH patients after blunt trauma*

# 4 MATERIALS AND METHODS

## 4.1 Patients

The Helsinki University Hospital's institutional review board has approved this retrospective study. As a part of Helsinki University Hospital, Töölö Hospital used to be the only level-1 trauma center in Finland with a catchment area of 1.67 million people. Patients with acute and severe trauma have been treated in Töölö Hospital since 1932, until all its facilities were transferred to the newly built Bridge Hospital trauma center located on the Meilahti main campus of the University hospital in February 2023, after which the historic Töölö hospital was decommissioned. All adult polytrauma cases including serious orthopedic and neurosurgical trauma have been routinely admitted to Töölö hospital for further evaluation and management, in addition to patients referred from lower- level trauma centers from both inside and outside the health care district

During daytime shifts, attending radiologists or residents under close supervision interpret and report all CT and MRI scans. At night, residents usually interpret CT scans, which undergo double reading by a specialist immediately the following morning. Any night-time MRI scans are interpreted by an on-call specialist. Patients under the age of 16 and ones with penetrating trauma were at that time generally referred to the main university hospital.

All patients in this study were managed at Töölö Hospital. Data including age, gender, trauma mechanism and energy, previous diagnoses concerning ankylosis of the spine, neurological status, information on medication, and the events of the hospitalization period were gathered from patients' electronic medical records.

### 4.1.1 Post-traumatic spinal hematoma in patients with ankylosing spondylitis (I) and DISH (III)

A manual review of emergency or urgent MRI referrals included scans of 2256 patients with a prior CT scan during a period of eight years and nine months

(January 2011 to September 2019). MRI scans with any mention of AS, spondyloarthropathy, spinal ankylosis, DISH, rheumatoid arthritis, spinal fracture, blunt trauma, neurological deterioration, spinal hematoma, or paraspinal fluid collection were manually reviewed on a radiology workstation, revealing 164 patients with spinal ankylosis and a fracture. Those cases were divided into patients with advanced spinal ankylosis comprising IVDs, facet, costotransversal, and costovertebral joints indicating SpA, and patients with spinal ankylosis from DISH. Insufficient image quality resulted in exclusion. In Study I, patients with advanced spinal ankylosis typical for SpA and ankylosis of the SI-joints were included even without a previous diagnosis in their electronic medical records. Study III included patients with ankylosis typical for DISH and a fracture in the ankylosed segment or in the vertebra adjacent to it. From manual review of 2256 MRI referrals, we found 28 AS patients for Study I and 70 DISH patients for Study III (Fig. 25).

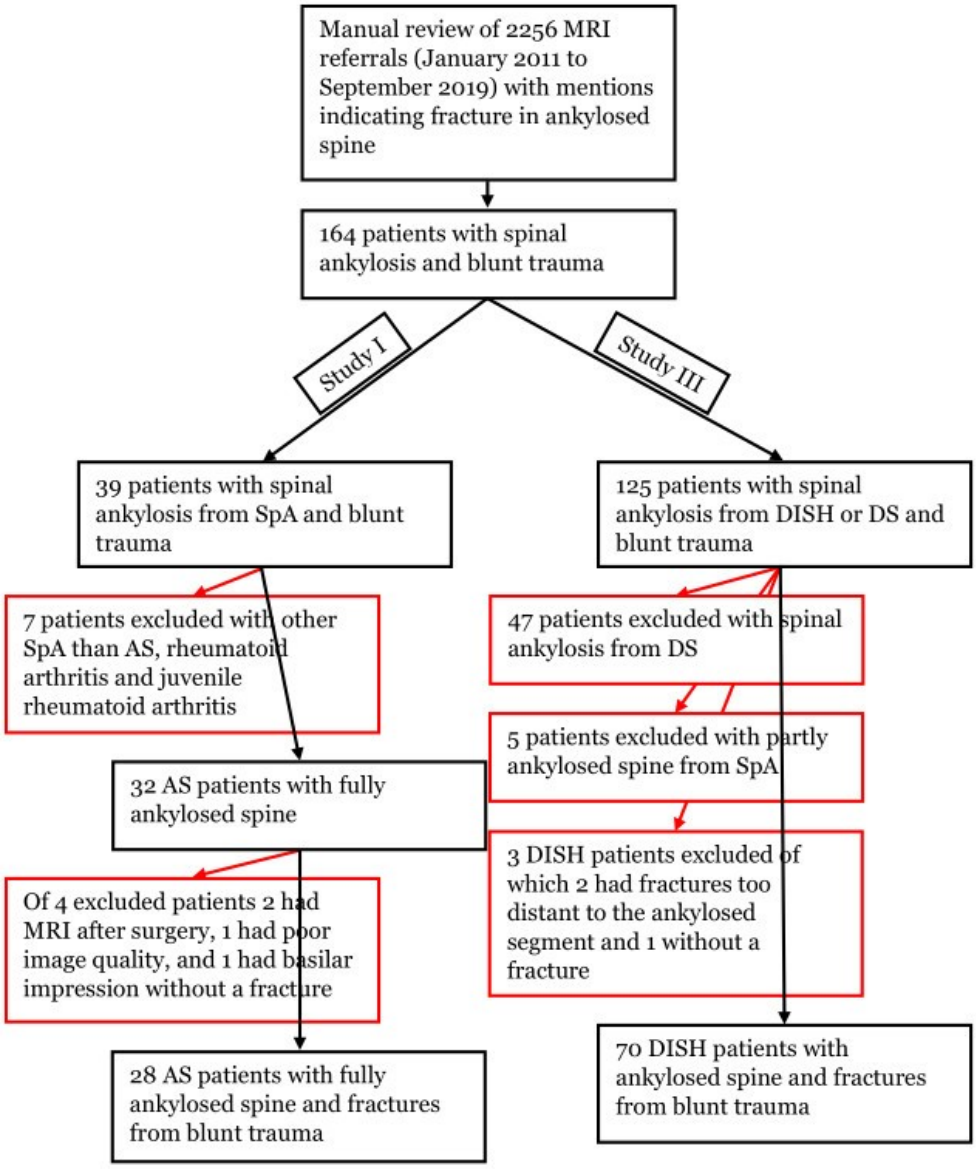


**Figure 25** Flow chart presenting the selection of patients for study I and III. Red arrows and red boxes indicate the excluded patients with the corresponding explanations.

### 4.1.2 BCVI of the ankylosed cervical spine after blunt trauma (II)

A manual review of CTAs imaged for detection of BCVI during a period of eight years and six months (October 2011 to March 2020) included 5867 patients. In the cervical spine of the 5867 patients with blunt trauma, 153 had ankylosis of at least three consecutive vertebral bodies visible in CT and were included in this study.

## 4.2 Methods

For both imaging of the spine and the craniocervical arteries, a 64-slice CT scanner (Discovery CT 750 HD, GE Healthcare, Milwaukee WI) acquired 2 mm coronal, sagittal, and axial reformats from the basic volumetric dataset with a slice thickness of 0.625 mm. The trauma protocol consists of a whole-body CT (WBCT) imaged with a split-bolus from clavicles to ischium with simultaneous arterial and venous phases including a non-enhanced head CT. Each WBCT starts with the cervical spine and the craniocervical arteries being imaged from the aortic arch to the skull base using an 80-ml contrast-media bolus continued by a second 50- ml bolus with a preceding 40-s delay. The first and second boluses have flow rates of 5 ml/s and of 4 ml/s.

In cases of facial trauma, the basic cervical CTA dataset is expanded to cover the facial bones from which the 2-mm slices for imaging facial fractures are reformatted. Reformats in axial, coronal, and sagittal planes with a slice thickness of 2 mm are then created in both soft tissue and bone kernel, in addition to maximum intensity projection (MIP) images.

If a patient is diagnosed with a BCVI, a follow-up CTA after two weeks is performed and immediate anticoagulation commenced.

MRI scans were imaged by a 1.5-T closed-bore scanner (Signa LX 1.5 T, GE Healthcare). The trauma protocol for MRI of the spine includes both T2- and T1-weighted images in sagittal and axial planes as well as STIR images in the sagittal plane. In the cervical spine, a coronal-plane fat-saturated T2-weighted sequence is included in addition to the aforementioned sequences. Additional optional sequences can be done at the attending radiologist's request. Patients in need of imaging of the craniocervical arteries, but for whom iodine is contraindicated, are imaged with magnetic resonance angiography (MRA). The protocol consists of unenhanced time-of- flight magnetic resonance angiography (TOF MRA) and T1-weighted, fat-saturated three-dimensional turbo spin-echo (3D TSE SPACE) sequences.

All CT, CTA, and MRI scans with the corresponding referrals were retrieved and reassessed manually in each study using the Impax Picture Archiving and Communications System (Impax 6, Agfa Healthcare NV, Mortsel, Belgium).

SPSS v.25 (IBM Corp., Armonk NY, USA) served for all statistical analyses. P-values < 0.05 we considered statistically significant.

Patients' neurological status regarding the SCI at each stage of the medical treatment period was concluded from their electronic medical records by use of Frankel grading (Table 1) (Frankel et al. 1969).

The radiologists who participated in the reading of images were R1, R2, R3, and R4 with their experience level in musculoskeletal and trauma radiology being a respective 5 months, 10 years, 15 years, and 16 years. R1 and R3 participated in all studies, R2 participated in Studies II and III, R4 participated in Study I.

The definition for the strength of agreement for Cohen's κ was as follows: values < 0, no agreement; 0–0.20, slight agreement; 0.21–0.40, fair agreement; 0.41–0.60, moderate agreement; 0.61–0.80, substantial agreement; 0.81–1, almost perfect agreement (Landis et al. 1977).

**Table 1** Description of Frankel grade classification used for clinical evaluation of neurological injury (Frankel HL, Hancock DO, Hyslop G, Melzak J, Michaelis LS, Ungar GH, Vernon JD, Walsh JJ. The value of postural reduction in the initial management of closed injuries of the spine with paraplegia and tetraplegia. I. Paraplegia. 1969;7(3):179-92.)

| Grade | Description of neurological deficit |
|---|---|
| A | Complete neurological injury with no motor or sensory function below level of lesion |
| B | Complete motor paralysis below level of lesion with possible sensory function present |
| C | Nonfunctional motor power present below level of lesion |
| D | Functionally useful motor power with possible partial sensory failure below level of lesion |
| E | Normal motor and sensory function with possible abnormal reflexes below level or lesion |

### 4.2.1 Post-traumatic spinal hematoma in patients with ankylosing spondylitis (I)

Fracture level and morphology were recorded, as well as the extent and dimensions of hematoma and spinal canal narrowing. Measurements of bony spinal canal and the definitive spinal canal narrowing, of which the latter comprised the spinal hematoma and bony fragments, were made from the midsagittal plane in the MRI. Spinal hematoma pressure displacing CSF was considered a significant indication of mass effect.

R1, R2, and R4 reviewed MRI scans independently and blinded to one another and to the initial reports. The variables for blinded review comprised the presence of spinal hematoma, mass effect, T1 and T2 signal intensity and

heterogeneity, SCI, and spinal cord impingement. Disagreements were settled by consensus.

Dual-energy x-ray absorptiometry (DEXA) scans, if available within two years of the injury, determined the presence of osteoporosis. If patients lacked DEXA scans, CT scans were evaluated for signs of visually decreased bone density.

Regular anticoagulation therapy was recorded.

The percentage of agreement and Krippendorff's alpha measured the inter-rater agreement between radiologists. The Mann-Whitney U test explored the association between Frankel grade after surgery and spinal cord impingement. The Wilcoxon signed-rank test compared Frankel grades before and after surgery. Hematoma T1- and T2 signal intensity and heterogeneity were compared to the delay between trauma and the initiation of the MRI by use of Mann-Whitney U and Kruskal-Wallis tests. Spearman's ρ evaluated the correlation between Frankel grade after surgery and bony spinal canal narrowing, as well as Frankel grade after surgery and the definitive spinal canal narrowing.

### 4.2.2 BCVI in patients with ankylosed cervical spine after blunt trauma (II)

BCVI and the associated stroke were primary variables. Predictive variables were cervical spine fracture, and facial-, and skull fracture. Other variables were age, gender, etiology, and levels of ankylosis, trauma mechanism, and traumatic brain injury (TBI).

Stroke was reviewed from nonenhanced head CT and from an MRI when available, as well as TBI defined as subdural, subarachnoideal, epidural, intraparenchymal hemorrhage, or contusion (visible only on MRI).

R1 and R3, blinded to the original reports, reviewed the 153 patients for the etiology of ankylosis. R1, R2, and R3 evaluated the 153 CTAs for BCVIs according to Biffl et al. (1999) (Fig. 15). Disagreements were settled by consensus.

Follow-up CTA classification was defined as grade 1, completely healed; grade 2, reduced Biffl grade; grade 3, no change; grade 4, increased Biffl grade.

The etiology of ankylosis included AS or SpA, DISH, DS, or surgical fusion.

Regular anticoagulation therapy was recorded.

Associations between the aforementioned variables and BCVI were analyzed as follows: cervical spine fracture, $\chi 2$ test; skull fracture, Fisher's test; gender, $\chi 2$ test; age, Mann-Whitney U test. Only those patients with a single fracture variable were involved in calculations for statistical association with BCVI. All variables except for age were analyzed by a logistic regression model to predict the relative risk for BCVI. Correlations between number of fractured vertebrae, as well as transversely fractured intervertebral discs, and the number of ankylosed vertebrae we evaluated with Spearman's ρ. Interobserver agreement on analysis of etiology in

ankylosis achieved between radiologists, as well as for BCVI findings between radiologists and the consensus reading were calculated using Cohen's κ (Landis et al. 1977).

### 4.2.3 Post-traumatic spinal hematoma in patients with DISH (III)

The AOSpine classification (Divi et al. 2019) and the three-column concept by Denis (1983) served for the classification of morphology and stability of spinal fractures. The extent and dimensions of spinal hematomas were recorded. A spinal hematoma was the primary outcome; SCI and spinal-cord impingement were the secondary outcomes. Patients with at least one injury in addition to a spinal fracture were defined as having polytrauma (Hebert et al. 2000). The width of the dural sac, measured from sagittal images at the narrowest point perpendicular to the spine at fracture level, defined the narrowing of the spinal canal. This narrowing, divided by the mean width of the adjacent levels, defined the relative spinal canal narrowing.

Neurological status was recorded at three points in time: paramedics' reports during their first encounter ($Frankel_{para}$), attending physicians' evaluation before the decision as to treatment method ($Frankel_{ward}$), and before transfer to a further-treatment unit ($Frankel_{final}$). Frankel Δ, calculated by ($Frankel_{final}$–$Frankel_{ward}$)/ $Frankel_{final}$, represented the change in neurological status after treatment.

Patients were divided into four groups: surgically treated cervical spine fractures (Group 1 with 26 patients), surgically treated thoracolumbar fractures (Group 2 with 19 patients), conservatively treated cervical spine fractures (Group 3 with 14 patients), and conservatively treated thoracolumbar spine fractures (Group 4 with 11 patients).

Spearman's ρ was allowed evaluation of the correlation between relative spinal canal narrowing and $Frankel_{ward}$. Association between spinal cord impingement and $Frankel_{ward}$ in all groups was analyzed with Mann-Whitney U test. Evaluation of the effect of spinal hematoma on neurological status was analyzed between decompressed patients and (spinal hematoma indicated as a dichotomic ordinal value) vs. Fankel Δ by the Mann-Whitney U test. The Wilcoxon signed-rank test compared the longitudinal change between $Frankel_{para}$ and $Frankel_{ward}$ in test 1 as well as between $Frankel_{ward}$ and $Frankel_{final}$ in test 2. Interobserver agreement between R1 and R2 for etiology of ankylosis and between R1 and R3 for MRI findings was calculated by Cohen's κ (Landis et al. 1977).

# 5 Results

## 5.1 General results

Demographic data including trauma mechanisms and relevant patient history is shown in Table 2, which serves as a reference for all three studies.

**Table 2** Demographics, trauma mechanisms, and primary variables in Studies I, II, and III. IQR, interquartile range; BCVI, blunt cerebrovascular injury; MVA, motor vehicle accident.

| Variable | Study I | Study II | Study III |
|---|---|---|---|
| | n = 28 | n = 153 | n = 70 |
| Median age | 55.5 (IQR: 49.3 – 76) | 75 (IQR: 67.5 – 82) | 73 (IQR: 66 – 81) |
| Men | 24, 86% | 111, 73% | 54, 77% |
| Women | 4, 14% | 42, 27% | 16, 23% |
| Trauma mechanisms | | | |
| Ground level fall | 20, 83% | 125, 82% | 48, 69% |
| MVA | 4, 14% | 14, 9% | 10, 14% |
| Bicycle | | 6, 4% | 3, 4% |
| Pedestrian struck | | 2, 1% | |
| Struck by object | | 1, < 1% | |
| Fall from > 2 meters | 3, 11% | 5, 3% | 9, 13% |
| Assault | 1, 4% | | |
| Spinal hematoma | 24, 86% | 20, 13% | 37, 53% |
| Spinal cord impingement | 15, 54% | 25, 16% | 47, 67% |
| SCI | 8, 29% | 17, 11% | 43, 61% |
| Patients with BCVI | | 29, 19% | 5, 7% |
| Strokes from BCVI | | 6, 4% | |

### 5.1.1 Post-traumatic spinal hematoma in patients with ankylosing spondylitis (I)

The 28 (24 men, median age 55.5) who had a fully ankylosed spine from AS and at least one spinal fracture included 24 with a pre-existing diagnosis of AS in their medical records.

The most common trauma mechanism was ground-level fall (71%), followed by MVA (14%) (Table 2); 32 fractures affected 41 vertebrae and 17 IVDs and were distributed as follows: 19 in the cervical spine, 12 in the thoracic spine, and one in the lumbar spine. The main fracture line ran through IVDs in 15, and through vertebrae in 17 fractures. All but one patient had unstable fractures.

Of the 32 fractures, 25 were treated with posterior fixation, 4 with anterior fixation, and one with both approaches.

Ten patients had regular anticoagulation therapy on admission.

Of the 28 patients, 24 had spinal hematomas, of which 19 were epidural, with an incidence of 68%, and 5 were subdural, incidence, 18%. Hematoma median transverse dimensions in the transverse and anteroposterior width as well as the median craniocaudal extent were, respectively, 1.8 cm (interquartile range (IQR) 1.6–2.2), 0.5 cm (IQR 0.2–0.8), and 13.3 cm (IQR 4.9–20.9). Of the 24 hematomas, 14 caused mass effect; 17 had T1 signal isointense and 7 hyperintense to muscle; 20 had T2 signal hyperintense, 3 hypointense, and 1 isointense to muscle; 7 had T1 signal heterogeneity; and 12 had T2 signal heterogeneity.

Though not statistically significant (Mann-Whitney U test, $p = 0.53$), the delay between injury and MRI scan seemed shorter in T1 hyperintense than in isointense hematomas, with respective median delays of 32.0 hours (IQR 9.0–72.0) and 72.0 hours (IQR 14.5–145.5).

The delay was significantly increased in T1-heterogenous hematomas with a median delay of 96.0 hours (IQR 42.0–216.0) compared to non-heterogenous hematomas with median delay of 22.0 hours (IQR 8.5–72.0) (Mann-Whitney U test, $p = 0.047$).

The small number of hematomas prevented statistical analysis. One was iso and three were hyperintense on T2WI, while the rest were hyperintense to muscle without statistical significance in relation to delay (Kruskal-Wallis test, $p = 0.24$).

The Mann–Whitney U test failed to indicate any association between the delay and T2-heterogenous or non-heterogenous hematomas with a median delay of the former of 72 hours (IQR 17.5–192) and of the latter of 23 hours (IQR 9.3–72.0) ($p = 0.22$).

Of the three patients with DEXA scans performed within two years of the trauma, one had overt osteoporosis (T-score < -2.5). Twelve patients had visibly decreased bone density on CT.

The difference between Frankel grades before and after surgery was statistically significant, with their ordinal median values being 4.0 (IQR 3.0–5.0) and 5.0 (3.3–5.0) (Wilcoxon signed-rank test, p = 0.008).

Frankel grades after surgery were higher for those who had no spinal cord impingement than for those who did, with their ordinal median values being 5.0 (IQR 5.0–5.0) and 4.0 (IQR 3.0–5.0) (Mann-Whitney U test, p = 0.012).

Spinal canal narrowing after surgery, caused by either hematoma and bony fragments (Spearman's ρ 0.010, p = 0.96) or by only the bony fragments (Spearman's ρ 0.062, p = 0.76), lacked any correlation with Frankel grade.

Variables including T2 signal, presence of spinal hematoma, and spinal cord impingement were 0.69, 0.61, and 0.69, reaching their best scores for substantial agreement (Table 3). Readings were consistent with values of Cohen's κ for strength of agreement.

**Table 3** Interobserver agreement among R1, R2, and R4 denoted with Krippendorff's alpha and Percentage agreement. CI, confidence interval. Reproduced and modified by permission of Springer Nature

| Variable | Krippendorff's alpha (95% CIs) | Percentage agreement |
|---|---|---|
| T1 heterogeneity | 0.32 (0.05; 0.59) | 32 |
| T1 signal | 0.22 (-0.15;0.46) | 36 |
| T2 heterogeneity | 0.45 (0.21; 0.66) | 40 |
| T2 signal | 0.69 (0.53; 0.95) | 64 |
| Presence of spinal hematoma | 0.61 (0.48; 0.74) | 63 |
| Mass effect of spinal hematoma | 0.37 (0.12; 0.59) | 32 |
| Spinal cord injury | 0.52 (0.31; 0.73) | 61 |
| Spinal cord impingement | 0.69 (0.51; 0.82) | 71 |

### 5.1.2 BCVI in patients with ankylosed cervical spine after blunt trauma (II)

Of the 153 patients with cervical ankylosis of at least three consecutive vertebrae and blunt trauma, 29 (19%) had 36 BCVIs with an incidence of 19%. Of the 36 BCVIs, 32 were in VAs (89%), 3 in ICAs (8%), and one in a CCA (3%). Of the 29 patients, 2 had ipsilateral BCVIs in the right VA, 4 had bilateral VAs, and one patient each had a BCVI in the right VA or in the left ICA. The distribution of BCVIs across the cervical spine is shown in Table 4. The 36 BCVIs were graded according to Biffl et al. (Fig. 15) as 17 grade II, 4 grade III, 14 grade IV, and one grade V (Biffl et al. 1999).

Of the 29 patients, 6 had subsequent strokes, of which 4 were acute, and 2 occurred within 2 and 3 days. The four acute strokes were caused by grade IV BCVI in the right CCA, a grade IV BCVI in the left ICA, a grade IV BCVI in the right VA, and by two ipsilateral grade II BCVIs in the right VA. A grade IV BCVI in the right VA and a grade II BCVI in the left VA caused strokes with a delay of a respective two and three days. Of the 4 patients with injured carotid arteries, 2 developed anterior circulation strokes, and 4 (15%) of the 26 patients with injured VAs developed posterior circulation strokes.

The most common trauma mechanism was a ground-level fall (82%) followed by MVA (9%) and some bicycle accidents (4%) (Table 2).

Of the 82 patients with cervical spine fractures, 7 had a simultaneous skull- or facial fracture. Of the 26 patients with injured VAs, 24 had a cervical spine fracture, and one, a skull fracture. Only one patient with an injured VA had no fractures.

A further 18 patients (12%) had facial and 20 (13%) had skull fractures; 12 patients had only facial fractures without BCVIs. Of 8 patients with only skull fractures, one had a grade III BCVI in the right ICA.

TBIs occurred in 38 (25%) patients, and 45 patients had MRI scans that found 20 spinal hematomas, 17 SCIs, and 25 spinal cord impingements.

Of the 29 patients with BCVI, 13 had follow-up CTAs, and one had MRA because of kidney failure. The 14 patients had a combined 20 BCVIs, of which 3 (2 grade II in VAs and one grade IV in VA) healed completely, 6 (3 grade II in VAs, 2 grade IV in VAs, and 1 grade V in VA) improved to a lower Biffl grade, 9 (3 grade II in VAs, one grade III in VA, 4 grade IV in VAs, and one grade III in ICA) showed no change, and 2 (2 grade II in VAs) had an increased Biffl grade.

Of 10 severely injured patients with a BCVI, 8 (5 injured VAs and 3 carotid injuries) died within 30 days, and 2 with VA injury died in a further treatment unit within 2 and 3 months. Of the 4 patients with carotid injuries, 3 belonged to the

group dying within 30 days after trauma, reaching a mortality rate of 75% for carotid artery injury.

The cause of ankylosis was DS in 84 (55 %) patients, DISH in 41 (27%), SpA in 18 (12%), and surgical fusion in 10 (6%). The 82 patients with cervical spine fractures together had injuries comprising 93 fractured vertebrae and 25 fractured IVDs. Of these fractures, 36%, 59%, and 5% were located above, within, or beneath the ankylosed segment. The 59% (69) of the fractured vertebrae and IVDs which were located within the ankylosed segment were evenly distributed. Of the 82 patients, 37 (45%) had no documentation of ankylosis in their electronic records. Patients with insufficiently recognized ankylosis had etiologies for DS in 23 (62%), DISH in 11 (30%), surgical fusion in 2 (5%), and AS in one (3%) patient. Of the 10 patients with surgical fusion, 1 with posterior fixation, and 3 patients with ACDF had BCVIs.

Of 15 patients on regular anticoagulation therapy with coumarin derivatives or platelet-aggregation blockers upon admission, 14 commenced additional low-molecular-weight heparin, and one continued with regular warfarin, 8 who were without regular anticoagulation medication commenced low-molecular-weight heparin therapy, 7 took no anticoagulation because of TBI, massive cerebral infarction, or other severe injuries, and one patient had a BCVI that was initially missed.

The only variable predicting BCVI in the logistic regression model was cervical spine fracture, with an odds ratio of 7.44 (95% confidence intervals: 2.22–24.98, $p < 0.001$). The number of fractured vertebrae and IVDs correlated with the number of ankylosed IVDs (Spearman's $\rho$ 0.214, $p < 0.01$). Interobserver agreement as to the etiology of ankylosis between R1 and R3 was substantial, which also reflected the discrepancy for DISH and DS in 20 patients (Cohen's $\kappa = 0.73$, $p < 0.001$). The consensus reading on BCVIs showed an almost perfect agreement (0.892 – 0.889, $p < 0.001$).

**Table 4** The 36 BCVIs in 29 patients with ankylosed cervical spine distributed according to spinal level. CCA, common carotid artery; ICA, internal carotid artery; VA, vertebral artery

| Right CCA | Right ICA | Right VA | Level | Left VA | Left ICA | Left CCA |
|---|---|---|---|---|---|---|
| | | 1 | **C0** | | | |
| | 1 | 2 | **C1** | 2 | | |
| | | 5 | **C2** | 5 | | |
| | | 1 | **C3** | | | |
| | | | **C4** | 3 | | |
| | | 2 | **C5** | 1 | | |
| | | 3 | **C6** | 2 | | |
| | | 2 | **C7** | 1 | | |
| 1 | | 2 | **Th1** | | | |
| 1 | 1 | 18 | **Sum** | 14 | 2 | |

### 5.1.3 Post-traumatic spinal hematoma in patients with DISH (III)

Of the 70 patients (54 men, median age 73) with anterior ankylosis of at least 4 consecutive vertebrae from DISH plus a spinal fracture, 37 (53%) had spinal hematoma, 47 (67%) had spinal cord impingement, and 43 (61%) had SCI (Table 2). Of the hematomas, 34 were epidural and 3 subdural, with incidences of 49% and 4%. Thirty patients had spinal cord impingement as well as spinal hematoma due to spinal fracture. Seven patients with SCI had hemorrhage within the spinal cord. A patient with a spinal epidural hematoma (SEH) causing spinal cord impingement refused surgical treatment, which ultimately resulted in SCI.

Hematoma median transverse dimensions in the transverse and anteroposterior width as well as the median craniocaudal extent were a respective 2.1 cm (IQR 1.8 – 2.4), 0.5 cm (IQR 0.5 – 0.7), and 7 cm (IQR 3.6 – 15).

The most common trauma mechanism was ground-level fall (69%), followed by MVA (14%) and a fall from a height of over 2 m (13%) (Table 2).

Of 21 patients with polytrauma, 5 had either TBI, skull fracture, or facial fracture, and 5 had a BCVI in addition to a spinal fracture.

Of the 70 patients, 66 (94%) had an unstable fracture out of the total of 153 fractures. Of 80 type B fractures, 60 ran transversely only through the vertebral body, and the rest continued also to the IVD; 21 fractures ran through the IVD. The 27 Type A fractures comprised 8 burst and 19 compression fractures. Two patients had a Jefferson's fracture and 3 had a Hangman's fracture. The distribution of fractures according to vertebral level showed peaks in the following order: at the CTJ, CCJ, and TLJ.

Of 45 patients treated surgically, 41 (91%) underwent posterior fixation. Four patients had unstable cervical spine fractures, of whom 2 had both anterior and posterior fixation as well as 2 with anterior fixation. Of 30 patients with spinal hematoma, 20 had decompression during posterior fixation. Of 25 conservatively treated patients, 10 had spinal hematoma.

The results of the statistical analysis are shown in Tables 5 to 7. The relative spinal canal narrowing correlated with neurological status before treatment ($Frankel_{ward}$) (Spearman's $\rho$ 0.519, $p < 0.001$). Spinal cord impingement had associations with $Frankel_{ward}$ in surgically ($p = 0.004$) and conservatively ($p < 0.001$) treated patients (Mann-Whitney U test). Patients who had decompression for the spinal hematoma showed no association with their change in neurological status (Frankel $\Delta$) (Mann-Whitney U test, $p = 0.53$). Variables of test 1 showed significance in Group 2 ($p = 0.024$) as well as variables of test 2 in Group 1 ($p < 0.001$) and Group 2 ($p = 0.004$) (Wilcoxon signed-rank test). For the etiology of ankylosis, the interobserver agreement was moderate between R1 and R2 ($\kappa = 0.570$, $p < 0.001$). For spinal hematoma, SCI, and spinal cord impingement, the agreement between R1 and R3 was respectively moderate ($\kappa = 0.602$) and substantial ($\kappa = 0.683$) and substantial ($\kappa = 0.664$), ($p < 0.001$).

**Table 5** Statistical results from Mann-Whitney U tests and Spearman's ρ

| Test variables | Statistical tests and results |
|---|---|
| Spinal canal narrowing vs. $Frankel_{ward}$ | Spearman's ρ 0.519, $p < 0.001$ |
| Spinal cord impingement in surgically treated patients vs. $Frankel_{ward}$ | Independent samples Mann-Whitney U test, $p = 0.004$ |
| Spinal cord impingement in conservatively treated patients vs. $Frankel_{ward}$ | Independent samples Mann-Whitney U test, $p < 0.001$ |
| Presence of spinal hematoma in patients treated with decompression vs. Frankel Δ | Independent samples Mann-Whitney U test, $p = 0.53$ |

**Table 6** Statistical results of longitudinal test 1. Patients: Group 1, surgically treated cervical spine fractures; Group 2, surgically treated thoracolumbar spine fractures; Group 3, conservatively treated cervical spine fractures; and Group 4, conservatively treated thoracolumbar spine fractures

| Groups | Test 1 variables | Related samples Wilcoxon signed-rank test |
|---|---|---|
| Group 1 | $Frankel_{para}$ vs. $Frankel_{ward}$ | $p = 0.129$ |
| Group 2 | $Frankel_{para}$ vs. $Frankel_{ward}$ | $p = 0.024$ |
| Group 3 | $Frankel_{para}$ vs. $Frankel_{ward}$ | $p = 0.257$ |
| Group 4 | $Frankel_{para}$ vs. $Frankel_{ward}$ | $p = 0.317$ |

**Table 7** Statistical results of longitudinal test 2. Patients: Group 1, surgically treated cervical spine fractures; Group 2, surgically treated thoracolumbar spine fractures; Group 3, conservatively treated cervical spine fractures; and Group 4, conservatively treated thoracolumbar spine fractures

| Groups | Test 2 variables | Related samples Wilcoxon signed-rank test |
|---|---|---|
| Group 1 | $Frankel_{ward}$ vs. $Frankel_{final}$ | $p < 0.001$ |
| Group 2 | $Frankel_{ward}$ vs. $Frankel_{final}$ | $p = 0.004$ |
| Group 3 | $Frankel_{ward}$ vs. $Frankel_{final}$ | $p = 0.063$ |
| Group 4 | $Frankel_{ward}$ vs. $Frankel_{final}$ | $p = 1$ |

# 6 Discussion

## 6.1 Post-traumatic spinal hematoma in patients with ankylosing spondylitis (I)

This study is based on the MRI features of spinal hematoma and neurological status in AS patients with spinal fracture. The literature prior to this study consisted of case reports including very few AS patients with SEH that coincided with spinal fracture (Foo & Rossier 1982, Jacobs & Fehlings 2008, Al-Mutair & Bednar 2010), of literature reviews (Westerveld et al. 2009b), and of a series of patients with different etiologies for ankylosis (Vazan et al. 2019). A study published at the same time as the current one, stood out for its high number of AS and DISH patients, in which 60 MRI-imaged AS patients had SEH at an incidence of 43% (Shah et al. 2021). Results of 68% and 18% for the incidence of SEH and of SSH far exceed the assumed expectations based on the studies mentioned above.

Because this topic continued to inspire interest, studies appeared as case reports of AS and with cohorts having both DISH and AS, without distinction between the two patient groups relating to spinal hematoma (Schwendner et al. 2021, Berglar et al. 2023). A study published right after Study I, found among 164 patients in a cohort gathered by artificial intelligence software from electronic medical records without a radiological blinded review for spinal hematoma nor with any inspection of the true etiology for the ankylosis, SEH with an incidence of 10.4% (Hanna et al. 2021). Despite the impressively large cohort, the authors stated that the incidence of SEH may be either over- or underestimated.

Although almost all fractures were caused by hyperextension and were unstable, the most common trauma mechanism was a low-energy ground-level fall, reflecting the biomechanically weakened state of the ankylosed spine. The lower part of the cervical spine is physiologically less mobile than the upper part (Nowitzke 1994, Jaumard et al. 2011, Dalley et al.2023). This immobility, when combined with ankylosis, osteoporosis (Bessant et al. 2002), and the pronounced thoracic kyphosis in AS patients, is closely tied to the majority of unstable fractures occurring in the area of the lower cervical spine and CTJ. This is also suggested in Study I and in many preceding studies (Caron et al. 2010, Lukasiewicz et al. 2016, Teunissen et al. 2017).

A large spinal hematoma with median thickness in the anteroposterior of 0.5 cm and in the median with a craniocaudal extent of over 13 cm can be expected to be clearly distinguishable on MRI. We, however, found a hyperintense T2 signal to be the only reliably identifiable MRI feature. A study with a larger cohort might confirm a possible relationship between T1 signal intensity of spinal hematoma and an imaging delay.

Surgery offered stabilization for the fracture and (a) generally improved neurological status. Because in AS patients, cervical spine fracture surpasses cardiovascular disease, pneumonia, and sepsis as the leading cause of death, timely management of the condition is crucial (Wysham et al. 2017). Patients with low-energy trauma and a current diagnosis or features of AS visible in radiographs should have an immediate CT or MRI scan; both may even be deemed necessary, for the timely diagnosis and appropriate management of a possible fracture.

Our small number of patients is this study's obvious limitation. The inclusion criteria required both CT and MRI scans be obtained for the appropriate diagnosis of spinal fracture and spinal hematoma in patients with advanced ankylosis from AS. That study design produced a selective cohort of patients, because emergency MRI scans were limited to patients with acutely decreased neurological status and already high suspicion of spinal-canal compromise. However, AS patients with a well-positioned but unstable spinal fracture usually are eventually imaged by either CT or MRI. In the absence of prospective studies, the true incidence of spinal hematoma remains obscure.

## 6.2 BCVI in patients with ankylosed cervical spine after blunt trauma (II)

The literature is scarce on ankylosed spine and BCVI in the context of spinal trauma. In one study of 253 patients with blunt trauma to the cervical spine, five patients had either AS or DISH, of which three had an injury in the VA (Lebl et al. 2013). For these patients, neither the length of the ankylosed segment nor its anatomical location appeared in the report. This very limited data suggests an association between BCVI in VA and ankylosed spine.

The present study found BCVI with an incidence of 19% in patients with ankylosed cervical spine of at least three consecutive vertebrae, which is over seven times as high as for the general blunt-trauma population (Weber et al. 2018, Bensch et al. 2019). With a ground-level fall being the most common trauma mechanism (82%), patients with ankylosed cervical spine are notably in danger of strokes after any seemingly harmless trauma. Though a previous study of elderly patients over age 65 found an incidence of 0.3% for BCVI from ground-level falls (Gorman et al. 2020), we found in the current study, for the same demographic and trauma mechanism, an incidence of 20.1%. This suggests that ankylosis of the cervical spine is a major risk factor for BCVI and increases the relative risk up to 67-fold in that demographic.

When examining trauma mechanisms and trauma energy experienced by patients with and without cervical spine ankylosis, a BCVI seems to occur from low-energy trauma in a ground-level fall for the former, and from high-energy trauma such as an MVA for the latter (Biffl et al. 2000, Cothren et al. 2004, Eastman et al. 2006, Stein et al. 2009, Bromberg 2010, Fleck et al. 2011, Wang et al. 2012, Esnault et al. 2017, Rutman et al. 2018, Weber et al. 2018, Bensch et al. 2019, Leichtle et al. 2020). Since BCVI naturally correlates with a concomitant cervical spine fracture, which is reflected in the original Denver criteria, but BCVI also correlates with chest injury in patients both with and without cervical spine ankylosis, an index of suspicion for BCVI should be high, even in the absence of cervical fracture (Bensch et al. 2019).

During a high-energy deceleration causing a chest injury, the inertia of especially the head with a fixated torso such as in a seat belt, can cause stretching and shearing of the cervical arteries. This is a typical mechanism of injury in BCVI for patients without ankylosed cervical spine (Rutman et al. 2018). In patients with an ankylosed cervical spine, a BCVI occurs mostly (89%) in the VAs at fracture level, indicating a direct crushing or shearing injury caused by the sharp fracture edges. Leverage forces of ankylosed segments may also cause distension of the cervical arteries adjacent to the fracture. With cervical spine fracture being a strong

predictive factor for BCVI, a patient experiencing a blunt trauma with an ankylosed cervical spine of at least three consecutive vertebrae is unlikely to have a BCVI without a cervical spine fracture. This finding might alleviate the difficulty of the workup in differential diagnosis of intimal irregularities caused by atherosclerosis and a suspected grade I BCVI.

We found most of the BCVI in this study in the VAs, with 15% suffering temporally related strokes, similar to the figure of 17% reported by Fink et al (2011). Nevertheless, the published literature suggests a wide range of incidences from 0 to 24%, which might reflect differences in imaging quality, small case numbers, or selection bias, to name just a few (Biffl et al. 2000, Cothren et al. 2004, Fassett et al. 2008, Berne et al. 2009, Fink et al. 2011, Lytle et al. 2018).

BCVIs are generally treated by anticoagulation medication, which might be contraindicated in polytrauma patients facing an unacceptable risk of hemorrhage, for instance in the CNS or in major organ disruption. The four patients with BCVIs in the CCA artery and three ICAs were excluded from anticoagulation due to massive infarction, TBI, or unconsciousness at admission. A recent study found that VA injuries already present on admission, or occurring within the first 24 hours, had a 13.6% stroke rate (Boggs et al. 2024). A patient in our study had a cerebellar infarction two days after the initial injury from a grade IV BCVI in the right VA. The Boggs study also claimed that anticoagulation can be safely deployed regardless of the grade of BCVI, obviously excluding grade V. A concomitant injury in polytrauma such as a TBI or spinal injury may delay or even prevent the initiation of anticoagulation treatment. A prospective multi-center study stated that the delay between injury and initiation of anticoagulation does not increase stroke rate but results in more severe injury (Appelbaum et al. 2022). This fact further emphasizes the need for timely diagnosis and initiation of treatment. All but one of the patients in this study had anticoagulation for the primary treatment method, as one had a grade V BCVI, became acutely unstable, and received endovascular treatment.

AS is the most commonly recognized cause of spinal ankylosis, and cervical spine fracture its most feared complication. As a relatively rare condition, it nevertheless was only the third most common cause of ankylosis of four causes we identified for this study, with the most common being DS and second most common, DISH. The high prevalence of DS is an expected feature of an aging population. A Norwegian study found that the annual rate of cervical spine fractures in AS patients dropped steadily, by up to 8.4% during its eight-year period (Rydning et al. 2024). Deployment of the relatively new class of biological disease-modifying antirheumatic drugs might explain those favorable results, assuming that AS patients receive the appropriate treatment before the spine becomes ankylosed.

The biomechanics of the ankylosed cervical spine is demonstrated by the highly significant correlation between the number of successively ankylosed vertebrae and the number of fractured vertebrae and IVDs. Although the

distribution of fractures within the ankylosed segment showed no obvious peak, the location of fractures outside the ankylosed segment emerged superiorly. The area of the CCJ situated between the ankylosed segment and the head is subject to increased forces due to residual flexion/extension and rotation taking place only in this still mobile segment, making it vulnerable to excessive forces. This reflects the peak of BCVIs at the C2 level, which is similar in patients without ankylosis of the cervical spine, who nevertheless have the majority of BCVIs in the ICAs (Bensch et al. 2019).

DS as the most common etiology for ankylosis was also least documented in the radiological reports, presumably since the majority of the patients had only a partly ankylosed spine, and the condition remained underappreciated. Raising awareness of ankylosis from DS as a risk factor for BCVI is likely to reduce serious strokes by facilitating access to screening, timely diagnosis, and earlier treatment.

The retrospective study design was a limitationas well, since not all patients had BCVI follow-up imaging. Furthermore, the limited number of cases prevented statistical analysis of some variables.

## 6.3 Post-traumatic spinal hematoma in patients with DISH (III)

Several studies have reported an incidence for spinal epidural hematoma in DISH patients after blunt trauma ranging from 0% to 19.2% with a mean value of 7.1% (Caron et al. 2010, Bransford et al. 2012, Balling & Weckbach 2015, Okada et al. 2017, Teunissen et al. 2017, Okada et al. 2019, Shah et al. 2021).

This study found spinal hematoma as a complication in blunt-trauma patients with DISH and spinal fractures at an incidence of 53%, of which 49% were SEHs and 4% were SSHs. Those incidences markedly exceed the previously published percentages, with the current study being the only one using double-blinded reading. Since SEH and especially SSH present a considerable diagnostic challenge, it seems likely that keyword searches without manual review will miss a large number of those cases. Moreover, likely contributing to the discrepancy is the overall experience level and exposure to spinal hematoma cases of the radiologists interpreting the images.

The majority of patients fell at ground level, while non-AS patients tended to experience higher trauma energies, reflecting the restrictions in activity that AS patients face (I).

The ankylosis of the thoracic spine typically seen in DISH patients did not particularly change the distribution of fractures, with the most common level for spinal fractures being in the lower cervical spine analogous to that in general-trauma populations (Niemi-Nikkola et al. 2018). With increasing trauma energy, the distribution might still have shifted towards the lumbar spine, as occurs in the general population of trauma patients, due to numerous factors (Bensch et al. 2004, Bensch et al. 2011, Balling & Weckbach 2015, Okada et al. 2019).

AOSpine classification type B fracture was most common, and the likely explanation is the hyperostotic syndesmophytes at the level of the IVDs. Those osteophytes are generally denser than the vertebral body, which seems to protect the disc space, whereas the vertebral body becomes more vulnerable to fractures (Westerweld et al. 2009a). Any fracture involving the middle column is, according to Denis (1983), considered unstable. If a fracture in a DISH patient without neurological deficit is considered isolated on CT images, the posterior ligaments in one study were injured in 18% (Shah et al. 2021).

Both spinal-canal narrowing and spinal cord impingement correlated with neurological status before treatment, reflecting earlier reports of an expansive spinal hematoma causing neurological deficits within hours (Lawton et al. 1995). On the other hand, in our own study, decompression did not affect neurological status among patients with spinal hematoma treated with posterior fixation, which

might be a result of relatively low case numbers. However, one patient developed permanent SCI from a spinal hematoma which was not evacuated since it was located on a separate level above the fracture. This confirms that a spinal hematoma itself is sufficient to cause severe SCI.

The neurological status of all surgically treated patients improved, confirming the benefits of operative management for neurological outcome. Patients with thoracolumbar fractures chosen for surgery developed neurological deficits after the initial injury, which suggests secondary neurological deterioration. Conservative treatment is a viable alternative in cases with unfavorable prognosis for surgical intervention due to severity of the injury or concomitant injuries, or because of other contraindications.

The small number of patients and retrospective study design were limitations of this study. Since particularly patients with clinical findings of neurological deterioration were subjected to MRI scans, selection bias is likely, favoring those patients over those without neurological deterioration, obscuring the true incidence of spinal hematoma. Because this study was conducted in a level-one trauma center with a focus on patients with severe injuries, selection bias may have affected the incidences.

# 7 Conclusions

## 7.1 Post-traumatic spinal hematoma in patients with ankylosing spondylitis (I)

Spinal hematoma is a common complication of blunt trauma in AS patients with advanced spinal ankylosis. As a concomitant injury generally following a fall at ground level, SEH shows an incidence of 68% and SSH of 18%. The deteriorating neurological status correlates with spinal cord impingement. These patients with unstable spinal fractures benefit from surgery. T1 heterogeneity is an MRI feature related to significant delay in imaging with a mean of four days after the initial injury.

## 7.2 BCVI in patients with ankylosed cervical spine after blunt trauma (II)

Even though trauma energies tend to be lower than in the general trauma population, ankylosis of at least 3 consecutive cervical vertebrae leads to an increased incidence of BCVI up to sevenfold. Of BCVIs in ankylosed spines, 89% were located in the VAs. The most common etiology of ankylosis was DS, a condition (which was) severely underreported both in patient records and in radiological reports.

## 7.3 Post-traumatic spinal hematoma in patients with DISH (III)

A fall from standing height may cause hyperextension injury in DISH patients, resulting in an unstable AOSpine classification type B spinal fracture. A spinal hematoma, spinal cord impingement, and SCI with incidences of 53%, 67%, and 61%, are common concomitant injuries in DISH patients with blunt trauma. A spinal hematoma, if not treated with decompression, has the potential of causing spinal cord impingement leading to permanent SCI.

# ACKNOWLEDGEMENTS

This study was carried out at HUS Diagnostic Center, in the Department of Radiology, at Töölö Hospital, and at the Bridge Hospital in 2019–2024. I thank Professor Taina Autti for acting as the custos and for providing excellent working and research facilities.

First and foremost, I'm thankful to my supervisors Docent Mika Koivikko and Frank Bensch MD, PhD, for the opportunity to do research in the first place, for the original ideas and concepts of the research, and for their constant support and trust in the face of a workload that sometimes seemed exhausting.
Thanks to Frank, for being able to prioritize this thesis in the midst of all the commotion, and for his comprehensive aid from the beginning till the very end.
Thanks to Mika, for being able to create a versatile view of (doing) research and for reminding me about more important things.
Both gentlemen had the open-mindedly positive attitudes which influenced my efforts and at the same time set examples of professionalism to strive for.

I warmly thank Docents Jaakko Niinimäki and Jukka Huttunen for evaluating this study and for the constructive feedback which gave the opportunity for improving it in many ways.

I express my sincere gratitude to Professor Roberto Blanco Sequeiros for being the opponent.

It's been a pleasure to work with the co-authors Ville Haapamäki MD, PhD, and Docents Liisa Kerttula and Jari Siironen. (Special thanks to Ville Haapamäki, who offered his immediate contributions, which repeatedly exceeded expectations in terms or speed and knowledge.) Your contributions sped up the research and provided an intriguing educational experience in science.

I truly appreciate the expert assistance I received from Paula H. Bergman and Olavi Koivisto for the statistical analysis. Thanks to Paula, for her patient and perceptive help in the consideration of the statistical setups, which significantly contributed to

the quality of the research. Thanks to Olavi, for taking on the pending work on such short notice, while staying on schedule.

I extend my warmest thanks to my fellow radiologists working in the Department of Musculoskeletal and Trauma Radiology and in other departments of Meilahti University Hospital for their constant encouragement, positive attitude, and occasional non-medical or non-scientific comments. I would especially like to thank Mari Nummela for her open and kind help, practical tips and instructions in making of this thesis.

Dearest thanks to my mother Annikki, to my late father Tapio, and to my older sister Inkeri for their love and support that I've always been so lucky to enjoy.

Finally, I am deeply grateful to Miia for love and patience. I am extremely lucky to share my days with her and with our wonderful children, Aleksi and Reetta, not to forget forever lovely Lissu.

This study was supported by grants from the Finnish Musculoskeletal Society and from the Finnish Radiological society.

Espoo, January 2025

# REFERENCES


Agostini A, Borgheresi A, Granata V, Bruno F, Palumbo P, De Muzio F, Bicci E, Grazzini G, Grassi F, Fusco R, Barile A, Miele V, Giovagnoni A. Technological advances in body CT: a primer for beginners. Eur Rev Med Pharmacol Sci. 2022;26(21):7918-7937.

Alaranta H, Luoto S, Konttinen YT. Traumatic spinal cord injury as a complication to ankylosing spondylitis. An extended report. Clin Exp Rheumatol. 2002;20(1):66-68.

Al-Mutair A, Bednar DA. Spinal epidural hematoma. J Am Orthop Surg. 2010;18(8):494-502.

Anipindi S, Ibrahim N. Epidural Haematoma Causing Paraplegia in a Patient with Ankylosing Spondylitis: A Case Report. Anesth Pain Med. 2017;7(2)e43873.

Appelbaum RD, Esposito E, Spaulding MC, Simpson JP, Dunn J, Zier LB, Burruss S, Kim PP, Jacobson LE, Williams JM, Nahmias J, Grigorian A, Harmon L, Gergen AK, Chatoor M, Rattan R, Young AJ, Pascual JL, Murry J, Ong AW, Muller A, Sandhu RS, Bugaev N, Tatar A, Zreik K, Lieser MJ, Stein DM, Scalea TM, Lauerman MH. Does treatment delay for blunt cerebrovascular injury affect stroke rate?: An EAST multicenter study. Injury. 2022;53(11):3702-3708.

Azhar S, Chong LR. Clinician's guide to the basic principles of MRI. Postgrad Med J. 2023;99(1174):894-903.

Bagheri H, Govsa F. Anatomy of the sacral hiatus and its clinical relevance in caudal epidural block. Surg Radiol Anat. 2017;39(9):943-951.

Balling H, Weckbach A. Hyperextension injuries of the thoracolumbar spine in diffuse idiopathic skeletal hyperostosis. Spine (Phila Pa 1976). 2015;40(2):E61-E67.

Bansal GJ. Digital radiography. A comparison with modern conventional imaging. Postgrad Med J. 2006;82(969):425-428.

Benek B, Yilmaz H, Akçay E, Yurt A. Bilateral vertebral artery occlusion after traumatic complete disruption of the cervical spine associated with ankylosing spondylitis. Ulus Travma Acil Cerrahi Derg. 2021;27(6):697-701.

Bensch FV, Kiuru MJ, Koivikko MP, Koskinen SK. Spine fractures in falling accidents: analysis of multidetector CT findings. Eur Radiol. 2004;14(4):618-624.

Bensch FV, Koivikko MP, Koskinen SK. MDCT findings in sports and recreational accidents. Acta Radiol. 2011;52(10):1107-1112.

Bensch FV, Varjonen EA, Pyhältö TT, Koskinen SK. Augmenting Denver criteria yields increased BCVI detection, with screening showing markedly

increased risk for subsequent ischemic stroke. Emerg Radiol. 2019;26(4):365-372.

Benson JC, Brinjikji W, Messina SA, Lanzino G, Kallmes DF. Cervical internal carotid artery tortuosity: A morphologic analysis of patients with acute ischemic stroke. Interv Neuroradiol. 2020;26(2):216-221.

Berglar IK, Williams GP, Catapano JS, Snyder LA. Spinal Subdural Hematoma in Ankylosing Spondylitis Patients Without Anticoagulation Therapy. Cureus. 2023;15(11):e48508.

Berne JD, Norwood SH. Blunt vertebral artery injuries in the era of computed tomographic angiographic screening. Incidence and outcomes from 8,292 patients. J Trauma. 2009;67(6):1333-1338.

Berne JD, Reuland KS, Villareal DH, McGovern TM, Rowe SA, Norwood SH. Sixteen-slice multi-detector computed tomographic angiography improves the accuracy of screening for blunt cerebrovascular injury. J Trauma. 2006;60(6):1204-1209.

Bessant R, Keat A. How should clinicians manage osteoporosis in ankylosing spondylitis? J Rheumatol. 2002;29(7):1511-1519.

Biffl WL, Moore EE, Elliott JP, Ray C, Offner PJ, Franciose RJ, Brega KE, Burch JM. The devastating potential of blunt vertebral arterial injuries. Ann Surg. 2000;231(5):672-681.

Biffl WL, Moore EE, Offner PJ, Burch JM. Blunt carotid and vertebral arterial injuries. World J Surg. 2001;25(8):1036-1043.

Biffl WL, Moore EE, Ryu RK, Offner PJ, Novak Z, Coldwell DM, Franciose RJ, Burch JM. The unrecognized epidemic of blunt carotid arterial injuries: early diagnosis improves neurologic outcome. Ann Surg. 1998;228(4):462-470.

Biffl WL, Ray CE Jr, Moore EE, Mestek M, Johnson JL, Burch JM. Noninvasive diagnosis of blunt cerebrovascular injuries: a preliminary report. J Trauma. 2002;53(5):850-856.

Biffl WL, Moore EE, Offner PJ, Brega KE, Fanciose RJ, Burch JM. Blunt carotid arterial injuries: implications of a new grading scale. J Trauma. 1999;47(5):845-553.

Blauth M, Bastian L, Knop C, Lange U, Tusch G. Inter-observer reliability in the classification of thoraco-lumbar spinal injuries [in German]. Orthopade. 1999;28(8):662-681.

Bogduk N, Mercer S. Biomechanics of the cervical spine. I: Normal kinematics. Clin Biomech (Bristol, Avon). 2000;15(9):633-648.

Bogduk N. Functional anatomy of the spine. Handb Clin Neurol. 2016:136:675-688.

Boggs HK, Tomihama RT, Tran Z, Mukherjee K, Turay D, Magtanong E, Pop A, Kiang SC. Medical Management of Traumatic Vertebral Artery Injury Is Safe Regardless of the Severity of Injury. Ann Vasc Surg. 2024:101:186-192.

Bradley WE Jr. MR appearance of hemorrhage in the brain. Radiology. 1993;189(1):15-26.

Bransford RJ, Koller H, Caron T, Zenner J, Hitzl W, Tomasino A, Mayer M. Cervical spine trauma in diffuse idiopathic skeletal hyperostosis: injury characteristics and outcome with surgical treatment. Spine (Phila Pa 1976). 2012;37(23):1923-1932.

Bromberg WJ, Collier BC, Diebel LN, Dwyer KM, Holevar MR, Jacobs DG, Kurek SJ, Schreiber MA, Shapiro ML, Vogel TR. Blunt cerebrovascular injury practice management guidelines: the Eastern Association for the Surgery of Trauma. J Trauma. 2010;68(2):471-477.

Brown CV, Antevil JL, Sise MJ, Sack DI. Spiral computed tomography for the diagnosis of cervical, thoracic, and lumbar spine fractures: its time has come. J Trauma. 2005;58(5):890-895.

Cairney J. Tortuosity of the Cervical Segment of the Internal Carotid Artery. J Anat. 1924;59(Pt 1):87-96.

Cappabianca S, Somma F, Negro A, Rotondo M, Scuotto A, Rotondo A. Extracranial internal carotid artery: anatomical variations in asymptomatic patients. Surg Radiol Anat. 2016;38(8):893-902.

Caron T, Bransford R, Nguyen Q, Agel J, Chapman J, Bellabarba C. Spine fractures in patients with ankylosing spinal disorders. Spine (Phila Pa 1976). 2010;35(11):E458-64.

Chance GQ. Note on a type of flexion fracture of the spine. Br J Radiol. 1948;21(249):452.

Chan BC, Cadarette SM, Wodchis WP, Krahn MC, Mittmann N. The lifetime cost of spinal cord injury in Ontario, Canada: A population-based study from the perspective of the public health care payer. J Spinal Cord Med. 2019;42(2):184-193.

Chelberg MK, Banks GM, Geiger DF, Oegema TR Jr. Identification of heterogenous cell populations in normal human intervertebral disc. J Anat. 1995;186 ( Pt1)(Pt1):43-53.

Cothren CC, Moore EE, Biffl WL, Ciesla DJ, Ray CE Jr, Johnson JL, Moore JB, Burch JM. Anticoagulation is the gold standard therapy for blunt carotid injuries to reduce stroke rate. Arch Surg. 2004;139(5):540-545.

Culleton S, Wiggins R, McNally JS. Imaging spectrum of extracranial arterial vascular pathology: pearls for the radiologist. Clin Radiol. 2022;77(3):167-178.

Dalley AF II, Agur AMR. Moore's Clinically Oriented Anatomy. Ninth edition. Lippincott Connect 2023.

Davis JW, Holbrook TL, Hoyt DB, Mackersie RC, Field TO Jr, Shackford SR. Blunt carotid artery dissection: incidence, associated injuries, screening, and treatment. J Trauma. 1990;30(12):1514-1517.

Denis F. The three column spine and its significance in the classification of acute thoracolumbar spinal inuries. 1983;8(8):817-831.

Divi SN, Schroeder GD, Oner FC, Kandziora F, Schnake KJ, Dvorak MF, Benneker LM, Chapman JR, Vaccaro AR. AOSpine—Spine Trauma Classification System: The Value of Modifiers: A Narrative Review With Commentary on Evolving Descriptive Principles. Global Spine J. 2019;9(1 Suppl):77S-88S.

D'Sa A, Alvin MD, Brody R, Javed S, Faro S, Nadgir RN. Imaging features of vertebral artery fenestration. Neuroradiology. 2020;62(5):587-592.

Duane TM, Young AJ, Vanguri P, Wolfe LG, Katzen J, Han J, Mayglothling J, Whelan JF, Aboutanos MB, Ivatury RR, Malhotra AK. Defining the cervical spine clearance algorithm: A single-institution prospective study of more Fthan 9,000 patients. J Trauma Acute Care Surg. 2016;81:(3):541-547.

Dvorak J, Panjabi M, Gerber M, Wichmann W. CT-functional diagnostic of the rotatory instability of upper cervical spine. 1. An experimental study on cadavers. Spine (Phila Pa 1976). 1987;12(3):197-205.

Eastman AL, Chason DP, Perez CL, McAnulty AL, Minei JP. Computed tomographic angiography for the diagnosis of blunt cervical vascular injury: is it ready for primetime? J Trauma. 2006;60(5):925-929.

Edelson JG, Nathan H. Stages in the natural history of the vertebral end-plates. Spine (Phila Pa 1976). 1988;13(1):21-26.

Einsiedel T, Schmelz A, Arand M, Wilke HJ, Gebhard F, Hartwig E, Kramer M, Neugebauer R, Kinzl L, Schultheiss M. Injuries of the cervical spine in patients with ankylosing spondylitis: experience at two trauma centers. J Neurosurg Spine. 2006;5(1):33-45.

Esnault P, Cardinale M, Boret H, D'Aranda E, Montcriol A, Bordes J, Prunet B, Joubert C, Dagain A, Goutorbe P, Kaiser E, Meaudre E. Blunt cerebrovascular injuries in severe traumatic brain injury: incidence, risk factors, and evolution. J Neurosurg. 2017;127(1):16-22.

Fabian TC, George SM Jr, Croce MA, Mangiante EC, Voeller GR, Kudsk KA. Carotid artery trauma: management based on mechanism of injury. J Trauma. 1990;30(8):953-961.

Farrell SF, Osmotherly PG, Cornwall J, Rivett DA. Morphology and morphometry of lateral atlantoaxial joint meniscoids. Anat Sci Int. 2016;91(1):89-96.

Fassett DR, Dailey AT, Vaccaro AR. Vertebral artery injuries associated with cervical spine injuries: a review of the literature. J spinal Disord Tech. 2008;21(4):252-258.

Fauny M, Morizot C, Allado E, Verhoeven F, Albuisson E, Semaan M, Pinzano A, Chary-Valckenaere I, Loeuille D. Consequences of spinal ankylosis on bone trabecular fragility assessed on CT scans in patients with ankylosing spondylitis. A retrospective study. Joint Bone Spine. 2020;87(6):625-631.

Fink KR, Fink JR, Cohen WA. Cervical collaterals may protect against stroke after blunt vertebral artery injury. Emerg Radiol. 2011;18(6):545-549.

Fleck SK, Langner S, Baldauf J, Kirsch M, Kohlmann T, Schroeder HWS. Incidence of blunt craniocervical artery injuries: use of whole-body computed tomography trauma imaging with adapted computed tomography. Neurosurgery. 2011;69(3):615-623.

Foo D, Rossier B. Post-traumatic spinal epidural hematoma. Neurosurgery. 1982;11(1 Pt 1):25-32.

Frankel HL, Hancock DO, Hyslop G, Melzak J, Michaelis LS, Ungar GH, Vernon JD, Walsh JJ. The value of postural reduction in the initial management of closed injuries of the spine with paraplegia and tetraplegia. I. Paraplegia. 1969;7(3):179-192.

Friedrich KM, Reiter G, Pretterklieber ML, Pinker K, Friedrich M, Trattnig S, Salomonowitz E. Reference data for in vivo magnetic resonance imaging properties of meniscoids in the cervical zygapophyseal joints. Spine (Phila Pa 1976). 2008;33(21):E778-783.

Fujimori T, Iwasaki M, Nagamoto Y, Ishii T, Kashii M, Murase T, Sugiura T, Matsuo Y, Sugamoto K, Yoshikawa H. Kinematics of the thoracic spine in trunk rotation: in vivo 3-dimensional analysis. Spine (Phila Pa 1976). 2012;37(21):E1318-1328.

Gellhorn AC, Katz JN, Suri P. Osteoarthritis of the spine: the facet joints. Nat Rev Rheumatol. 2013;9(4):216-224.

Gorman E, DiMaggio C, Frangos S, Klein M, Berry C, Bukur M. Elderly Patients With Cervical Spine Fractures After Ground Level Falls Are at Risk for Blunt Cerebrovascular Injury. J Surg Res. 2020:253:100-104.

Gornik HL, Persu A, Adlam D, Aparicio LS, Azizi M, Boulanger M, Bruno RM, de Leeuw P, Fendrikova-Mahlay N, Froehlich J, Ganesh SK, Gray BH, Jamison C, Januszewicz A, Jeunemaitre X, Kadian-Dodov D, Kim ES, Kovacic JC, Mace P, Morganti A, Sharma A, Southerland AM, Touzé E, van der Niepen P, Wang J, Weinberg I, Wilson S, Olin JW, Plouin PF. First International Consensus on the diagnosis and management of fibromuscular dysplasia. Vasc Med. 2019;24(2):164-189.

Guglielmi V, Compagne KCJ, Sarrami AH, Sluis WM, van den Berg LA, van der Sluijs PM, Mandell DM, van der Lugt A, Roos YBWEM, Majoie CBLM, Dippel DWJ, Emmer BJ, van Es ACGM, Coutinho JM; MR CLEAN trial and MR CLEAN Registry Investigators. Assessment of Recurrent Stroke Risk in Patients With a Carotid Web. JAMA Neurol. 2021;78(7):826-833.

Han PP, Theodore N, Porter RW, Detwiler PW, Lawton MT, Spetzler RF. Subdural hematoma from a Type I spinal arteriovenous malformation. Case report. J Neurosurg. 1999;90(2 Suppl):255-257.

Hanna G, Uddin SA, Trontis A, Ross L, Drazin D, Kim TT, Johnson JP. Epidural hematoma in patients with ankylosing spondylitis requiring surgical stabilization: a single-institution retrospective review with literature analysis. Neurosurg Focus. 2021;51(4):E5.

Hebert JS, Burnham RS. The effect of polytrauma in persons with traumatic spine injury. A prospective database of spine fractures. Spine (Phila Pa 1976). 2000;25(1):55-60.

Hendee WR, Becker GJ, Borgstede JP. Addressing overutilization in medical imaging. Radiology. 2010; 257(1): 240-245.

Hoffman JR, Mower WR, Wolfson AB, Todd KH, Zucker MI. Validity of a set of clinical criteria to rule out injury to the cervical spine in patients with blunt trauma. National Emergency X-Radiography Utilization Study Group. N Engl J Med. 2000;343(2):94-99.

Holdsworth F. Fractures, dislocations, and fracture-dislocations of the spine. J Bone Joint Surg Br. 1963;45(1):6-20.

Jacobs WB, Fehlings MG. Ankylosing spondylitis and spinal cord injury: origin, incidence, management, and avoidance. Neurosurg Focus. 2008;24(1):E12.

Jaumard NV, Welch WC, Winkelstein BA. Spinal facet joint biomechanics and mechanotransduction in normal, injury, and degenerative conditions. J Biomech Eng. 2011;133(7):071010.

Joaquim AF, de Oliveira SA, Appenzeller S, Patel AA. Spine Surgery and Ankylosing spondylitis: Optimizing Perioperative Management. Clin Spine Surg. 2023;36(1):8-14.

Kim MS. Developmental anomalies of the distal vertebral artery and posterior inferior cerebellar artery: diagnosis by CT angiography and literature review. Surg Radiol Anat. 2016;38(9):997-1006.

Kohler FC, Schenk P, Bechstedt-Schimske M, Ullrich BW, Klauke F, Hofmann GO, Mendel T. Open versus minimally invasive fixation of thoracic and lumbar

spine fractures in patients with ankylosing spinal diseases. Eur J Trauma Emerg Surg. 2022;48(3):2297-2307.

Koivikko MP, Koskinen SK. MRI of cervical spine injuries complicating ankylosing spondylitis. Skeletal Radiol. 2008;37(9):813-819.

Kuperus JS, Mohamed Hoesein FAA, de Jong PA, Verlaan JJ. Diffuse idiopathic skeletal hyperostosis: Etiology and clinical relevance. Best Pract Res Clin Rheumatol. 2020;34(3):101527.

Kuperus JS, Waalwijk JF, Regan EA, van der Horst-Bruinsma IE, Oner FC, de Jong PA, Verlaan JJ. Simultaneous occurrence of ankylosing spondylitis and diffuse idiopathic skeletal hyperostosis: a systematic review. Rheumatology (Oxford). 2018;57(12):2120-2128.

Landis JR, Koch GG. The measurement of observer agreement for categorical data. Biometrics. 1977;33(1):159-174.

Lantsman CD, Barkay G, Friedlander A, Barbi M, Stern M, Eshed. Whole Spine CT Scan for the Detection of Acute Spinal Fractures in Diffuse Idiopathic Skeletal Hyperostosis Patients Who Sustained Low-energy Trauma. Spine (Phila Pa 1976) 45(19):1348–1353.

Lawton MT, Porter RW, Heiserman JE, Jacobowitz R, Sonntag VK, Dickman CA. Surgical management of spinal epidural hematoma: relationship between surgical timing and neurological outcome. J Neurosurg. 1995;83(1):1-7.

Lebl DR, Bono CM, Velmahos G, Metkar U, Nguyen J, Harris MB. Vertebral artery injury associated with blunt cervical spine trauma: a multivariate regression analysis. Spine (Phila Pa). 2013;38(16):1352-1361.

Leichtle SW, Banerjee D, Schrader R, Torres B, Jayaraman S, Rodas E, Broering B, Aboutanos MB. Blunt cerebrovascular injury: The case for universal screening. J Trauma Acute Care Surg. 2020;89(5):880-886.

Leone A, Marino M, Dell'Atti C, Zecchi V, Magarelli N, Colosimo C. Spinal fractures in patients with ankylosing spondylitis. Rheumatol Int. 2016;36(10):1335-1346.

Lukasiewicz AM, Bohl DD, Varthi AG, Basques BA, Webb ML, Samuel AM, Grauer JN. Spinal Fracture in Patients With Ankylosing Spondylitis: Cohort Definition, Distribution of Injuries, and Hospital Outcomes. Spine (Phila Pa 1976). 2016;41(3):191-196.

Lytle ME, West J, Burkes JN, Beteck B, Fisher T, Daoud Y, Gable DR, Shutze WP. Limited Clinical Relevance of Vertebral Artery Injury in Blunt Trauma. Ann Vasc Surg. 2018;53:53-62.

Marchand F, Ahmed AM. Investigation of the laminate structure of lumbar disc anulus fibrosus. Spine (Phila Pa 1976). 1990;15(5):402-410.

Martin CJ, Barnard M. How much should we be concerned about cumulative effective dose in medical imaging? J Radiol Prot. 2022;42(1).

Matsunaga S, Kabayama S, Yamamoto T, Yone K, Sakou T, Nakanishi K. Strain on intervertebral discs after anterior cervical decompression and fusion. Spine (Phila Pa 1976). 1999;24(7):670-675.

Mercer S, Bogduk N. The ligaments and annulus fibrosus of human adult cervical intervertebral discs. Spine (Phila Pa 1976). 1999;24(7):619-626.

Mettler FA, Huda W, Yoshizumi TT, Mahadevappa M. Effective doses in radiology and nuclear medicine: a catalog. Radiology 2008; 248(1):254-263.

Misaki H, Morino T, Hino M, Murakami Y, Imai H, Miura H. Can Diffuse Idiopathic Skeletal Hyperostosis Be Diagnosed by Plain Lumbar Spine X-Ray Findings Alone? Global Spine J. 2022;12(2):198-203.

Mokin M, Waqas M, Chin F, Rai H, Senko J, Sparks A, Ducharme RW, Springer M, Borlongan CV, Levy EI, Ionita C, Siddiqui AH. Semi-automated measurement of vascular tortuosity and its implications for mechanical thrombectomy performance. Neuroradiology. 2021;63(3):381-389.

Morita K, Ohashi H, Kawamura D, Tani S, Karagiozov K, Murayama Y. Thoracic and lumbar spine pedicle morphology in Japanese patients. Surg Radiol Anat. 2021;43(6):833-842.

Nageler G, Gergel I, Fangerau M, Breckwoldt M, Seker F, Bendszus M, Möhlenbruch M, Neuberger U. Deep Learning-based Assessment of Internal Carotid Artery Anatomy to Predict Difficult Intracranial Access in Endovascular Recanalization of Acute Ischemic Stroke. Clin Neuroradiol. 2023;33(3):783-792.

Nicoll EA. Fractures of the dorso-lumbar spine. J Bone Joint Surg Br. 1949;31B(3):376-394.

Niemi-Nikkola V, Saijets N, Ylipoussu H, Kinnunen P, Pesälä J, Mäkelä P, Alen M, Vainionpää A. Traumatic Spinal Injuries in Northern Finland. Spine (Phila Pa 1976). 2018;43(1):E41-E51.

Noordhoek I, Koning MT, Vleggeert-Lankamp CLA. Evaluation of bony fusion after anterior cervical discectomy: a systematic literature review. Eur Spine J. 2019;28(2):386-399.

North American Symptomatic Carotid Endarterectomy Trial Collaborators; Barnett HJM, Taylor DW, Haynes RB, Sackett DL, Peerless SJ, Ferguson GG, Fox AJ, Rankin RN, Hachinski VC, Wiebers DO, Eliasziw M. Beneficial effect of carotid endarterectomy in symptomatic patients with high-grade carotid stenosis. N Engl J Med. 1991;325(7):445-453

Nowitzke A, Westaway M, Bogduk N. Cervical zygapophyseal joints: geometrical parameters and relationship to cervical kinematics. Clin Biomech (Bristol, Avon). 1994;9(6):342-348.

Oda J, Tanaka H, Tsuzuki N. Intervertebral disc changes with aging of human cervical vertebra. From the neonate to the eighties. Spine (Phila Pa). 1988;13(11):1205-1211.

Okada E, Yoshii T, Yamada T, Watanabe K, Katsumi K, Hiyama A, Watanabe M, Nakagawa Y, Okada M, Endo T, Shiraishi Y, Takeuchi K, Matsunaga S, Maruo K, Sakai K, Kobayashi S, Ohba T, Wada K, Ohya J, Mori K, Tsushima M, Nishimura H, Tsuji T, Okawa A, Matsumoto M, Watanabe K. Spinal fractures in patients with Diffuse idiopathic skeletal hyperostosis:A nationwide multi-institution survey. J Orthop Sci. 2019;24(4):601-606.

Okada E, Tsuji T, Shimizu K, Kato M, Fukuda K, Kaneko S, Ogawa J, Watanabe K, Ishii K, Nakamura M, Matsumoto M. CT-based morphological analysis of spinal fractures in patients with diffuse idiopathic skeletal hyperostosis. J Orthop Sci. 2017;22(1):3-9.

Oliver M, Inaba K, Tang A, Branco BC, Barmparas G, Schnüriger B, Lustenberger T, Demetriades D. The changing epidemiology of spinal trauma: a 13-year review from a Level I trauma centre. Injury. 2012;43(8):1296-1300.

Panjabi MM, O'Holleran JD, Crisco JJ 3rd, Kothe R. Complexity of the thoracic spine pedicle anatomy. Eur Spine J. 1997;6(1):19-24.

Paykin G, O'Reilly G, Ackland HM, Mitra B. The NEXUS criteria are insufficient to exclude cervical spine fractures in older blunt trauma patients. Injury. 2017;48(5):1020-1024.

Pearcy MJ, Tibrewal SB. Axial rotation and lateral bending in the normal lumbar spine measured by three-dimensional radiography. Spine (Phila Pa 1976). 1984;9(6):582-587.

Pierce JL, Donahue JH, Nacey NC, Quirk CR, Perry MT, Faulconer N, Falkowski GA, Maldonado MD, Shaeffer CA, Shen FH. Spinal Hematomas: What a Radiologist Needs to Know. Radiographics. 2018;38(5):1516-1535.

Reina MA, De Leon Casasola O, López A, De Andrés JA, Mora M, Fernández A. The origin of the spinal subdural space: ultrastructure findings. Anesth Analg. 2002;94(4):991-995.

Resnick D, Niwayama G. Radiographic and pathologic features of spinal involvement in diffuse idiopathic skeletal hyperostosis (DISH). Radiology. 1976;119(3):559-568.

Roberts GJ, Jacobson LE, Amaral MM, Jensen CD, Cooke L, Schultz JF, Kinstedt AJ, Saxe JM. Cross-sectional imaging of the torso reveals injuries in asymptomatic blunt trauma patients. World J Emerg Surg. 2020;15:5.

Roberts S, Evans H, Trivedi J, Menage J. Histology and pathology of the human intervertebral disc. J Bone Joint Surg Am. 2006:88 Suppl 2:10-4.

Rogalla P, Kloeters C, Hein PA. CT technology overview: 64-slice and beyond. Radiol Clin North Am. 2009;47(1):1-11.

Rosenthal BD, Boody BS, Jenkins TJ, Hsu WK, Patel AA, Savage JW. Thoracolumbar Burst Fractures. Clin Spine Surg. 2018;31(4):143-151.

Rudwaleit M, van der Heijde D, Landewé R, Listing J, Akkoc N, Brandt J, Braun J, Chou CT, Collantes-Estevez E, Dougados M, Huang F, Gu J, Khan MA, Kirazli Y, Maksymowych WP, Mielants H, Sørensen IJ, Ozgocmen S, Roussou E, Valle-Oñate R, Weber U, Wei J, Sieper J. The development of Assessment of SpondyloArthritis international Society classification criteria for axial spondyloarthritis (part II): validation and final selection. Ann Rheum Dis. 2009;68(6):777-783.

Rustagi T, Drazin D, Oner C, York J, Schroeder GD, Vaccaro AR, Oskouian RJ, Chapman JR. Fractures in Spinal Ankylosing Disorders: A Narrative Review of Disease and Injury Types, Treatment Techniques, and Outcomes. J Orthop Trauma. 2017;31 Suppl 4:S57-S74.

Rutman AM, Vranic JE, Mossa-Basha M. Imaging and Management of Blunt Cerebrovascular Injury. Radiographics. 2018;38(2):542-563.

Rydning PNF, Linnerud H, Mirzamohammadi J, Brommeland T, Rønning PA, Evjensvold M, Aarhus M, Bakland G, Helseth E. Decreasing incidence of cervical spine fractures in patients with ankylosing spondylitis: a population-based study in Southeast Norway. Spine J. 2024;24(8):1502-1509.

Sarzi-Puttini P, Atzeni F, Fumagalli M, Capsoni F, Carrabba M. Osteoarthritis of the spine. Semin Arthritis Rheum. 2005;34(6 Suppl 2):38-43.

Sasaki E, Ono A, Yokoyama T, Wada K, Tanaka T, Kumagai G, Iwasaki H, Takahashi I, Umeda T, Nakaji S, Ishibashi Y. Prevalence and symptom of ossification of posterior longitudinal ligaments in the Japanese general population. J Orthop Sci 2014;19(3):405-411.

Schaefer-Prokop CM, De Boo DW, Uffmann M, Prokop M. DR and CR: Recent advances in technology. Eur J Radiol. 2009;72(2):194-201.

Schwendner M, Seule M, Meyer B, Krieg SM. Management of spine fractures in ankylosing spondylitis and diffuse idiopathic skeletal hyperostosis: a challenge. Neurosurg Focus. 2021;51(4):E2.

Sebro R. Confirmation of the Influence of Descending Aorta on Osteophyte Formation in Dish. J Clin Rheumatol. 2018;24(6):351-353.

Shah NG, Keraliya A, Nunez DB, Schoenfeld A, Harris MB, Bono CM, Khurana B. Injuries to the Rigid Spine: What the Spine Surgeon Wants to Know. Radiographics. 2019;39(2):449-466.

Shah NG, Keraliya A, Harris MB, Bono CM, Khurana B. Spinal trauma in DISH and AS: is MRI essential following the detection of vertebral fractures in CT? Spine J. 2021;21(4):618-626.

Shahan CP, Magnotti LJ, McBeth PB, Weinberg JA, Croce MA, Fabian TC. Early antithrombotic therapy is safe and effective in patients with blunt cerebrovascular injury and solid organ injury or traumatic brain injury. J Trauma Acute Care Surg. 2016;81(1):173-177.

Shin JH, Wang S, Yao Q, Wood KB, Li G. Investigation of coupled bending of the lumbar spine during dynamic axial rotation of the body. Eur Spine J. 2013;22(12):2671-2677.

Sieper J, Poddubnyy D. Axial spondyloarthritis. Lancet. 2017;390(10089):73-84.

Sim E, Vaccaro AR, Berzlanovich A, Thaler H, Ullrich CG. Fenestration of the extracranial vertebral artery: review of the literature. Spine (Phila Pa 1976). 2001;26(6):E139-142.

Skjødt MK, Nicolaes J, Smith CD, Libanati C, Cooper C, Olsen KR, Abrahamsen B. Healthcare costs associated with opportunistically identifiable vertebral fractures. Bone. 2023:175:116831.

Slonimsky E, Lidar M, Stern M, Eshed I. Degenerative changes of the thoracic spine do exist in patients with diffuse idiopathic skeletal hyperostosis: a detailed thoracic spine CT analysis. Acta Radiol. 2018;59(11):1343-1350.

Smith GB, Barton FL, Watt JH. Extensive spread of local anaesthetic solution following subdural insertion of an epidural catheter during labour. Anaesthesia. 1984;39(4):355-358.

Smits AJ, Ouden LPD, Deunk J, Bloemers FW; LNAZ Research Group. Incidence of Traumatic Spinal Fractures in the Netherlands: Analysis of a Nationwide Database. Spine (Phila Pa 1976). 2020;45(23):1639-1648.

Stein DM, Boswell S, Sliker CW, Lui FY, Scalea TM. Blunt cerebrovascular injuries: does treatment always matter? J Trauma. 2009;66(1):132-143.

Stiell IG, Wells GA, Vandemheen KL, Clement CM, Lesiuk H, De Maio VJ, Laupacis A, Schull M, McKnight RD, Verbeek R, Brison R, Cass D, Dreyer J, Eisenhauer MA, Greenberg GH, MacPhail I, Morrison L, Reardon M, Worthington J. The Canadian C-spine rule for radiology in alert and stable trauma patients. JAMA. 2001;286(15):1841-1848.

Takagi H, Ota H, Natsuaki Y, Komori Y, Ito K, Saiki Y, Takase K. Identifying the Adamkiewicz artery using 3-T time-resolved magnetic resonance angiography: its role in addition to multidetector computed tomography angiography. Jpn J Radiol. 2015;33(12):749-756.

Takahashi T, Yoshii T, Mori K, Kobayashi S, Inoue H, Tada K, Tamura N, Hirai T, Sugimura N, Nagoshi N, Maki S, Katsumi K, Koda M, Murata K, Takeuchi K, Nakashima H, Imagama S, Kawaguchi Y, Yamazaki M, Okawa A. Comparison of radiological characteristics between diffuse idiopathic skeletal hyperostosis and ankylosing spondylitis: a multicenter study. Sci Rep. 2023;13(1):1949.

Taterra D, Skinningsrud B, Pękala PA, Hsieh WC, Cirocchi R, Walocha JA, Tubbs RS, Tomaszewski KA, Henry BM. Artery of Adamkiewicz: a meta-analysis of anatomical characteristics. Neuroradiology. 2019;61(8):869-880.

Teunissen FR, Verbeek BM, Cha TD, Schwab JH. Spinal cord injury after traumatic spine fracture in patients with ankylosing spinal disorders. J Neurosurg Spine. 2017;27(6):709-716.

Travan L, Saccheri P, Gregoraci G, Mardegan C, Crivellato E. Normal anatomy and anatomic variants of vascular foramens in the cervical vertebrae: a paleo-osteological study and review of the literature. Anat Sci Int. 2015;90(4):308-323.

Vaccaro AR, Lehman RA Jr, Hurlbert RJ, Anderson PA, Harris M, Hedlund R, Harrop J, Dvorak M, Wood K, Fehlings MG, Fisher C, Zeiller SC, Anderson DG, Bono CM, Stock GH, Brown AK, Kuklo T, Oner FC. A new classification of thoracolumbar injuries: the importance of injury morphology, the integrity of the posterior ligamentous complex, and neurologic status. Spine (Phila Pa 1976). 2005;30(20):2325-2333.

Vaccaro AR, Hulbert RJ, Patel AA, Fisher C, Dvorak M, Lehman RA Jr, Anderson P, Harrop J, Oner FC, Arnold P, Fehlings M, Hedlund R, Madrazo I, Rechtine G, Aarabi B, Shainline M; Spine Trauma Study Group. The subaxial cervical spine injury classification system: a novel approach to recognize the importance of morphology, neurology, and integrity of the disco-ligamentous complex. Spine (Phila Pa 1976). 2007;32(21):2365-2374.

Vaccaro AR, Oner C, Kepler CK, Dvorak M, Schnake K, Bellabarba C, Reinhold M, Aarabi B, Kandziora F, Chapman J, Shanmuganathan R, Fehlings M, Vialle L; AOSpine Spinal Cord Injury & Trauma Knowledge Forum. AOSpine thoracolumbar spine injury classification system: fracture description, neurological status, and key modifiers. Spine (Phila Pa 1976). 2013;38(23):2028-2037.

van der Linden S, Valkenburg HA, Cats A. Evaluation of diagnostic criteria for ankylosing spondylitis. A proposal for modification of the New York criteria. Arthritis Rheum. 1984;27(4):361-368.

Vandenabeele F, Creemers J, Lambrichts I. Ultrastructure of the human spinal arachnoid mater and dura mater. J Anat. 1996;189 ( Pt2)(Pt2):417-430.

Vazan M, Ryang YM, Barz M, Török E, Gempt J, Meyer B. Ankylosing Spinal Disease-Diagnosis and Treatment of Spine Fractures. World Neurosurg. 2019:123:e162-e170.

Wang AC, Charters MA, Thawani JP, Than KD, Sullivan SE, Graziano GP. Evaluating the use and utility of noninvasive angiography in diagnosing traumatic blunt cerebrovascular injury. J Trauma Acute Care Surg. 2012;72(6):1601-1610.

Weber CD, Lefering R, Kobbe P, Horst K, Pishnamaz M, Sellei RM, Hildebrand F, Pape HC; TraumaRegister DGU. Blunt Cerebrovascular Artery Injury and Stroke in Severely Injured Patients: An International Multicenter Analysis. World J Surg. 2018;42(7):2043-2053.

Weinfeld RM, Olson PN, Maki DD, Griffiths HJ. The prevalence of diffuse idiopathic skeletal hyperostosis (DISH) in two large American Midwest mertropolitan hospital populations. Skeletal Radiol. 1997;26(4):222-5.

Werner BC, Samartzis D, Shen FH. Spinal Fractures in Patients With Ankylosing Spondylitis: Etiology, Diagnosis, and Management. J Am Acad Orthop Surg. 2016;24(4):241-249.

Westerveld LA, van Bemmel JC, Dhert WJ, Oner FC, Verlaan JJ. Clinical outcome after traumatic spinal fractures in patients with ankylosing spinal disorders compared with control patients. Spine J. 2014;14(5):729-740.

Westerveld LA, van Ufford HM, Verlaan JJ, Oner FC. The prevalence of diffuse idiopathic skeletal hyperostosis in an outpatient population in The Netherlands. J Rheumatol. 2008;35(8):1635-1638.

Westerveld LA, Verlaan JJ, Lam MG, Scholten WP, Bleys RL, Dhert WJ, Oner FC. The influence of diffuse idiopathic skeletal hyperostosis on bone mineral density measurements of the spine. Rheumatology (Oxford). 2009;48(9):1133-1136.

Westerveld LA, Verlaan JJ, Oner FC. Spinal fractures in patients with ankylosing spinal disorders: a systematic review of the literature on treatment, neurological status and complications. Eur Spine J. 2009;18(2):145-156.

Wysham KD, Murray SG, Hills N, Yelin E, Gensler LS. Cervical Spine Fracture and Other Diagnoses Associated with Mortality in Hospitalized Ankylosing Spondylitis Patients. Arthritis Care Res (Hoboken). 2017;69(2):271-277.

Xu R, Burgar A, Ebraheim NA, Yeasting RA. The quantitative anatomy of the laminas of the spine. Spine (Phila Pa 1976). 1999;24(2):107-113.

Yaprak F, Ozer MA, Govsa F, Eraslan C. Variations of the extracranial segment of vertebral artery as a bleeding risk factor. Surg Radiol Anat. 2021;43(10):1735-1743.

Yoshimura N, Nagata K, Muraki S, Oka H, Yoshida M, Enyo Y, Kagotani R, Hashizume H, Yamada H, Ishimoto Y, Teraguchi M, Tanaka S, Kawaguchi H, Toyama Y, Nakamura K, Akune T. Prevalence and progression of radiographic ossification of the posterior longitudinal ligament and associated factors in the Japanese population: a 3-year follow-up of the ROAD study. Osteoporos Int. 2014;25(3):1089-1098.

Yu J, Fairbank JC, Roberts S, Urban JP. The elastic fiber network of the anulus fibrosus of the normal and scoliotic human intervertebral disc. Spine (Phila Pa 1976). 2005;30(16):1815-1820.

# ORIGINAL PUBLICATIONS